DISSERTATIONES CHIMICAE UNIVERSITATIS TARTUENSIS
68

# CHARGE STATE OF DOPANTS AND ORDERED CLUSTERS FORMATION IN $CaF_2$:Mn AND $CaF_2$:Eu LUMINOPHORS

**AIME LUST**

TARTU UNIVERSITY
PRESS

Institute of Chemical Physics, Department of Chemistry, University of Tartu, Estonia

Dissertation is accepted for the commencement of the degree of Doctor of Philosophy in Chemistry on June 29, 2007, by the Doctoral Committee of the Department of Chemistry, University of Tartu.

Dissertant: Aime Lust (MSc), Analytical and Physical Chemistry

Supervisor: senior researcher Mikhail Danilkin (PhD)

Opponents: academician, professor Enn Mellikov (DSc), Director of Institute of Material Science, Tallinn University of Technology, Estonia (ennm@staff.ttu.ee)

senior researcher Irina A. Kamenskikh (phys.-math. cand.), Optics and Spectroscopy Chair of Physics Department of M.V. Lomonosov Moscow State University (iak@neurok.ru)

Commencement: August 29, 2007, 11 AM, at 18 Ülikooli St., room 204

Publication of this dissertation is granted by University of Tartu

ISSN 1406–7366
ISBN 978–9949–11–661–4 (trükis)
ISBN 978–9949–11–662–1 (PDF)

Autoriõigus Aime Lust, 2007

Tartu Ülikooli Kirjastus
www.tyk.ee
Tellimus nr. 284

# CONTENTS

# LIST OF ORIGINAL PUBLICATIONS

This thesis is based on five papers, listed below, and discussion of the results. These papers are referred to by Roman numerals from I to V in the text. The discussion of the results summarises and supplements the original papers.

I. Determination of Manganese in Thermoluminescence Materials by Inductively Coupled Plasma Atomic Emission Spectroscopy and Spectrophotometry. Lust, A.; Paama, L.; Kerikmäe, M.; Must, M.; Perämäki, P. *Proc. Estonian Acad. Sci. Chem.*, **2002**, 51(2), 126–133.
II. OSL of Some TLD Detectors as the Indicator of Absorbed Dose. Jaek, I.; Kerikmäe, M.; Lust, A. *Rad. Prot. Dosim.*, **2002**, 100(1–4), 459–462.
III. $CaF_2$:Mn extreme dosimeter: Effects on Mn concentration on thermoluminescence mechanisms and properties. Danilkin, M.; Lust, A.; Kerikmäe, M.; Seeman, V.; Mändar, H.; Must, M. *Rad. Meas.*, **2006,** 41, 677–681.
IV. Magnetic manifestations of thermoluminescence excitation in $CaF_2$:Mn (TLD-400). Danilkin, M.; Kirillov, A.; Klimonsky, S.; Kuznetsov, V.; Lust, A.; Mändar, H.; Seeman, V. *Rad. Meas.*, **2007** (available online at http://dx.doi.org/10.1016/j.radmeas.2007.01.079).
V. $Eu^{2+}$ and $Eu^{3+}$ centers formation at synthesis of $CaF_2$:Eu luminophors. Danilkin, M.I.; Beloussov, A.P.; Klimonsky, S.O.; Kuznetsov, V.D.; Lust, A.L.; Nikiforov, V.N.; Paama, L.N.; Rammo, I.H.; Seeman, V.O. (submitted for publication to *Journal of Applied Spectroscopy, Minsk*).

**Author 's contribution**

**Paper I:** The main contributor of work. One of two contributors to writing the text.
**Paper II:** The synthesis of samples; helped to prepare manuscript.
**Paper III:** One of main contributors (synthesis and analysis of samples, sample irradiation arrangements, discussion, helped to prepare the manuscript).
**Paper IV:** The synthesis of samples, analysis of manganese concentrations, sample irradiation arrangements.
**Paper V:** One of main contributors (the synthesis of samples, data calculations, discussion and manuscript preparation).

# INTRODUCTION

All branches of science, industry and medicine, where ionising radiation is used, require exact radiation dose monitoring. Thermoluminescence dosimeters (TLD) are among the well-known radiation measuring means. Despite of many minerals and synthetic compounds possessing thermoluminescence (TL) phenomena, only few of them are suitable TLD. Calcium fluoride doped with manganese ($Mn^{2+}$) is one of perfect materials. It is used mostly in an environmental dosimetry [1–4] rather than in personal dosimetry, because it absorbs radiation like bones, not like tissues. $CaF_2$:Mn is called for as extreme dosimeter due to the linear response of TL intensity in the wide range of the radiation doses (from 0.5 mGy to about $10^3$ Gy) [2,5]. $CaF_2$:Mn has a single TL peak well above room temperature (570–580 K). There are no losses of dose information from this TL peak at room temperature, and dose information can be stored for years. Many attempts have been made during the last 40 years to understand the TL mechanism of $CaF_2$:Mn, nevertheless the issue is still open for investigations. This is mostly due to the substantial dependence of thermoluminescence characteristics on actual concentration, distribution, and charge state of the doping agent ($Mn^{2+}$). The single high-temperature peak at glow curve appears only when $CaF_2$ is doped with a high manganese concentration, being close, but still below the decomposition threshold of a solid solution. This point is very important background making the present study up to date.

$CaF_2$:Eu is well-known scintillation crystal for X-ray and particle detection. It shows mostly $Eu^{2+}$ luminescence with relatively high light output. There were many separate studies of $Eu^{2+}$ [6,7] and $Eu^{3+}$ [8,9] luminescence, and also two-photon processes on $Eu^{2+}$[10]. A new scintillation material was reported recently, namely, a single crystal of $Ca_{0.65}Eu_{0.35}F_{2.35}$[11], with europium being totally in triple charged state. It is positioned for scintillation detectors in security X-ray tomography systems. Despite of good luminescence characteristics, this material is quite expensive one in comparison with, for example, sintered ceramics. This makes a practical challenge to develop the method of controlling the charge state of europium in $CaF_2$:Eu luminophors. Moreover, the problem of charge transformations of Eu is not extensively studied in $CaF_2$:Eu, being connected in publications only with thermoluminescence mechanism [12]. The ordered clusters were studied in connection with $Eu^{3+}$ [8,9] luminescence solely, and no explanation were given to very different appearance of EPR spectra of $Eu^{2+}$ [13,14] in $CaF_2$:Eu. However, the ordered clusters of dopant influence the luminescence output very essentially, and they need to be studied.

All the unsolved problems mentioned above, and also practical importance of the materials under investigation, make the present work up to date.

The purpose of present study was to adapt the co-precipitation synthesis method for $CaF_2$:Mn and $CaF_2$:Eu luminophors, to control suitable concentra-

tion and charge state of a dopant, and also, the conditions when ordered clusters are formed in solid solutions.

A brief review of synthesis methods of $CaF_2$:Mn and $CaF_2$:Eu luminophors (known from existing publications) is given in the first chapter. The luminescence and thermoluminescence studies of these materials are also shortly reviewed here. The second chapter describes the synthesis procedure developed by the author of dissertation for $CaF_2$:Mn and $CaF_2$:Eu luminophors, and also the methods of analysis of the concentration of dopant in final product. The third chapter deals with the dopant clustering effects on thermoluminescence, luminescence and magnetic properties of luminophors.

# INVESTIGATION GOALS

The goals of present work are the following:

- to adapt the co-precipitating synthesis method for $CaF_2$:Mn luminophors;
- to find the solubility threshold and optimal manganese concentration in $CaF_2$:Mn solid solution;
- to control the ordered clusters formation and Mn oxidation state in $CaF_2$:Mn;
- to study thermoluminescence mechanism of $CaF_2$:Mn and possibility of readout by the method of optically stimulated afterglow (OSA);
- to compare the co-precipitating and mechanical mixing synthesis methods for $CaF_2$:Eu luminophors;
- to study europium charge transformations at synthesis of $CaF_2$:Eu luminophors;
- to control charge state of europium in $CaF_2$:Eu luminophor in order to obtain the material with a low $Eu^{2+}$ concentration;
- to study the ordered clusters formation in $CaF_2$:Eu and the influence of Eu clusters on the luminescence and magnetic properties of $CaF_2$:Eu.

# 1. SYNTHESIS AND PROPERTIES OF $CaF_2$:Mn AND $CaF_2$:Eu LUMINOPHORS (LITERATURE OVERVIEW)

## 1.1. $CaF_2$:Mn

One of the first $CaF_2$:Mn synthesis methods [5,15–21] was based on the following reaction:

$$CaF_2 + NH_4MnF_3.nH_20 \rightarrow CaF_2:Mn + NH_3 + nH_2O$$

$CaF_2$ and doping agent in the form of $NH_4MnF_3.nH_20$ were mixed mechanically, then placed into platinum crucible and annealed at 1473 K for 16 hours in an inert gas atmosphere. The Pt is capable to catalyse a reaction of $NH_3$ with oxygen traces, and thus products like NO and $NO_2$ were released and partially stored in a host lattice, causing the further oxidation of $Mn^{2+}$. Oxidised to a higher than 2+ oxidation state, manganese is no more luminescence activator. So, the effective activator concentration decreases, and low-temperature peaks appear on the glow curve. The replacement of platinum crucible with a graphite one does not give better results. CO and $CO_2$ are formed in this case, and CO reduces $Mn^{2+}$ to base metal. As a result, the thermoluminophors synthesized in graphite crucibles have also low-temperature peaks on a glow curve.

Another method suggested in [22–24] was based on adding HF to suspension of $CaCO_3$ and $MnCO_3$. Some part of manganese was oxidised during separation of precipitate, and also, precipitate was contaminated with traces of $CaCO_3$, thus making worse the properties of thermoluminophor. The desired single high-temperature peak has occurred at so high activator concentrations [23] that thermoluminophor was unstable at reuse in routine dosimetry due to decomposition of the solid solution.

When $CaF_2$ was obtained by a reaction [5]:

$$HF + CaCl_2 \rightarrow CaF_2 + 2HCl$$

the optimal concentration of $Mn^{2+}$ was found to be 1,5 at.%, and no low-temperature peaks were observed on the glow curve. Niewiadomski [25] has proposed to precipitate $CaF_2$ :$MnF_2$ by adding reaction equivalent amount of $NH_4F$ to water solutions of $CaCl_2$ and $MnCl_2$.

An essential fact was reported in paper [16] where the substantially non-uniform distribution of manganese in final product was discovered when Mn impurity was mechanically mixed with the other reagents. The final annealing temperature occurs to be too low for successful diffusion of a doping agent. Hence, one needs at the same time to avoid the oxidation of $Mn^{2+}$ and to get an uniform distribution of activator in the final product. This can be achieved by

introducing the $Mn^{2+}$ into $CaF_2$ lattice at an early stage of synthesis by co-precipitation. Then, oxidizing during firing should be avoided. The co-precipitation procedure was first proposed by Palmer *et al* [22,23]. The initial compounds were $CaCO_3$, $MnCO_3$, and HF. However, the described process has also yielded to a partial oxidation of manganese during high-temperature annealing. The final product needed washing with hot concentrated hydrochloric acid to remove traces of $Mn^{4+}$.

We have modified this method and succeeded in developing the synthesis technology giving the TL material, which is free of oxygen traces and very stable against oxidation. The apparatus, and co-precipitation conditions have been worked out. The oxygen-free salts of calcium and manganese are to be used in our process [26,27].

As it was already mentioned in the introduction, $CaF_2$:Mn has extremely wide range of linearity of response to radiation dose [2,5,28], so it may be used either in routine or in accident dosimetry. The thermoluminophor $CaF_2$:Mn has low information losses due to deep traps, and it is insensitive to a daylight [29,30]. The luminophor has a single TL peak at 513–553 K. However, some researchers consider that this peak consists of several unresolved peaks with different types of trapping centres [31–33].

The conventional way to measure a thermoluminescence response to dose assumes heating TLD below incandescence temperature after it has been exposed to ionising radiation. Also, the other ways of readout are becoming more and more popular, namely, optically stimulated luminescence (OSL) [34], cryogenic optically stimulated luminescence (COSL) [30,35,36], and laser beam stimulation [37,38]. The OSL and COSL methods give a possibility to use organic binders and plastic materials in the construction of TLD [39]. S.D. Miller *et al* [40] have demonstrated optical cleaning out the dose in $CaF_2$:Mn. The laser suitable for optical readout of $CaF_2$:Mn is a 326 nm helium-cadmium ultraviolet laser. A complete cycle of readout and annealing of the $CaF_2$:Mn (COSL) can be accomplished now without heating the dosimeters above room temperature. This is essential for creating a proton-recoil-based fast neutron dosimetry systems, based on COSL technique.

Besides being suitable TLD material, $CaF_2$ doped with both manganese and rare earth ions is a model object for studying mechanisms of resonance energy transfer in solids, important for development of different luminophors, laser materials etc. [41–43]. Also, isotropic fluorite crystals are promising materials for short-wavelength ($h\nu \geq 6$ eV) laser optics [44,45]. Physical processes in $CaF_2$:Mn excited with photons of high energies ($h\nu \geq 6$ eV) are reported in papers [46,47].

Many attempts have been made during the last 40 years to understand the TL mechanism of $CaF_2$:Mn. Very different approaches have been used and different models were suggested. A brief overview of the investigations and ideas is given below.

Alonso and Alcala [48,49], Alonso *et al* [50], Alcala *et al* [51], Jain and Jahan [52] have investigated the TL response of $CaF_2$:Mn below room temperature. V.K. Jain [53] has studied optical absorption, ESR, and TL emission spectrum to identify the type of charge carriers and involved traps and luminescent centres in $CaF_2$:Mn. However, the exact trap/luminescent centre correlation has not been revealed.

Mathur *et al* [54], McKeever *et al* [55], Allen and McKeever [56] have suggested the defects involved in thermoluminescence processes to be complexes of Mn and radiation induced defects (e.g. Mn/F centres).

Jose Luis Pasqual *et al* [57] have performed *ab initio* calculations of the optical absorption spectrum of $Mn^{2+}$-doped $CaF_2$. The calculations were based on a $MnF_8^{6-}$ cluster, where electrostatic and quantum embedding effects have been considered. The same authors [58] have extended their calculations to include the effects of dipole polarization and site relaxation of lattice ions external to the $MnF_8^{6-}$ cluster. Their calculations predict essential local distortions around $Mn^{2+}$ impurity in $CaF_2$ lattice.

A.C. Lewandovski and T. Wilson [59] have also performed *ab initio* multi-configuration self-consistent field calculations of the excited states of Mn impurity in $CaF_2$. The $[MnF_8]^{6-}$ $O_h$ cluster have been chosen to represent the isolated $Mn^{2+}$ substitutional impurity. The crystal field splitting diagrams for the light-coordinated $Mn^{2+}$ impurity in $O_h$ symmetry are calculated.

M.T. Barriuso and M. Moreno [60] investigated the $Mn^{2+}$-$F^-$ distance for $Mn^{2+}$ in fluoride lattices with hexahedral coordination. Their work is based on EPR data analysis and also predicts essential distortions in $CaF_2$ lattice caused by $Mn^{2+}$ impurity.

A lot of papers are concerned with EPR studies of $CaF_2$:Mn [62–64].

J.H. Barkoumb and A.N. Mansour [65] have measured the XANES spectra of the Ca and Mn at K edges in crystalline $CaF_2$:Mn. They determined the lattice distortion produced by the manganese center. The significance of shell contraction and a disorder caused by Mn impurity is discussed in terms of possible defect structure in this material.

K. Chakrabati, J.H. Barkoumb, V.K. Mathur [66] found that at higher $Mn^{2+}$ concentrations (more than 3 %) $Mn^{2+}$ - $Mn^{2+}$ pairs appear causing the deeper traps and background problems.

R. Lindner *et al* [67] have studied time-dependent luminescence of self-trapped excitons in alkaline earth fluorides excited by femto-second laser pulses. They proposed the model that the levels of several STE configurations are occupied at room temperature. The temporal and spectral behavior of the luminescence decay is believed to be characteristic either for the exciton configurations or transformations of one configuration into another.

V.P. Denks *et al* [68] have measured fluorescent characteristics of series of powder $CaF_2$:Mn phosphors (prepared in our laboratory, with concentration of Mn in mixture ranging from 0.01 to 2.47 weight %) excited by VUV radiation with quantum energies up to 14 eV at 293 K and up to 12 eV at 85 K. Narrow

excitation bands of $Mn^{2+}$ centres found at 7.9 and 8.6 eV (at 293 K) are assigned to partially forbidden transitions from the ground state $^6S$ split by crystalline field in two sublevels to the excited level corresponding to the $^6D$ term of a free $Mn^{2+}$-ion ($3d^5 \rightarrow 3d^4 4s$ transitions). A wide elementary excitation band in region 9.1–10.3 eV is interpreted as photogeneration of near-activator D-excitations. The channels of energy transfer in the $CaF_2$:Mn luminophor are briefly analysed.

## 1.2. $CaF_2$:Eu

First studies were undertaken using natural fluorite crystals. Rare earth impurities are also natural impurities in fluorite. Doping of finished single crystals is not so easy task. Very common method uses to insert a single crystal into previously doped powder and anneal at temperature of about 80% of melting point. This method was the only possible one before the synthetic fluorite crystals have been grown. Since then a dopant is introduced into the melt (for example, [69]), and no special preparation details are marked out in the description of experimental setup in different papers. The only point we know concerns avoiding contamination of crystals with oxygen. For example, $PbF_2$ was added into the raw materials as oxygen scavenger [70]. What concerns the powder samples, both mechanical mixing [71] and co-precipitation techniques [72] were used in preparation of $CaF_2$:Eu samples. Mechanically mixed precursors were annealed at 1173 K for 4 days [71]. The co-precipitation procedure [72] makes possible to decrease the annealing time, however, calcium nitrate used as a starting material provides oxygen traces capable to stabilize $Eu^{3+}$ near interstitial $O^{2-}$. $Ca_{1-X}Eu_XF_{2+X}$ nano-particles were obtained recently [73] by co-precipitation method in alcohol from starting $CaCl_2$, $EuCl_3$, and $NH_4F$. Low solubility of $NH_4F$ in alcohol was used to restrict the growth rate of nano-particles. Actually, our procedure uses the same starting materials, except being conducted in triply distilled water. Another waterless synthesis of $Ca_{1-X}Eu_XF_{2+X}$ nano-particles was suggested [74], using nano-reactors formed of isopropanol droplets in tetrahydrofuran. Waterless calcium nitrate was used in the procedure as a starting material. The reaction yield is high enough (90%), and the remaining nitrate traces are washed out with isopropanol and tetrahydrofuran in a repeated sequence washing procedure. The absence of interstitial oxygen was checked by measuring luminescence spectra.

Luminescence and EPR studies of $CaF_2$:Eu have a very long history. Absorption and luminescence of $Eu^{2+}$ in natural and synthetic fluorites was studied yet by Feofilov [75]. $CaF_2$:Eu single crystals are now available commercially as scintillators, they are used in nuclear physics and even for dark matter detection [76]. There are many applications of rare earth doped fluorite crystals in laser physics, and there are many papers, from two-photon processes [10] and spectral hole burning [77] to laser-beam damage of fluorite crystals [78]. The

detailed structure of $Eu^{3+}$ centres in $CaF_2$ is reported in papers [8,9,79]. In the absence of oxygen contamination, the charge compensation is performed through interstitial $F^-$ ions. The local compensation occurs in this way, that besides additional interstitial fluoride, there are also pairs of displaced fluoride ions and anion vacancies around rare earth impurity ions. The total amount of interstitial fluoride exceeds the amount of triple charged rare earth ions, by one ion per cluster. This is regarded as the reason for creation large clusters at annealing, with excess interstitial fluoride being scavenged away [9,79].

There were also many studies of thermoluminescence mechanisms in $CaF_2$ doped with rare earth ions. The model of charge transformations of rare earth impurities was checked and rejected in paper [12]. The low-temperature peaks were mostly connected with decay of $V_K$ centres with released holes re-combining with electrons trapped at anion vacancies near rare-earth impurities [70].

# 2. SYNTHESIS AND ANALYSIS OF $CaF_2$ BASED LUMINOPHORS

## 2.1. $CaF_2$:Mn

The co-precipitation of host material together with Mn dopant was proceeded in a specially designed apparatus made of fluoroplast-4. The initial compounds, concentration of a dopant in the initial solutions, and co-precipitation conditions like temperature, rate of solutions adding, time of product ageing in mother liquor, were varied. Various calcium salts were used as initial compounds. Most suitable were $CaCl_2$ and $MnCl_2$ (no manganese oxidation). In case of $Ca(NO_3)_2$, a small part of $Mn^{2+}$ was oxidised to $Mn^{4+}$ during final annealing due to traces of oxygen remained in precipitate. All the initial compounds were of special purity. HF contained less than $1x10^{-5}$% of heavy and transition metals. $CaCl_2$ contained less than $1x10^{-5}$% of Al, Cu, Ag, Fe, Mn, Mg, less than $1x10^{-3}$% of Ba and Sr, and less than $1x10^{-4}$% of Pb, Bi, Cr, Si. Triply distilled water was used to prepare solutions and mother liquor. The dilute solutions of $CaCl_2$, $MnCl_2$ and HF were added simultaneously at a regulated rate into the reaction vessel using peristaltic pumps. The reaction vessel was kept at an elevated temperature using vapour bath, and incoming solutions were agitated with a fluoroplast-made stirring rod. The precipitate was aged in the mother liquor for 2–3 hours. Then, the precipitate was decanted and washed carefully, dried, and pre-annealed in air at 673 K for two hours to remove the traces of water and hydrofluoric acid. Traces of water cause oxidation of $Mn^{2+}$ as well as oxygen traces. Pre-annealed precipitate was then placed into carbon-glass crucible and fired for ½ hour at 1423 K in a quartz atmospheric tube under a protective flow of high-purity (99.999%) argon or nitrogen. When necessary, the finished thermoluminophor was pressed into tablets and fired in a protective atmosphere once again. The resulting concentration of manganese in the finished thermoluminophor depends not only on the amount of manganese in the initial solutions but also on the precipitation conditions and on the presence of additional dopants. The amount of manganese was varied in the starting solutions from 0.01 weight % to 2 weight %, while the actual concentration of Mn was assessed by spectrophotometric analysis [I].

The results of photometric analysis were checked with data obtained by inductively coupled plasma atomic emission spectroscopy (ICP-AES). A sequential PU 7000 Philips (Unicam Analytical Systems, Cambridge, UK) inductive coupled plasma atomic emission spectrometer (University of Oulu, Finland) was used for the measurements. The spectrophotometric measurements were performed with Lambda 2S Perkin-Elmer UV/VIS spectrophotometer. Both methods, ICP-AES and spectrophotometry, give the consistent results. The ICP-AES method is more rapid and convenient compared with spectrophotometric method, which is more complicated and time-consuming. The man-

ganese concentration in precipitate changes non-monotonically with the increase of manganese amount in the starting solution, giving a maximum near 1.0 weight % of Mn in $CaCl_2$ solution [I]. The results of analysis are represented in Table 1.

**Table 1** The comparison of ICP-AES and spectrophotometric analytical results for both precipitate $CaF_2$:$MnF_2$ and finished $CaF_2$:Mn thermoluminescent material.

| Sample | Mn, % (m/m) | | | | |
|---|---|---|---|---|---|
| | Added to the initial solutions | ICP-AES | | Spectrophotometry | |
| | | $C_{AVER}$ ± SD | RSD, % | $C_{AVER}$ ± SD | RSD, % |
| $CaF_2$:$MnF_2$ precipitate | | | | | |
| 1 | 0.01 | 0.12 ± 0.0012 | 1.00 | 0.10 ± 0.0018 | 1.80 |
| 2 | 0.05 | 0.27 ± 0.0026 | 0.98 | 0.28 ± 0.0027 | 0.96 |
| 3 | 0.10 | 0.51 ± 0.0049 | 0.96 | 0.49 ± 0.0098 | 2.00 |
| 4 | 0.20 | 0.62 ± 0.0055 | 0.88 | 0.59 ± 0.012 | 2.03 |
| 5 | 0.40 | 1.49 ± 0.0044 | 0.90 | 1.54 ± 0.028 | 1.82 |
| 6 | 0.80 | 2.20 ± 0.0094 | 0.63 | 2.12 ± 0.044 | 2.08 |
| 7 | 1.00 | 2.53 ± 0.017 | 0.69 | 2.50 ± 0.048 | 1.92 |
| 8 | 1.20 | 2.39 ± 0.019 | 0.80 | 2.46 ± 0.042 | 1.71 |
| 9 | 1.60 | 1.63 ± 0.011 | 0.65 | 1.55 ± 0.029 | 1.87 |
| 10 | 2.00 | 1.78 ± 0.016 | 0.65 | 1.73 ± 0.040 | 2.31 |
| $CaF_2$:Mn thermoluminophor | | | | | |
| 1 | 0.10 | 0.58 ± 0.0042 | 0.72 | 0.62 ± 0.014 | 2.26 |
| 2 | 0.20 | 0.68 ± 0.0051 | 0.76 | 0.73 ± 0.013 | 1.78 |
| 3 | 0.40 | 1.46 ± 0.010 | 0.68 | 1.44 ± 0.028 | 1.94 |
| 4 | 0.80 | 1.66 ± 0.012 | 0.70 | 1.56 ± 0.031 | 1.99 |

The Mn concentration in the final product is also controlled by the rate of solutions adding into the mother liquor. The Mn concentration dependence on $CaCl_2$ solution adding rate is represented in Fig. 1.

The other parameters were kept constant (Mn concentration in initial solution, HF adding rate, temperature). The Mn concentration in final product decays exponentially with the increase of adding rate of $CaCl_2$ solution. The amount of manganese in the precipitate is affected not only by the rate of adding solutions into the reaction vessel but also by the ratio of calcium and fluoride ions and by the ageing time in mother liquor. The amount of manganese in precipitate versus the ageing time at different adding rates of $CaCl_2$ solution is shown in Table 2.

At ageing, the smallest micro-crystalls are dissolved, while the larger are growing up. This makes the influence of both ageing time and solutions adding rate on the amount of Mn in the final product non-monotonical, because the larger micro-crystals appear at lower adding rate, and they undergo essential further transformations in the mother liquor at ageing. The optimum ageing time was found to be 2 hours, with the adding rate of $CaCl_2$ solution being 2.4–2.5 ml/min.

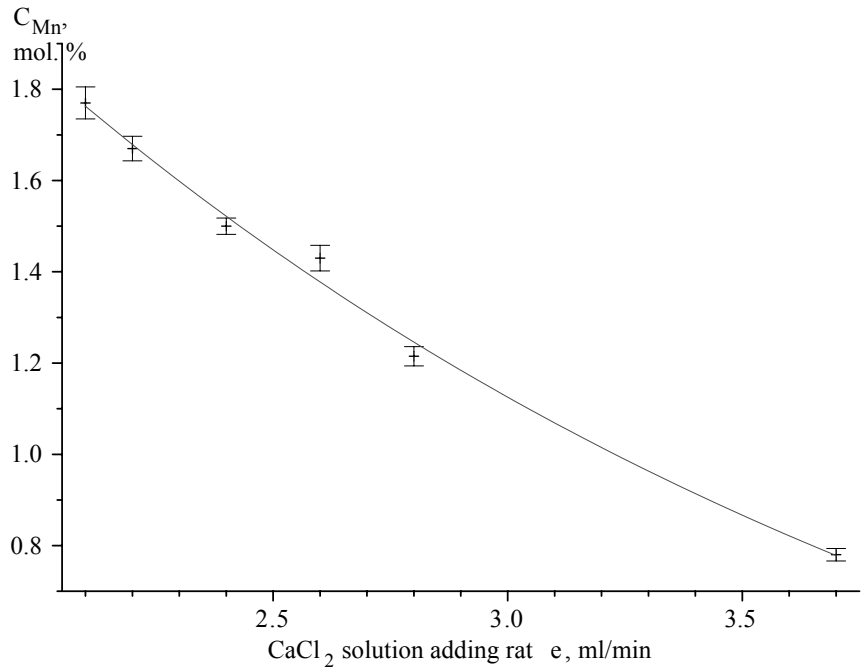


**Fig. 1.** Concentration of manganese in precipitate versus the adding rate of $CaCl_2$ solution. HF adding rate was kept at 2.4 ml/min, amount of Mn in initial solution 0.567 at%.

**Table 2.** Amount of Mn in precipitate versus ageing time of precipitate in the mother liquor measured for different adding rates of $CaCl_2$ solution. Adding rate of HF was kept at 2.8 ml/min, and the amount of manganese in the initial solutions was 1.13 at.%.

| Adding rate of $CaCl_2$, ml/min | Ageing time, hours | Mn concentration in coprecipitate, at.% |
|---|---|---|
| 1.5 | 1 | 1.72 ± 0.03 |
| 1.5 | 2 | 1.72 ± 0.03 |
| 1.5 | 3 | 1.41 ± 0.03 |
| 1.8 | 1 | 1.56 ± 0.03 |
| 1.8 | 2 | 2.12 ± 0.04 |
| 1.8 | 3 | 2.69 ± 0.04 |
| 2.4 | 0 | 3.82 ± 0.04 |
| 2.4 | 1 | 3.68 ± 0.03 |
| 2.4 | 2 | 3.68 ± 0.03 |
| 2.4 | 3 | 3.55 ± 0.04 |

The dependence of the concentration of manganese in the final product on the $Ca^{2+}$: $F^-$ ratio in the mother liquor is shown in Table 3 [III].

**Table 3.** Dependence of co-precipitated Mn on the $Ca^{2+}$ to $F^-$ ratio*

| Concentration of $Mn^{2+}$ in the initial solution, at. | Ratio of $[Ca^{2+}]$:$[F^-]$ | Concentration of $Mn^{2+}$ in the co-precipitate, at.% |
|---|---|---|
| 0.262 | 1:2.5 | 2.32 |
| 0.262 | 1:2.2 | 1.59 |
| 0.262 | 1:1.9 | 1.07 |
| 0.262 | 1:1.7 | 0.49 |

* Solutions were added at a rate of 2.4 $cm^3$/min, ageing time was 3 hours

The excess of $F^-$ ions increases the amount of manganese in precipitate. In order to obtain a precipitate of $CaF_2$-$MnF_2$ in the form of fine microscopic crystals one should add the solutions into reaction vessel very slowly. The most suitable co-precipitation conditions are the following: $CaCl_2$ adding rate – 2.5 ml/min; HF – 2.8 ml/min, ageing time – 2 hours [III].

The total amount of manganese in the final product is limited by the solubility threshold of Mn in $CaF_2$. $Mn^{2+}$ is smaller than $Ca^{2+}$, and it causes lattice distortions and stress [60,65]. The concentration of manganese in thermoluminophor should be below the decomposition threshold, because re-using of TLD requires high stability. We checked the crystal lattice distortions and lattice constant changes with increase of $Mn^{2+}$ concentration using XRD analysis [III].

X-ray powder diffraction (XRPD) method was used for crystal phase analysis and cell parameter determination. XRPD data were collected using a

computer-controlled Bragg-Brentano θ-2θ powder diffractometer (equipped with a goniometer GUR-5 from diffractometer DRON-1). It has a 180 mm radius and works at 40 kV (20 mA) with CuKα (λ=1.5405981 Å) radiation collimated with Soller slits (aperture 2.5°) and a 1 mm divergence slit. Soller slits (aperture 1.5°) were also used in the diffracted beam. A 0.03 mm Ni filter, a 0.25 mm receiving slit and a scintillation detector were used in the step-scanning mode (5 s for each step of 0.02°2θ) in the angular range of 8–160°2θ. A software system AXES [80] was used to treat raw data (peak detection, fitting with pseudo-Voigt function and cell refinement). For cell refinement, an independent zero angle correction was made and applied to the diffraction angle. Rietveld analysis (computer program FULLPROF, by Rodriguez-Carvajal [81]) was used to determine the lattice stoichiometry.

X-ray diffraction analysis has not revealed separate phases of Mn-containing substances. However, the lattice constant decreases slightly but systematically by increasing the concentration of Mn ions [III]. The stoichiometry analysis has not revealed any changes in the occupancies of Ca and F atoms in the lattice, the only exception being the sample with the highest concentration of $Mn^{2+}$ (2.76 at%). The best fit between the observed and calculated diffraction pattern has been obtained for this sample with the occupancy of Ca equal to 0.88(±0.05) and the occupancy of F equal to 0.85(±0.05). This sample demonstrates also a TL peak of a lower intensity with the maximum situated at a lower temperature when compared with the sample with 2.39 at.% of Mn (to be described below). This indicates that the Mn concentration of 2.76 at.% lies close to the threshold of the solid solution decomposition [III].

The variation of crystal lattice constant with manganese concentration is shown in Fig. 2.

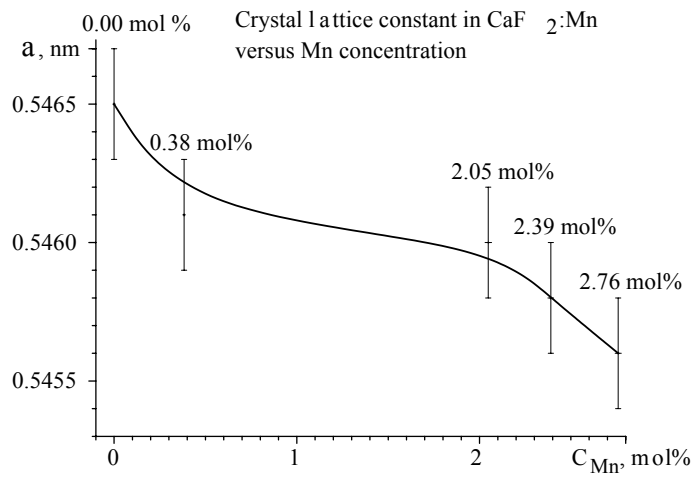


**Fig. 2.** Crystal lattice constant of $CaF_2$:Mn versus Mn concentration

## 2.2. $CaF_2$:Eu

The synthesis of $CaF_2$:Eu was performed using two different methods to introduce the activator into the host material:

1. Mechanical mixing of activator compound [$Eu_2(CO_3)_3$] with solid $CaF_2$ followed by high-temperature firing in atmosphere of high-purity nitrogen (99.999 %) during 45 minutes. Temperature of firing was varied from 1173 to 1373 K, and concentration of Eu – from 0.05 to 0.2 weight %. The final luminophors demonstrate typical blue emission of $Eu^{2+}$ under ultraviolet excitation [V].
2. Co-precipitation of the host material $CaF_2$ together with the activator compound. The co-precipitation was proceeded in the same specially designed apparatus as $CaF_2$:Mn. Dilute solutions of $CaCl_2$, $Eu_2(CO_3)_3$ and $NH_4F$ were simultaneously added at a regulated rate into reaction vessel using peristaltic pumps. The mother liquor was based on triply distilled water acidified with HCl. The reaction vessel was kept at elevated temperature by water vapours, and the incoming solutions were agitated with a fluoroplast-made stirring rod. The precipitate was aged in the mother liquor for two hours. The activator compound was added either into mother liquor only or both into the mother liquor and $CaCl_2$ solution before co-precipitating. The concentration of $Eu^{3+}$ in solutions was varied from 0.2 to 0.6 weight %. After ageing, the precipitate was decanted, washed, dried and pre-annealed at 673 K for two hours. The pre-annealed precipitate was placed into carbon-glass crucible and fired for 45 minutes at 1373 K in a quartz atmospheric tube under protective flow of high purity nitrogen. The final luminophors showed both $Eu^{2+}$ and $Eu^{3+}$ luminescence under ultraviolet excitation.

The actual concentration of Eu in phosphors synthesized by co-precipitation was found by inductively coupled plasma atomic emission spectroscopy using the installation described in the previous subsection. About 60–80 mg of sample was dissolved in 1 ml of concentrated $HNO_3$, and the volume was coupled to 100 ml. Reference solutions used were 0.1 μg/ml – 100 μg/ml and 1 μg/ml – 50 μg/ml. Emission line of Eu(II) = 381.967 nm was used for measurements. The details of this method are given in paper [82]. The description of all the prepared samples, including the concentrations determined by ICP-AES analysis, are shown in Table 4 [V].

**Table 4.** The list of samples $CaF_2$:Eu with actually determined Eu concentrations.

| № | Concentration of Eu in the initial solutions, at.% | Concentration of Eu determined by ICP-AES analysis, at.% | Concentration of Eu added by mixing, at.% | Annealing temperature K |
|---|---|---|---|---|
| 1 | 0.1028 in the mother liquor and 0.1028 in $CaCl_2$ | 1.467 | —— | 1373 |
| 2 | 0.1028 in the mother liquor | 1.493 | —— | 1373 |
| 3 | 0.2056 in the mother liquor and 0.2056 in $CaCl_2$ | 2.727 | —— | 1373 |
| 4 | 0.2056 in the mother liquor | 1.639 | —— | 1373 |
| 5 | 0.3084 in the mother liquor and 0.3084 in $CaCl_2$ | 4.351 | —— | 1373 |
| 6 | 0.3084 in the mother liquor | 2.137 | —— | 1373 |
| 7 | Mechanical mixing of $Eu_2(CO_3)_3$ with solid $CaF_2$ | —— | 0.0257 | 1373 |
| 8 | Mechanical mixing of $Eu_2(CO_3)_3$ with solid $CaF_2$ | —— | 0.0514 | 1373 |
| 9 | Mechanical mixing of $Eu_2(CO_3)_3$ with solid $CaF_2$ | —— | 0.1028 | 1173 |
| 10 | Mechanical mixing of $Eu_2(CO_3)_3$ with solid $CaF_2$ | —— | 0.1028 | 1373 |

# 3. THE EFFECT OF IMPURITY CLUSTERING ON THE LUMINESCENCE, THERMOLUMINESCENCE AND MAGNETIC PROPERTIES OF $CaF_2$-BASED LUMINOPHORS

## 3.1. $CaF_2$:Mn

The TL curve appearance in $CaF_2$:Mn depends on the manganese concentration and distribution. The TL curves were measured with a semiautomatic TLD reader based on thermocontroller OMRON E5CK and a photomultiplier with current to frequency converter. The pulses were counted by microprocessor and transferred to computer by data acquisition system. The measurements were carried out at a constant heating rate (0,5 K/s). The TL materials were irradiated with a $^{60}$Co γ-radiation source (doses 100, 200 and 400 Gy) to study the radiation effects and other manifestations of stored dose information. The reference dose irradiator 6527B (Sweden) equipped with $^{90}$Sr/$^{90}$Y $\beta$-radiation source was used to produce lower irradiation doses (0.1–1.0 Gy).

The TL curves for different manganese concentrations [I,III] are shown in Fig. 3.

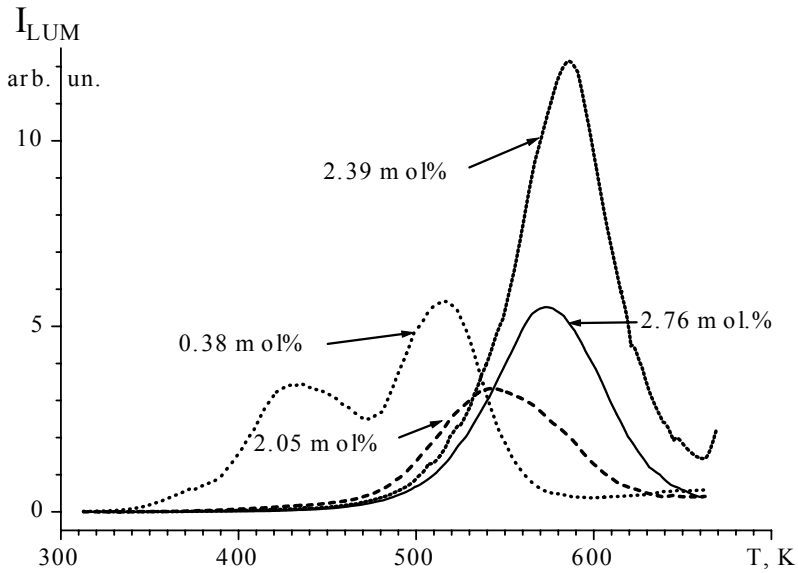


**Fig. 3.** TL curves after 0.25 Gy irradiation for different concentrations of Mn in $CaF_2$.

The TL curve is composed of several peaks overlapping each other if the manganese concentration is low. At higher Mn concentrations, a single strong TL peak appears near 590–600 K. Fractional annealing shows, however, that the TL peak is not elementary and still consists of several close overlapping peaks. Nevertheless, the distribution of the activation energies of the traps becomes narrower at higher concentrations of Mn. This fact assumes probably that the disorder caused by Mn impurity in $CaF_2$ lattice turns into some ordered clusters when the concentration of Mn increases. This could be a preliminary stage of manganese falling out of a solid solution [III]. The EPR spectra of $Mn^{2+}$ were studied with X-band EPR spectrometers (8,87 GHz with 100 KHz magnetic field modulation and 9,1 GHz with a 975 KHz magnetic field modulation). EPR studies show that $Mn^{2+}$ lines become broader with the Mn concentration increase. The mechanism of broadening EPR lines is connected not only with the exchange interactions in clusters but also with increased super hyperfine interaction of the $Mn^{2+}$ $3d^5$ electrons with the nuclei of surrounding $F^-$ ions. The super hyperfine structure (SHFS) caused by eight closest $^{19}F$ nuclei can be only resolved in single crystals. In our powder samples, only the hyperfine structure from $^{55}Mn$ is observed. However, due to the displacement of $Mn^{2+}$ and $F^-$ ions at increasing Mn concentration, the average distance between $Mn^{2+}$ and $F^-$ decreases and the interaction with $^{19}F$ nuclei becomes stronger causing the extra broadening of the averaged EPR lines. The broadening of the EPR lines of $Mn^{2+}$ is illustrated in Fig. 4.

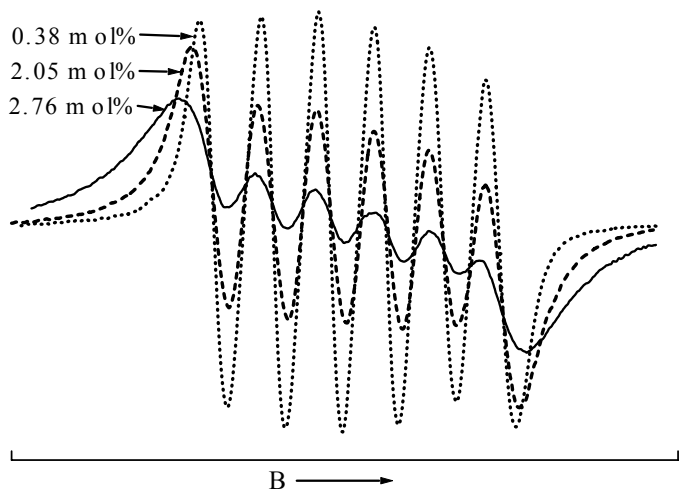


**Fig. 4**. EPR spectra of $Mn^{2+}$ for different concentrations of Mn in $CaF_2$.

The clustering of $Mn^{2+}$ is as well observed in our samples through the deviations of magnetic susceptibility from Curie-Weiss law about temperatures of 30–50 K [IV].

We have studied also the EPR spectra of the samples irradiated with different doses, from 0.25 to 400 Gy. Radiation has been proved to produce no effect on the amount of $Mn^{2+}$ in $CaF_2$:Mn. This means that energy storage can not be explained by charge transformations of $Mn^{2+}$. The absence of non-linear quenching effects of known quenching impurities (Co, Ni, Fe) as well as the absence of charge transformations of $Mn^{2+}$ makes the usual electron-hole recombination models for the energy storage and transfer untenable [III]. Hence, the process of energy storage should be explained with some intracentre mechanism. One more experimental fact is very helpful in understanding this mechanism. The observed deviations of magnetic susceptibility from Curie-Weiss law decrease and disappear after the samples are irradiated with doses about 250–500 Gy [IV]. The dependence of magnetic susceptibility on temperature was measured using quantum (SQUID) magnetometer equipped with superconductive magnet and superconductive screen (device is assembled and operating at Physics chair of D. Mendeleev University of Chemical Technology of Russia). The thermal insulation of sample from liquid He environment makes the measurements possible in a wide range of temperatures (2–350 K). The changes of magnetic susceptibility behaviour due to the stored radiation dose [IV] are shown in Fig. 5.

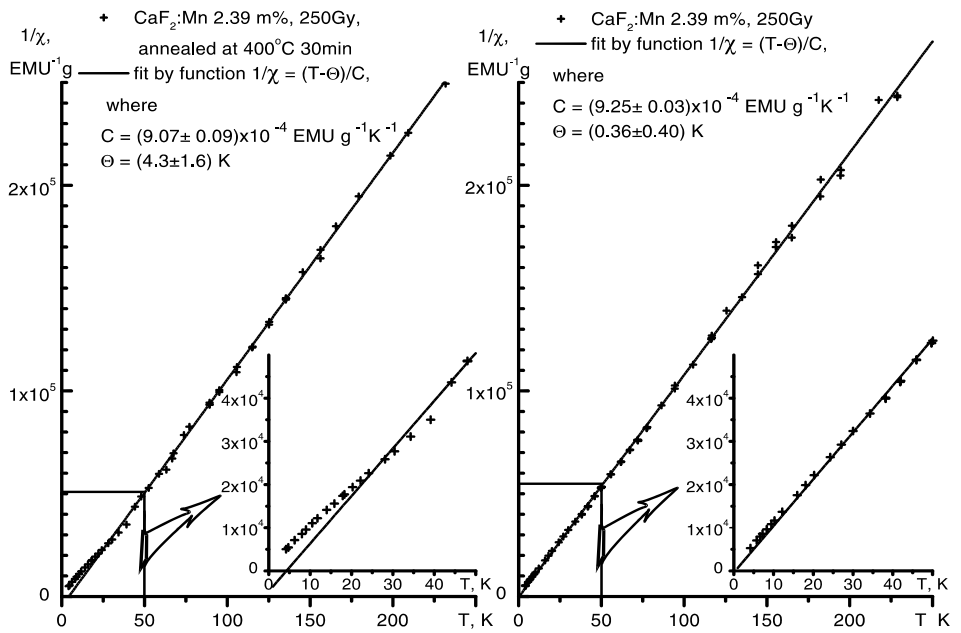


**Fig. 5**. Inverse magnetic susceptibility versus temperature. Deviations from Curie-Weiss law are observable at low temperatures when sample is annealed after irradiation, while there are practically no deviations in the sample irradiated with a dose of 250 Gy.

As we have seen from the EPR spectra (Fig. 4) [III], the electronic configuration of $Mn^{2+}$ becomes more and more overlapped with surrounding fluoride ions by increasing concentration of manganese. Hence, fluoride ions can transfer the exchange interaction between $Mn^{2+}$ ions. This interaction yields to the observed deviations of magnetic susceptibility from Curie-Weiss law. The stored radiation dose removes or decreases the exchange interactions due to the removal of one or more fluorines from the surrounding of the $Mn^{2+}$. Radiation damage is, however, reversible: the removed fluorine returns to its' normal place after annealing, and this process is accompanied with the thermoluminescence. $Mn^{2+}$- $F^{-}$ distances are smaller than $Ca^{2+}$- $F^{-}$ ones. Hence, the $Mn^{2+}$ substitution for $Ca^{2+}$ causes stress and distortions in the $CaF_2$ lattice. The larger is Mn concentration, the larger clusters of manganese are formed in $CaF_2$, and the stronger are local lattice distortions and stress. The removal of fluorine from the vicinity of $Mn^{2+}$ ions causes partial relaxation of lattice stress. The mechanism of relaxation is based on the redistribution of electron density from anion vacancy among the neighbouring $Mn^{2+}$ ions. As a result, a new mixed electronic configuration is formed in the Mn cluster. The more $Mn^{2+}$ ions are involved, the more stable configuration appears. $Mn^{2+}$ is distributed in $CaF_2$ non-uniformly. It is clustered into certain configurations, depending on the solid solution proportions. Transition from one cluster configuration to another is accompanied with very abrupt changes in TL curve structure, while accretion of same-type clusters causes only smooth changes in existing trapping energies. This mechanism explains the glow curve transformations [I,III] with increase of Mn concentration. At low Mn concentration, both electronic and hole processes can take place. When concentration of Mn is already close to the decomposition threshold of the solid solution, the electron from anion vacancy gives a very stable configuration with surrounding $Mn^{2+}$ ions, and the only possible recombination mechanism proceeds through the return of removed fluorine, effectively carrying hole. The fluorine returns to its' own place through intermediate hops, and also, there could be some distribution of Mn clusters in size. These are the basic reasons for the TL peak to be non-elementary and show transformations at intermediate annealing [III]. What concerns the detailed mechanism of energy storage, it could go through simultaneous F-centre (anion vacancy) and $V_K$ centre formation inside the $Mn^{2+}$ cluster [III]. This process is most probably connected with excitons produced or stopped near $Mn^{2+}$ clusters [IV]. The most essential point is the relaxation of lattice stress through configurational transformation. This transformation should be fast enough to occur at the time of exciton decay, preventing from immediate energy transformation into the luminescence or heat (quenching). Then, the $V_K$ centre should be further transformed into some defect which is yet more stable, for example, two of interstitial fluorines could combine together into interstitial neutral molecule. The next interesting point concerns the return of fluorine back – the configuration produced at the moment of return should be capable of energy transfer to $Mn^{2+}$. As we can see, this should be true for $CaF_2$:Mn with a high Mn

concentration. Thermoluminophors with actual concentration of manganese about 2.4 at.% are shown to be most suitable for TLD production. However, the single TL peak suitable for dosimetry is situated at very high temperature. The position of TL maximum at about 600 K means that the TLD should be annealed at still higher temperature before re-using in order to clean up the previous dose information. However, high-temperature annealing can cause either oxidation of $Mn^{2+}$ to higher charge states or decomposition of solid solution, thus making TLD unsuitable for repeated using.

Optically stimulated luminescence (OSL) readout [II] can solve the problem, giving the possibility to employ TLD with as high as possible concentration of Mn yet being below the decomposition threshold of solid solution.

OSL has some advantages for indicating absorbed dose compared with TL. The repeated readout of the information is the most important one. Most conventional TL and OSL dosimeters have relatively low luminescence yield under stimulation. This means that the measuring technique based on simultaneous stimulation and registration of output light has limited possibilities because the spectral separation of luminescence and stimulating light cannot be very effective. Thus, only the quanta of lower energies than luminescence output are commonly used for stimulation. The complete stimulation spectrum can be measured using time-resolution instead of spectral separation. The intensity of optically stimulated afterglow (OSA) versus time is measured after a certain delay following the stimulating pulse of light [II]. This method is also applicable for luminescence centres with forbidden transitions using the longer delays, because the stimulating light can cause the direct excitation of luminescence centres. This is the case for $Mn^{2+}$ in $CaF_2$. The OSA measurements for $Mn^{2+}$ in TLD $CaF_2$:Mn required the delay time of 150 ms. Measurements have been carried out at room temperature. The OSA stimulation spectra have been corrected with regard to the light intensity spectral distribution of the excitation radiation source (Xe lamp + SPM monochromator). The integrated emission value is acquired by PMT with a quartz window. Irradiation dose was given with X-rays. The heating rate was about 1 K/s when glow curves and thermo-optical bleaching (TOB) were measured. TOB is measured using intermittent heating. The OSA stimulation spectrum for $CaF_2$:Mn is shown in Fig. 6.

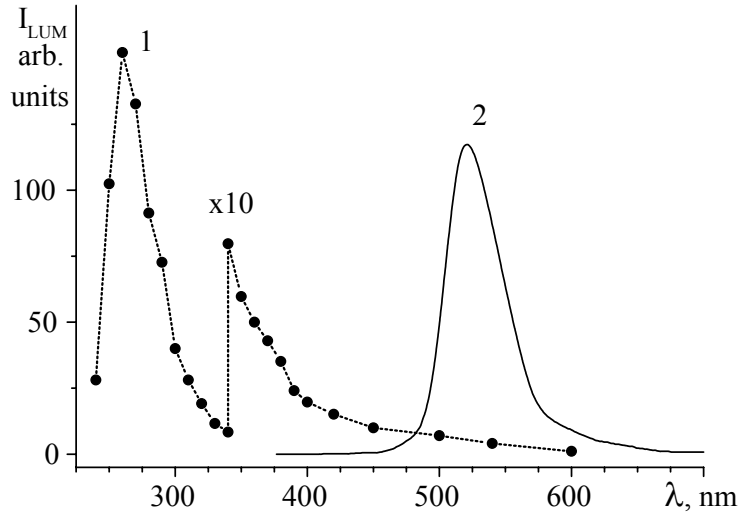


**Fig. 6.** The OSA stimulation spectrum (curve 1) and X-ray excited luminescence (curve 2) of $CaF_2$:Mn. The delay time is 150 ms.

## 3.2. $CaF_2$:Eu

The luminescence of $CaF_2$:Eu was studied using luminescence spectrophotometer Hitachi 650–60. It consists of two similar monochromators (200–850 nm scan, 1.5 nm resolution). The installation is equipped with a 150 W Xe-arc lamp. The data acquisition system transferred data to computer, data discretization was better than 12 bit. The spectra were measured at room temperature. Intra-centre excitation was used, 350 nm for $Eu^{2+}$ and 392 nm for $Eu^{3+}$. The luminescence spectra with a better resolution were measured with MDR-6 monochromator (LOMO) equipped with PMT FEU-100. The samples were excited with a direct-current high-pressure Hg-arc lamp SVD-305–3. The ultraviolet Hg emission line at 365 nm was selected with filter UFS-6. To decrease the scattered exciting light, ZhS-18 filter was put in front of the entrance slit of the monochromator. The used setup provided spectral resolution of about 0.7 nm.

The luminescence of the samples prepared by mechanical mixing (see previous Chapter) shows the only band of $Eu^{2+}$ which have the excitation maximum at 350 nm. The luminescence band maximum is shifted slightly but steadily with the increase of Eu concentration towards the longer wavelengths, from 423 to 427.5 nm (a shift of about 0.03 eV). The $Eu^{2+}$ luminescence intensity increases with the increase of Eu concentration. What concerns the samples obtained by co-precipitation, they demonstrate quite another behaviour of $Eu^{2+}$ luminescence [V]. The $Eu^{2+}$ luminescence intensity decreases with the

increase of the total europium amount, and the decrease is most pronounced for the samples where europium was added both to $CaCl_2$ solution and to the mother liquor, despite of the total added amount of europium being twice greater. The $Eu^{2+}$ luminescence band maximum is shifted only slightly with the Eu concentration increase being located at about 425–426 nm. The scene is changed when luminescence is excited near 392 nm. All the samples prepared by co-precipitation method demonstrate the line spectrum of $Eu^{3+}$ at this excitation, and the broad band of $Eu^{2+}$ is also observable. This is useful to observe the simultaneous $Eu^{2+}$ portion decrease and $Eu^{3+}$ portion increase with the increase of total Eu amount in the luminophor. $Eu^{3+}$ is produced most effectively when the dopant is added both into $CaCl_2$ solution and into the mother liquor. The luminescence spectra for samples №№1–5 are shown in Fig. 7.

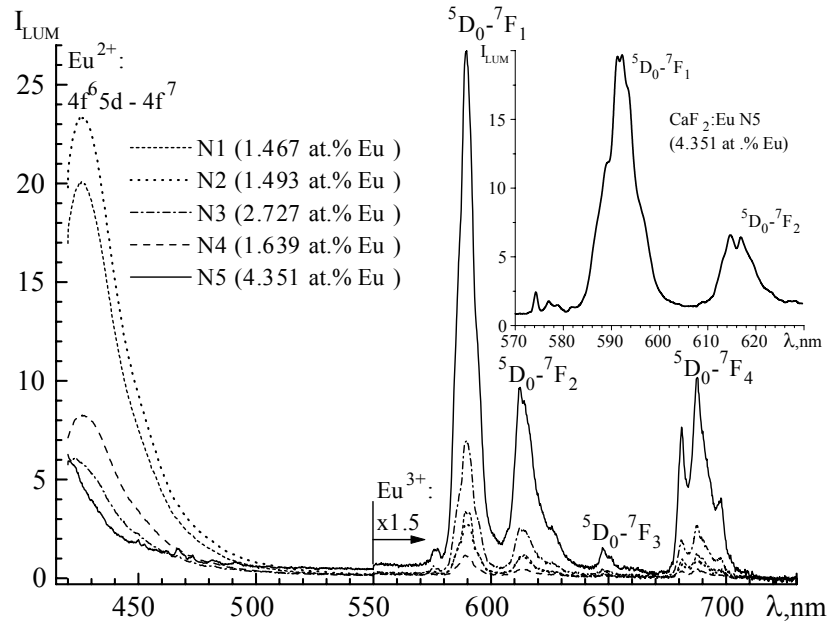


**Fig. 7.** The luminescence spectra of $CaF_2$:Eu №№1–5. Excitation wavelength 392 nm, T=300 K. The spectral part above 550 nm is multiplied by a factor of 1.5. The insertion shows the luminescence of the sample №5 recorded at 300 K with better resolution (0.7 nm).

The sample №10 also demonstrated a very weak line spectrum of $Eu^{3+}$, not shown, however, in this figure. The presence of $Eu^{3+}$ luminescence in one of the samples prepared by mechanical mixing, namely, in the sample with a maximal Eu concentration among the other mechanically mixed samples, shows a tendency for Eu to become $Eu^{3+}$ by the increase of total concentration. However, the synthesis conditions also influence the $Eu^{3+}$ to $Eu^{2+}$ ratio in $CaF_2$:Eu.

The forbidden transitions of rare earth triple charged ions are very sensitive to the site symmetry. Thus, the structure of emission and excitation spectra of $Eu^{3+}$ helps to understand the structure and symmetry of luminescence centres. The $Eu^{3+}$ ion is most sensitive to the presence or absence of inversion symmetry at the site. The most common approach was formulated by G. Blasse [83]: when the inversion symmetry is present, the magnetic-quadrupole transition $^5D_0 - {}^7F_1$ prevails, giving a group of lines around 590 nm; when the inversion symmetry is absent, the electric-dipole transitions $^5D_0 - {}^7F_J$ with J=2,4,6, are dominating, giving groups of lines in the red and infrared region. The first of dipole transitions, $^5D_0 - {}^7F_2$, is hypersensitive to the site symmetry and will prevail absolutely when the deviation from the inversion symmetry is very small.

One can conclude from the first glance that the centres with inversion symmetry are prevailing, while the centres with deviations from inversion symmetry are present too, and these deviations are quite essential, because the transitions $^5D_0 - {}^7F_2$ and $^5D_0 - {}^7F_4$ show almost the same intensity. The ratio of the intensities of red and infrared electric dipole transitions to the intensity of the magnetic-quadrupole transition are given in Table 5.

**Table 5.** The ratio of the $Eu^{3+}$ spectral line intensities representing different radiative transitions. The samples were prepared by a co-precipitation method.

| | samples | | | | |
|---|---|---|---|---|---|
| transitions: | Nr5 | Nr4 | Nr3 | Nr2 | Nr1 |
| $^5D_0 - {}^7F_1$ | 1.00 | 1.00 | 1.00 | 1.00 | 1.00 |
| $^5D_0 - {}^7F_2$ | 0.34 | 0.42 | 0.35 | 0.37 | 0.36 |
| $^5D_0 - {}^7F_4$ | 0.38 | 0.42 | 0.38 | 0.35 | 0.36 |

Only the sample №4 falls slightly out of set of the spectral line ratios. The deviation can be explained, however, by the weakness of the luminescence and uncertainty caused by a background subtraction.

The structure of various $Eu^{3+}$ luminescence centres and the mechanisms of their formation were thoroughly studied by laser spectroscopy and subsequent annealings [8,9,79]. The model of luminescence centres could be suggested on the basis of comparison of our spectra with the data given in papers [8,9]. We can say that there should be the centres of R and Q type, namely, dimers, trimers, or probably more complex $Eu^{3+}$ clusters [V]. The insufficient resolution of the luminescence spectra given in Fig. 7 makes it reasonable both to check the excitation spectra and to measure the luminescence with a better resolution (see the insertion in Fig. 7). The excitation spectrum for the sample №5 (having the maximal $Eu^{3+}$ content) is shown in Fig. 8. The luminescence was registered

for the transition $^5D_0 - {}^7F_1$ near 590 nm. The spectral region shown in Fig. 8 demonstrates three groups of excitation lines characteristic only of clusters containing two, three or more of $Eu^{3+}$ ions with proper charge compensators (interstitial $F^-$) [8,9,79]. The luminescence spectrum of the same sample taken with a better resolution is shown in the insertion of Fig. 7. The $Eu^{3+}$ lines are not resolved as nicely as one could expect, however, the reason of this could be revealed: the lines are inhomogeniously broadened by some natural reason. Also, the structure of spectrum is more complicated than one could expect from the simple superposition of luminescence of dimers (R) and trimers (Q). The inhomogenious broadening and complex structure of spectrum allows one to suppose that $Eu^{3+}$ is not uniformly dissolved in $CaF_2$ producing large clusters containing large amount of $Eu^{3+}$ ions.

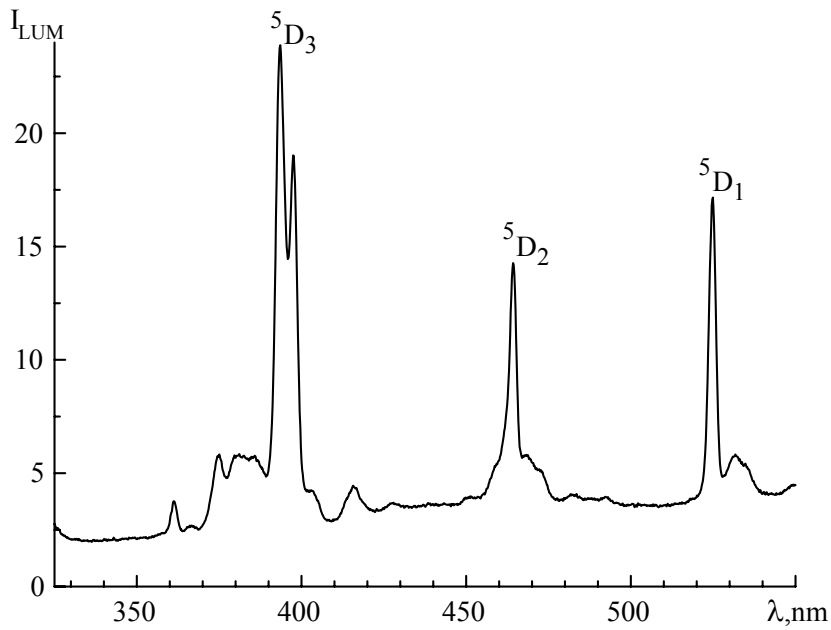


**Fig. 8.** The excitation spectrum of the sample №5 for the transition $^5D_0 - {}^7F_1$ (luminescence in the vicinity of 590 nm) measured at T=300 K

It is possible that the structure of these clusters is close to the structure of a calcium-europium fluoride single crystal $Ca_{0.65}Eu_{0.35}F_{2.35}$ which was grown recently [11]. The luminescence spectra of both our samples and $Ca_{0.65}Eu_{0.35}F_{2.35}$ single crystal are quite similar.

The non-uniformity of the $CaF_2$:Eu solid solution strongly affects its' magnetic properties. The Curie-Weiss law is valid only in the range of temperatures 4–70 K, while there are strong deviations at temperatures above 100 K [V].

There is a magnetic transition about 170 K where the effective Curie constant decreases by several times (Fig. 9).

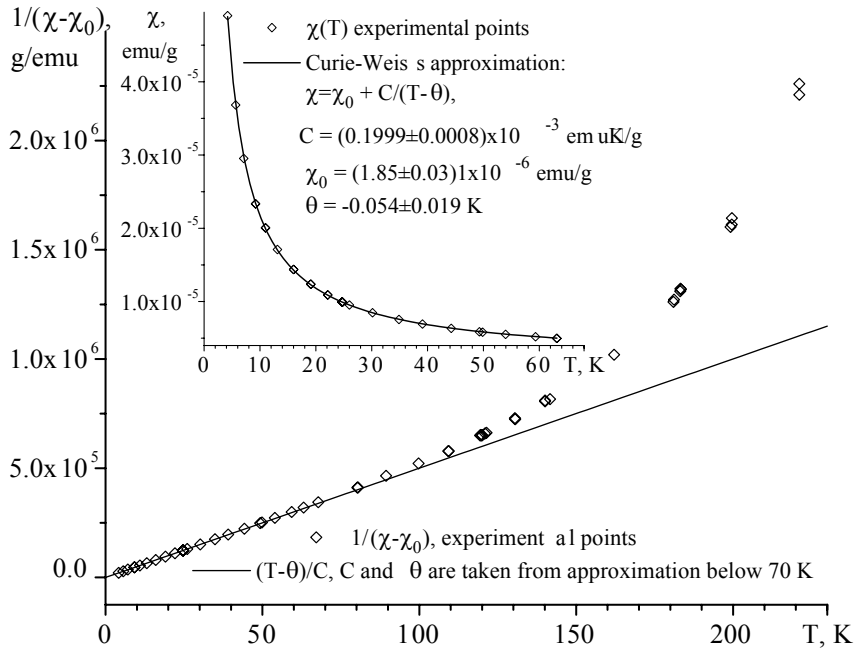


**Fig. 9.** The inverse magnetic susceptibility versus temperature for the sample №3. The insertion shows a low-temperature region where the Curie-Weiss law is valid.

One could suppose that there is a strong exchange interaction between $Eu^{2+}$ ions at low temperatures. A very large paramagnetic Curie temperature Θ (about 150 K or still larger) indicates that there should be very big Eu clusters where $Eu^{2+}$ ions are ordered. The strong exchange interaction could affect the luminescence band position. Actually, there could be two reasons for the observed $Eu^{2+}$ luminescence band shift: changes in the crystal lattice constant and lattice field, and also exchange interactions capable of direct displacement of the ground level of $Eu^{2+}$. To decide which reason is more essential, one needs to study the temperature dependences of luminescence in $CaF_2$:Eu with anomalous magnetic properties. It is interesting to note that the deviations from Curie-Weiss law and also the exchange interactions are stronger in samples with the higher $Eu^{3+}$ concentration. This fact supports the idea of how the large ordered $Eu^{2+}$ clusters are formed.

The co-precipitated precursor contains only $Eu^{3+}$ and demonstrates only orange $Eu^{3+}$ line at 580 nm.

After high-temperature annealing, some part of $Eu^{3+}$ is reduced to $Eu^{2+}$. The matter is that $Eu^{3+}$ extra positive charge is compensated by the interstitial flouride anion. Most of $Eu^{3+}$ pairs and more complex centres contain an extra interstitial fluoride, one per each $Eu^{3+}$ complex. So, there is a mechanism of extra flourine scavenging with the simultaneous increasing of cluster complexity and number of involved $Eu^{3+}$ ions [9,79]. When the extra fluorine goes out of balance, $Eu^{3+}$ is easily reduced to $Eu^{2+}$. The ionic radius of Eu increases, and its' motion away from cluster becomes difficult. So, $Eu^{2+}$ remains in the ordered cluster where it can be involved into a strong exchange interaction. This is the way large ordered magnetic clusters formation in $CaF_2$:Eu. The excess of fluorine, however, may act quite differently. Only a small excess acts as an oxidizer, while the large excess reduces Eu. An analogous effect of halogens was observed in CaS:Eu [84]. This usefull feature allows to control the charge state of Eu in $CaF_2$.

EPR of $Eu^{2+}$ in $CaF_2$ was studied both for single crystals and powder samples, however, different researchers give very different results on g-tensor and show different spectra [13,14]. The differences are mostly caused by the very strong exchange interaction distorting EPR spectrum of $Eu^{2+}$. When the concentration of Eu is about 0.1 at.%, there are no single $Eu^{2+}$ ions even in the samples prepared by mechanical mixing. When $Eu^{2+}$ appears as the result of reduction of $Eu^{3+}$, the situation becomes still more complex, because of the powerfull self-ordering mechanism of $Eu^{3+}$.

Let us compare the EPR spectra of samples №10 and №3 shown in Fig. 10.

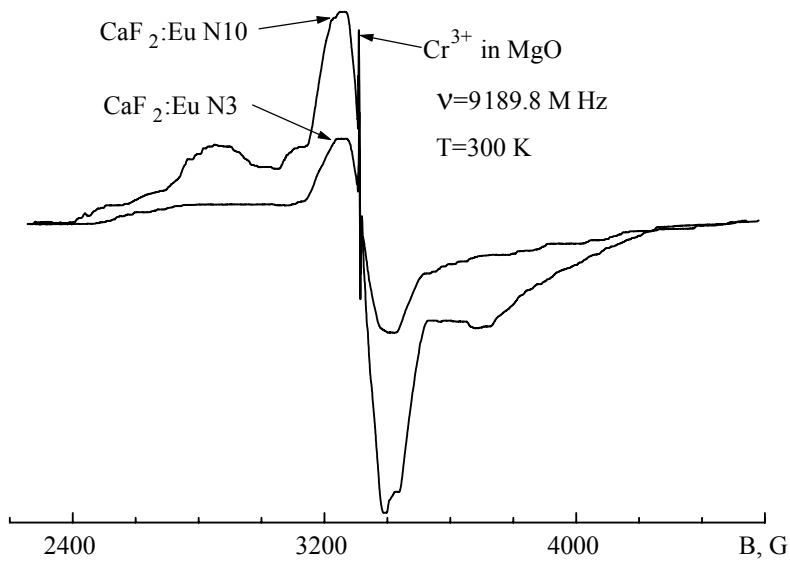


**Fig. 10.** EPR spectra of $CaF_2$:Eu №10 and №3 measured at 300 K. The signal of $Cr^{3+}$ in MgO single crystal was used for magnetic field calibration.

First, the spectra are spread over the very wide range of magnetic fields. What concerns the structure, some residual smoothed structure still persists in the spectrum of sample №10. The EPR spectrum of sample №3 is much smoother and does not show any structure. The deviations of magnetic susceptibility from Curie-Weiss law are also stronger in case of the sample №3 obtained by co-precipitation method. The $Eu^{3+}$ is prevailing in this sample, and this is $Eu^{3+}$ which provokes the ordered clustering and provides after reduction the $Eu^{2+}$ involved into strong exchange interactions.

# SUMMARY

1. Our experimental research succeeded in developing very stable against oxidation of Mn thermoluminophor $CaF_2$:Mn working in air without essential changes of its' properties up to a hundred of exposure-readout cycles. The new stable thermoluminescent material has a single TL peak and a lower detection threshold compared with that of previously known TLD based on $CaF_2$:Mn. This material is foreseen for detection of high (extreme) doses in radiation accidents due to an extraordinary wide range of linearity of dose response (up to $4x10^3$ Gy).
2. Manganese ions are non-uniformly distributed in $CaF_2$ lattice, however, this is an essential point for TLD material. TL curve structure and main dosimetry peak position is shown to depend on Mn concentration. The TL peak is shifted towards higher temperatures and becomes narrower at higher Mn concentrations when the clusters containing several Mn ions are created. The most suitable TL properties are obtained with Mn concentrations being close to the decomposition threshold of the solid solution, about 2.3–2.4 at.%. The developed co-precipitation procedure provides the reproducible synthesis of TLD material with required properties.
3. The thermoluminescence mechanism in $CaF_2$:Mn thermoluminophor is connected with the partial relaxation of lattice stress induced by smaller $Mn^{2+}$ ion substituting $Ca^{2+}$ in regular sites. Radiation dose storage produces interstitial fluorine. The remained in anion vacancy electron is redistributed among Mn ions and turns into a new stable covalent electronic configuration. When fluorine returns to own place by annealing, the TL takes place. The higher is Mn concentration, the more stressed is lattice, and the deeper relaxation occurs at dose storage yielding a shift of TL peak towards higher temperatures.
4. $CaF_2$:Eu luminophors can be synthesized both by through mechanical mixing of $CaF_2$ with a dopant and through the co-precipitation procedure. Mechanical mixing gives more $Eu^{2+}$ versus $Eu^{3+}$, while co-precipitation method increases the portion of $Eu^{3+}$. However, there is a general tendency of Eu transformation into $Eu^{3+}$ at increasing total concentration of Eu, regardless the synthesis method. $Eu^{3+}$ portion becomes prevailing when Eu is introduced at co-precipitation both into $CaCl_2$ solution and into mother liquor. Fine control of $Eu^{3+}/Eu^{2+}$ ratio can be performed through the exact balance of fluorine excess, because the interstitial fluoride compensates $Eu^{3+}$ extra positive charge in oxygen-free $CaF_2$:Eu.
5. The luminescence of $Eu^{2+}$ is slightly shifted towards a longer wavelength at increasing Eu amount. The luminescence of $Eu^{3+}$ demonstrates essential clustering of $Eu^{3+}$ according to the known mechanism of fluorine excess scavenging (fluorine balance in large clusters is better). The clusters of $Eu^{3+}$ could be large enough to speak about formation of mixed calcium-europium fluoride inclusions. The luminescence spectra of our samples are very

similar to those in recently grown single crystals $Ca_{0.65}Eu_{0.35}F_{2.35}$ [11]. This fact encourages to propose the new scintillating material based on sintered $CaF_2$:Eu ceramics which is essentially more cost-effective.

6. The changes in fluorine balance at the final annealing cause some part of $Eu^{3+}$ to be transformed into $Eu^{2+}$, however, it remains included in large ordered clusters. This causes $Eu^{2+}$ to be involved in very strong exchange interaction yielding to anomalous magnetic behaviour of $CaF_2$:Eu solid solutions.

# SUMMARY IN ESTONIAN

## Aktivaatorite laenguolek ja korrapärastatud klastrite moodustumine $CaF_2$:Mn ja $CaF_2$:Eu luminofoorides

1. Käesoleva töö raames töötati välja sünteesi metoodika, mis garanteeris oksüdatsioonile vastupidava termoluminofoori $CaF_2$:Mn saamise. Termoluminofoori omadused ei muutu praktilisel kasutamisel isegi saja tsükli korral. Termoluminofoori $CaF_2$:Mn termovälja kiirguskõveral esineb vaid üks kõrgetemperatuurne maksimum ja tal on madalam detekteerimise lävi kui varem tuntul. $CaF_2$:Mn termoluminofoor on sobiv kõrgete dooside mõõtmiseks tänu kiirgusdoosi lineaarsele vastusele laias doosi piirkonnas (kuni $4x10^3$ Gy).
2. Mangaani ioonid jaotuvad $CaF_2$ kristallvõres ebaühtlaselt, mis on väga oluline TLD materjalide puhul. TL kõvera struktuur ja dosimeetrilise maksimumi positsioon sõltub Mn kontsentratsioonist. Mangaani kontsentratsiooni tõustes nihkub maksimum kõrgemate temperatuuride poole, muutudes kitsamaks Mn suuremate klastrite moodustumise tõttu. Kõige sobivamad omadused on proovidel, kus Mn kontsentratsioon on minimaalselt väiksem Mn konsentratsioonist, mille juures tahke lahus laguneb (2.3–2.4 at.%). Väljatöötatud kaasasadestamismeetod võimaldab sünteesida nõutavate omadustega TLD materjale. Meetod on hästi reprodutseeritav.
3. $CaF_2$:Mn termoluminofoori TL mehhanism on seotud võre pinge osalise relaksatsiooniga. Võre pinget põhjustab $Ca^{2+}$ iooni asendumine väiksema ioonraadiusega $Mn^{2+}$ iooniga. Radioaktiivse kiirguse toimel nihkub fluori ioon võrevahelisele positsioonile. Anioonvakantsile jäänud elektron jaotub mitme $Mn^{2+}$ iooni vahel, tekitades uue stabiilse kovalentse elektroonilise konfiguratsiooni. Kuumutamisel pöördub fluor tagasi oma kohale, millega kaasneb termoluminestsents. Mida suurem on Mn kontsentratsioon, seda rohkem pingestunud on kristallvõre ja seda suurem on ka relaksatsioon doosi salvestamisel, mistõttu nihkub TL maksimum kõrgemate temperatuuride poole.
4. $CaF_2$:Eu luminofoore võib sünteesida kas aktivaatori mehhaanilisel segamisel põhiainega või aktivaatori kaasasadestamisel põhiainega. Mehhaanilisel segamisel läheb euroopium kristallvõresse peamiselt $Eu^{2+}$-na, kaasasadestamisel aga suureneb $Eu^{3+}$ hulk kristallvõres. Siiski ilmneb tendents, et euroopiumi üldise kontsentratsiooni tõustes suureneb ka $Eu^{3+}$ hulk kristallvõres, olenemata sünteesi meetodist. $Eu^{3+}$ hulk on ülekaalus, kui kaasasadestamisel viia euroopiumi ühend nii $CaCl_2$- kui emalahusesse. $Eu^{3+}/Eu^{2+}$ suhet saab suunata fluori liia täpse doseerimisega, kuna võrevaheline fluoriidioon kompenseerib $Eu^{3+}$ üleliigse positiivse laengu hapnikuvabades $CaF_2$:Eu proovides.

5. $Eu^{2+}$ sisalduse suurenemisel on tema luminestsents vähesel määral nihutatud pikemate lainepikkuste poole. $Eu^{3+}$ luminestsents näitab, et $Eu^{3+}$ ioonid moodustavad suuri klastreid vastavalt fluori liia eemaldamise tuntud mehhanismile (suurematel klastritel on parem fluori bilanss). $Eu^{3+}$ klastrid võivad olla nii suured, et $CaF_2$ kristallvõres moodustub juba uus aine (kaltsium-europiumfluoriid). Meie poolt sünteesitud proovide luminestsentsspektrid on väga sarnased hiljuti kasvatatud monokristallide $Ca_{0.65}Eu_{0.35}F_{2.35}$ spektritega [11]. See tähendab, et kuumpressimisega on võimalik valmistada $CaF_2$:Eu keraamika, mis on oluliselt odavam.
6. Fluori tasakaalu muutused algsegu kuumutamisel põhjustavad $Eu^{3+}$ osalise taandumise $Eu^{2+}$-ks, siiski viimase jäädes suurte korrapärastatud klastrite koostisse. See tingib $Eu^{2+}$ ioonide tugeva vahetusinteraktsiooni, mis omakorda põhjustab $CaF_2$:Eu tahke lahuse anomaalse magneetilise käitumise.

# REFERENCES


1. Zarate-Morales, A.; Buentil, A.E. *Health Physics*, **1996** ,71(3), 358–361.
2. Fehl, D.L.; Muron, D.I.; Suijka, B.R.; Vehar, D.W.; Lorence, L.I.; Westfall, R.L.; Jones, S.C.; Sweet, I.A. *Review of Scientific Instruments*, **1994**, 65(10), 3243–3251.
3. Nicolae, M.; Lazar, E. *Revue Roumine de Physique*, **1985**, 30(3), 207–214.
4. Kalchgruber, R.; Göksu, H.J.; Hochnauser, E.; Wagner, G.A. *Radiat. Meas.*, **2002**, 35, 585–590.
5. Schulman, J.R.; Ginther, R.J.; Kirk, R.D.; Goulart, H.S. *Nucleonics*, **1960**, 18, 92–102.
6. Kisliuk, P.; Tippins, H.H.; Moore, C.A.; Pollack, S.A. *Phys.Rev.*, **1968,** 171(2), 336–342.
7. Nikiforov, A.E.; Zaharov, A.Y.; Chernyshov, M.Y.; Ugrymov, M.Y.; Kotomanov, S.V. *Fizika tverdovo tela*, **2003,** 45(5), 822–825 (in Russian).
8. Hamers, R.J.; Wietfeldt, J.R.; Wright, J.C. *J. Chem. Phys.*, **1982,** 77(2), 683–692.
9. Cirillo-Penn, Kathleen M.; Wright, J.C. *Phys.Rev.B*, **1990**, 41(15), 10799–10807.
10. Kaiser,W.; Garrett, C.G.B. *Phys. Rev. Lett.*, **1961**, 7, 229–231.
11. Shimamura, K.; Shiran, N.; Gektin, A.; Voronova, V.; Nesterkina, V.; Ichinose, N.; Villora, E.; Shshido, T. *Functional materials*, **2004**, 11(4), 676–679.
12. Dhopte, S.M.; Muthal, P.M.; Kondawar, V.K.; Moharil, S.V. *J. Lumin.*, **1992**, 54, 95–101.
13. Baker, J.M.; Bleaney, B.; Hayes, W. *Proc. of the Royal Soc. of London*, **1958,** 247A, 141–151.
14. Upadeo, S.V.; Gundurao, T.K.; Muharil, S.V. *J. Phys.: Condens. Matter*, **1994,** 6, 9459–9468.
15. Schmid, W.E.; Mooney, R.W. *J. Electrochem. Soc.*, **1963**, 110, 340–345.
16. Ginther, B.J. *J. Electrochem. Soc.*, **1954**, 10, 248–257.
17. Frank, M.; Herforth, J. *Kernenergie*, **1962**, 5, 173–176.
18. Smith, A.L. *J. Electrochem. Soc.*, **1954**, 101,189–194.
19. Ginther, R.J.; Kirk, R.D. *Rep. of NRL Progress*, **1956**, sept., 12–20.
20. Ginther, R.J.; Kirk, R.D. *J. Electrochem. Soc.*, **1957**, 104, 365–369.
21. Erdey, l.; Kasa, I.; Kovacs, L. *Periodica Polytechnica*, **1965**, 9, 223–230.
22. Palmer, R.C.; Blase, E.F. Pat.USA, No 3282855, cl. 252–301,Hj, **1966**.
23. Palmer, R.C.; Blase, E.F. Poirier, V.D. *Int. J. Appl. Rad. Isot.*, **1965**, 16, 737–735.
24. Palmer, R.C.; Poirier, V.D. Blase, E.F. Pat.Fr.No 1365883, cl. CO1F ;GO1J, 1964.
25. Niewiadomski, T. *Nukleonika*,**1967**, 12, 281–301.
26. Lust, A. „Method of synthesis of $CaF_2$ : Mn thermoluminescent material and detectors“ **1997**, M.Sci Thesis, University of Tartu (in Estonian).
27. Allsalu, M.-L.J.; Kilk, I.R.; Kuus, H.J.; Lust, A.L.; Pedak, E.J. **1980,** Inventors Certificate of SU, No 749085.
28. Prokert, K.; Sommer, M. *Rad. Prot. Dosim.*, **1998**, 78 (4), 249–257.
29. Chakrabati, K.; Sharma, J.; Mathur, N.K. *Rad. Prot. Dosim.*, **1993**, 47, 155–159.
30. Miller, S.D.; McDonald,J.; Eichner, F.N.; Tomeraasen, P.L. US Patent No 4954707, **1990**.
31. Puite, K.J.; Arends, J. The third International Conference on Luminescence Dosimetry, Risö, Denmark, 11–14 October, 1971. Proceedings, Risö Report No 249, 680–691.
32. Puite, K.J. *Int. J. Appl. Radiat. Isot.,* **1968**, 19(4), 397–402.

33. Da Rosa, L.A.R.; Nette, H.P. *Int. J. Appl. Radiat. Isot.,* **1988**, 39(3), 191–197.
34. Miller, S.D. US Patent, No 5272348 (**1993**).
35. Miller, S.D.; McDonald, J.C.; Eichner, F.N.; Tomeraasen, L.P. Us Patent No 5025159 (**1991**).
36. Miller, S.D. US Patent No 5196704 (**1994**).
37. Gasiot, J.; Braunlich, P.F.; Fillard, J.P. US Patent No 4507562 (**1985)**.
38. Braunlich, P,F.; Tetzlaff, W. US Patent No 4906848 (**1990**).
39. Miller, S.D. US Patent No 5569927 (**1996**).
40. Miller, S.D.; Stahl, K.A.; Endres, G.W.R.; McDonald, J.C. *Rad. Prot. Dosim.*, **1989,** 29(3), 195–198.
41. Jassemnejad, B.; Abbundi, R.J.; Brown, M.D.; McKeever, S.W.S. *Phys. stat. sol. A*, **1988**, 108(2), 753–764.
42. Sen, S.C.; Bose, H.N. *Z. Physik*, **1967**, 201 (4), 368–373.
43. Bozhevolnov, V.E.; Ivanov, L.N.; Kozlov, V.K.; Voronov, Yu.V.; Timofeev, Yu.P., Karelin, V.V. *Phys. stat. sol. B*, 1976, 78(2), 483–487.
44. Mizuguchi, M.; Hosono, H.; Kawazoe, H.; Ogawa, T. *J. Vac. Sci. Technol. A*, **1998**, 16(5), 3052–3057.
45. Denks, V.; Maaroos, A.; Nagirnyi, V.; Savikhina, T.; Vassiltsenko, V. J. *Phys.: Condens. Matter*, **1999**, 11(15), 3115–3125.
46. Lushchik, N.E.; Soovik Kh. A. In Spectroscopy of crystals, ed. By S.V. Grum-Grzhimailo, B.S. Skorobogatov, P.P. Feofilov and V.I. Cherepanov (Nauka, Moscow 1970), 258 (in Russian).
47. Niewiadomski, T.; Bilski, P.; Budzanowski, M.; Olko, P.; Ryba, E.; Waligorski, M.P.R. *Nukleonika*, **1996,** 41(2), 93–104.
48. Alonso, P.J.; Alcala, R. *J. Lumin.*, **1981**, 22, 321–333.
49. Alonso, P.J.; Alcala, R. *J. Lumin.*, **1980**, 21, 147–152.
50. Alonso, P.J.; Orera,V.M.; Alcala, R. *Phys. stat. sol.(b)*, **1980**, 99, 585–591.
51. Alcala,R.; Alonso, J.P.; Lalinde, G.; Carretero, A. *Phys. stat. sol. (b)*, **1980**, 98, 315–322.
52. Jain, V.K.; Shah Jahan, M. *Phys. stat. sol. (b)*, **1985**, 131, K161–K166.
53. Jain, V.K. *Radiat. Phys. Chem.*, **1990**, 36(1), 47–57.
54. Mathur, V.K.; Abbundi, R.J.; Brown, M.D.; McKeever, S.W.S. *Rad. Effects*, **1986**, 99, 9–14.
55. McKeever, S.W.S.; Jassemnejad, B.; Landreth, J.F.; Brown, M.D., *J. Appl. Phys.*, **1986**, 60(3), 1124–1130.
56. Allen, P.; McKeever, S.W.S., *Rad. Prot. Dosim.*, **1990**, 33 (1–4), 19–22.
57. Pascual, J.L.; Seijo, L.; Barandiarán, Z. *J. Chem. Phys.*, **1995**, 103(12), 4841–4846.
58. Pascual, J.L.; Seijo, L. *J. Chem. Phys.*, **1995**, 102(13), 5368–5376.
59. Lewandowski, A.C.; Wilson, T.M. *Phys. Rev. B*, **1994**, 50(5), 2780–2790.
60. Barriuso, M.T.; Moreno, M., *Chem. Phys. Lett.*, **1984**, 112(2), 165–168.
61. Garifullina, R.L.; Stepanov, V.G. *Fizika tverdogo tela*, **1973**, 15(7), 2169–2172 (in Russian).
62. Lay, F.Min-tsong; Nolle, A.W. *Phys. Rev.*, **1967**, **163**(2), 266–275.
63. Gehlhoff, W.; Ulrici, W., *Phys. stat. sol.(b)*, **1980**, 102, 11–59.
64. Kuroda, S.; Marumoto,K.; Kihara, H.; Ofuchi, H.; Tabuchi, M.; Takeda, Y.; Banshchikov, A.G.; Sokolov, N.S.; Yakovlev, N.L. *Jpn. J. Appl. Phys.*, **2001,** 40, L1151-L1153.
65. Barkoumb, J.H.; Mansour, A.N., *Phys. Rev. B*, **1992**, 46(14), 8768–8776.

66. Chakrabati, K.; Barkoumb, J.H.; Mathur, V.K. Conference on Quantum Electronics and Laser Science, Anaheim, California, May 10–15, 1992. Technical Digest Series vol.13, **1992**, 66.
67. Lindner, R.; Williams, R.T.; Reichling, M., *Phys. Rev. B*, **2001**, 63, 075110, 1–7.
68. Denks, V.P.; Kerikmyae, M.P.; Lust, A.L.; Savikhina, T.I. *Physics of the solid state*, **2000**, 42(2), 261–269.
69. Tsuboi, T.; Silfsten, P. *J. Phys. Condens. Matter*, **1991,** 3, 9163–9167.
70. Radzabov, E. *J. Phys. Condens. Matter*, **2001**, 13, 10955–10967.
71. Caldino, U.; Munoz, A.F.; Rubio, J.O. *J. Phys. Condens. Matter*, **1990**, 2, 6071–6078.
72. Faulques, E.; Wery, J.; Dulieu, B.; Seybert, C.; Perry, D.L. *J. Fluorescence*, **1998**, 8 (4), 283–287.
73. Wang, F.; Fan, X.; Pi, D.; Wang, M. *Sol. Stat. Commun.*, **2005**, 133, 775–779.
74. Laberguerie, J.; Gredin, P.; Mortier, M.; Patriarche, G.; Kozak, A. *Z. Anorg. Allg. Chem.*, **2006**, 1538–1543.
75. Feofilov, P.P. Optika i spektroskopia, **1956**, 1(7), 992–1001 (in Russian).
76. Shimizu, Y.; Minowa, M.; Suganuma, W.; Inoue, Y. *Phys. Lett. B*, **2006**, 633, 195–200.
77. Silversmith, A.J.; Macfarlane, R.M. *Phys. Rev. B*, **1992**, 45(11), 5811–5818.
78. Mizuguchi, M., Hosono, H., Kawazoe, H., and Ogawa, T. *JOSA B*, **1999**, 16(7), 1153–1159.
79. Cirillo-Penn, K.M.; Wright, J.C. *J. Lumin.*, **1991**, 48&49, 505–508.
80. Mändar, H.; Felsche, J.; Mikli, V.; Vajakas, T. *J. Appl. Cryst.*, **1999**, 32, 345–350.
81. Rodriguez-Carvajal, **1997**. J. FULLPROF version 3.5, Laboratoire Leon Brillouin (CEA-CNRS), F-91191 Gif sur Yvette, France.
82. Paama, L.; Pärnoja, E.; Must, M.; Perämäki, P. *J. Anal. At. Spectrom.*, **2001**, 16, 1333–1336.
83. G.Blasse: in Luminescence of Inorganic Solids, edited by B.Di Bartolo, Plenum Press, New York and London, **1978**, 505–508.
84. Danilkin, M.; Must, M.; Pedak, E.; Pärnoja, E.; Ryasnyi, G.; Seeman, V.; Shpinkov, I.; Spinkova, L. *Zhurnal prikladnoi spektroskopii***, 1995,** 62(3), 186–191 (in Russian).

# ACKNOWLEDGEMENTS

I am very thankful to my supervisor, senior researcher Mikhail Danilkin (PhD) for the support and inspiration of the present work.

I would like to acknowledge the help of all our luminescence research group, specially Viktor Seeman (phys.-mat. cand.) for fruitful discussions and EPR measurements.

I am thankful to all the staff of the Institute of Chemical Physics for the friendly support.

The support from the Estonian Science Foundation (grants No. 5198 and 5779) is greatfully acknowledged.

# PUBLICATIONS

# I

Determination of Manganese in Thermoluminescence Materials by Inductively Coupled Plasma Atomic Emission Spectroscopy and Spectrophotometry.
Lust, A.; Paama, L.; Kerikmäe, M.; Must, M.; Perämäki, P.
*Proc. Estonian Acad. Sci. Chem.*, **2002**, 51(2), 126–133.

Proc. Estonian Acad. Sci. Chem., 2002, **51**, 2, 126–133

# Determination of manganese in thermoluminescent materials by inductively coupled plasma atomic emission spectrometry and spectrophotometry

Aime Lust[a], Lilli Paama[a*], Mihkel Kerikmäe[a], Mare Must[a], and Paavo Perämäki[b]

[a] Institute of Chemical Physics, University of Tartu, Jakobi 2, 51014 Tartu, Estonia
[b] Department of Chemistry, University of Oulu, FIN- 90401 Oulu, Finland

Received 15 October 2001, in revised form 7 December 2001

**Abstract.** The content of manganese in the mixed fluorides $CaF_2$: $MnF_2$ and $CaF_2$: Mn thermoluminophors was determined by inductively coupled plasma atomic emission spectrometry (ICP-AES) and spectrophotometry. The various Mn emission lines were compared and the manganese emission line at 257.610 nm was used for ICP-AES analysis. For the spectrophotometric determination the manganese(II) ions were oxidized to intensively coloured permanganate ions using potassium periodate. No statistically significant differences were found between the results of ICP-AES and spectrophotometric methods of analysis. The thermoluminophors were synthesized by coprecipitation of manganese with $CaF_2$, varying the concentration of manganese in the initial solutions in the range of 0.01–2.0% (m/m). The coprecipitated mixed fluorides $CaF_2$: $MnF_2$ were heated at 1423 K. The glow curves of synthesized $CaF_2$: Mn thermoluminophors were measured.

**Key words:** manganese determination, ICP-AES spectrophotometry, thermoluminophors $CaF_2$: Mn, glow curves.

## INTRODUCTION

Chemical characterization of advanced materials such as thermoluminophors, semiconductors, and conducting materials requires highly accurate methods for the determination of main and trace elements [1–3]. The large acceptance of

* Corresponding author, lilli@chem.ut.ee

inductively coupled plasma atomic emission spectrometry (ICP-AES) can be explained by some excellent characteristics such as high precision, high sensitivity as well as low limit of detection, a large linear dynamic range, and low matrix effects [4–6].

The thermoluminophor $CaF_2$: Mn is used in environmental dosimetry [7–11]. It is applied in accident dosimetry because of the linear response of the thermoluminescence intensity in the large range of the radiation dose (0.5 mGy to $10^3$ Gy) [12–14]. The fading of these thermoluminophors is low due to the relatively deep electron traps of $CaF_2$: Mn, and the luminophors are not sensitive to daylight [15, 16]. The thermoluminescence properties of $CaF_2$: Mn thermoluminophor depend mainly on the concentration of manganese.

The content of manganese in the semimagnetic semiconductors, bulk crystals, and epitaxially grown layers was examined by X-ray spectrometry [17]. A simple and fast analytical procedure was proposed for simultaneous spectrophotometric determination of manganese, lanthanum, and holmium in synthetic ceramics by using 2-(5-bromo-2-pyridylazo)-5-diethylaminophenol (5-Br-PADAP) [18]. Small quantities of manganese are readily determined photometrically by the oxidation of Mn(II) to the coloured permanganate ion. Potassium periodate is an effective oxidizing reagent for this purpose and permanganate solutions that contain excess of periodate are quite stable.

In earlier reports we discussed photoluminescence of $CaF_2$: Mn phosphors excited by vacuum ultraviolet (VUV) radiation. Spectra of emission, excitation of steady-state luminescence, and phosphorescence of samples excited by monochromatic VUV radiation with quantum energies up to 14 eV at 293 K and up to 12 eV at 85 K were measured [19]. The conditions of coprecipitation of manganese with $CaF_2$ and the synthesis of $CaF_2$: Mn thermoluminophor at high temperature were worked out earlier [20, 21].

In the present study the content of the activator (manganese) was determined spectrophotometrically and using the ICP-AES method. The aim of the study reported here was to develop spectrochemical and spectrophotometric methods for the analyses of different powders of $CaF_2$: $MnF_2$ and $CaF_2$: Mn thermoluminophors and to find suitable concentrations of the activator.

## EXPERIMENTAL

### Instrumentation and operating technique

A sequential PU 7000 Philips (Unicam Analytical Systems, Cambridge, UK) inductive plasma atomic emission spectrometer was used for the measurements. The design of this spectrometer includes a 40.68-MHz free-running oscillator for driving the plasma, an echelle grating for wavelength separation, and a grid nebulizer for sample introduction. The system is equipped with a Gilson 221 autosampler and is controlled by a Philips P3230 computer. The ICP-AES instrumental parameters are summarized in Table 1.

**Table 1.** Instrumental parameters of ICP-AES

| | |
|---|---|
| Injector tube (quartz) | 1.50 mm i.d. |
| Plasma power | 1.0 kW |
| Coolant argon flow | 13.0 L/min |
| Nebulizer argon pressure | 280 kPa (40 psi) |
| Sample uptake | 1.0 mL/min |
| Sample read delay | 40 s |
| Autosampler wash delay | 20 s |
| Integration time | 3 s |
| Number of integrations | 3 |
| Mn(II)[a] | 257.610 nm |

[a] ion line

A spectrometer Lambda 2S Perkin Elmer UV/Vis was used for spectrophotometric measurements.

The glow curves of thermoluminophors were measured by a thermoluminescence reader (TLD reader) UPF-02 (Moscow, Russia).

## Reagents and standards

All reagents were of analytical grade (Merck). The sulphuric, nitric, and hydrochloric acids were ultrapure (Merck). Deionized water (18 MΩ/cm) was used for the preparation of the solutions for ICP-AES analysis.

The stock solution, containing 1000 mg/L of manganese, was prepared from $MnSO_4 \cdot 5H_2O$ (anal. gr., Merck). The working standard solutions for ICP-AES were obtained by serial dilution of stock solution with deionized water (18 MΩ/cm). The concentrated $HNO_3$ (5% v/v) and concentrated $H_2SO_4$ (2% v/v) were added to the working standard solutions.

The calibration standards for spectrophotometric determination were prepared by serial dilution of the stock solution with deionized water. Six standard solutions in the range of 0.01–0.25 mg manganese in 50 mL were prepared for spectrophotometric measurements.

## Samples, their decomposition and procedures

The powders of $CaF_2$: $MnF_2$ were synthesized by coprecipitation using $CaCl_2$, HF, and $MnCl_2$ solutions. The $MnCl_2$ was added into solution of $CaCl_2$ and the excess of fluoride ions was used. The heating of powders was carried out at 1323 K during 30 min in special quartz apparatus in the argon atmosphere [20, 21].

The samples (0.05–0.06±0.0002 g) were weighed into a fluoroplastic crucible and 5 mL concentrated $H_2SO_4$ (Suprapur, Merck) was added. The samples were heated until HF vapours separated. For ICP-AES analysis 5 mL $HNO_3$ (65% v/v, Suprapur, Merck) was added. The solution was allowed to cool and then transferred into a 100 mL calibrated flask and coupled to volume with deionized water.

For spectrophotometric analysis the samples (after heating with concentrated $H_2SO_4$ on a hot plate) were transferred into a 100 mL baker. Then 14 mL of concentrated $H_2SO_4$ was added, diluted to 70 mL, and heated to dissolve the precipitate. After cooling the solution was transferred into a 100 mL calibrated flask and coupled to volume 100 mL with deionized water. For oxidation of manganese(II) to permanganate ions 25 mL aliquot part of sample solution was transferred into a 100 mL baker, 25 mL $H_3PO_4$ (85% v/v) and 1 g $KJO_4$ were added. The solution was heated to boiling and kept at 95 °C during 15 min. The solution was allowed to cool and transferred into a 50 mL calibrated flask and coupled to volume with deionized water. The absorbance of the solutions was measured at 545 nm to blank solution.

## RESULTS AND DISCUSSION

Spectral lines for ICP-AES measurements were selected on the basis of minimum spectral line interferences and maximum sensitivity. Three emission lines Mn(II) at 257.610 nm, Mn(II) at 259.373 nm, and Mn(II) at 293.306 nm were compared. The Mn emission line Mn(II) at 257.610 nm was found to be the most suitable for source peaking (to find an optimum viewing position in the ICP discharge) and the detection limits (3 s of the blank prepared as samples) were all in the 0.007–0.01 mg/L range (Table 2). The concentration of Ca in the analysed solution can affect the determination of Mn by ICP-AES. The matrix effects due to calcium were tested by measuring analyte intensities of 1.0 mg/L of manganese in solutions containing 500 mg/L of calcium. The actual concentration of Ca in the decomposed samples was about 200–300 mg/L. The influence of calcium matrix on the Mn emission signal at 257.610 nm was <1%. The precision of determination (RSD) ranged from 0.5% to 0.9% (Table 2). On the basis of optimized experimental conditions the Mn(II) emission line at 257.610 nm was selected for the spectrochemical determination of manganese in the samples of thermoluminescence materials. The following five manganese calibration standards were used: 0.05, 0.1, 1.0, 5.0, 10.0 mg/L. A scan of the

**Table 2.** Wavelength, excitation potentials (EP), ionization potential (IP), and detection limits (DL) of determination of Mn in solutions containing 1.0 mg/L manganese and 500 mg/L calcium

| Manganese line | Wavelength, nm | EP, eV | IP[a] + EP, eV | DL, mg/L | Found[b], mg/L | |
|---|---|---|---|---|---|---|
| | | | | | $\bar{c} \pm s$ | RSD, % |
| Mn(II)[c] | 257.610 | 4.813 | 12.248 | 0.007 | 0.994±0.0054 | 0.54 |
| Mn(II) | 259.373 | 4.784 | 12.222 | 0.009 | 0.983±0.0076 | 0.77 |
| Mn(II) | 293.306 | 4.228 | 11.663 | 0.010 | 1.052±0.0096 | 0.92 |

[a] IP Mn(II) = 7.435
[b] four replicates
[c] ion line

measurement lines showed neither background shifts nor sloped background, and therefore it was not necessary to introduce background correction (Fig. 1).

The results of analysis of laboratory synthesized powders of $CaF_2$: $MnF_2$ and $CaF_2$: Mn thermoluminophors by ICP-AES and spectrophotometry are shown in Table 3. Statistical tests applied (*t*-test, *F*-test) showed no significant differences between the results of ICP-AES and spectrophotometric analysis [22]. The RSD ranged from 0.63% to 1.0% for ICP-AES and from 0.96% to 2.3% for the spectrophotometric method.

Luminescence properties of thermoluminophors are determined by their glow curves. The glow curves measured by a TLD reader UPF-02 with rising the temperature 2°C/s are shown in Fig. 2. The shape of the glow curves, the temperature, and the intensity of the thermoluminescence peak depend mainly on the concentration of manganese in luminophors and the heating conditions. The increasing of the concentration of manganese reduces the intensity of the low-temperature thermoluminescence peak and increases the intensity of the high-temperature thermoluminescence peak. The most suitable concentration of the activator in the thermoluminophors seems to be in the range of 1.5–2.0% m/m. These thermoluminophors and detectors have only one thermoluminescence peak at 290°C. A higher concentration than 2.0% m/m is not recommended because of oxidation of Mn(II) in the case of reuse of detectors. These detectors are not sensitive to visible light and the fading is also very low because no low-temperature thermoluminescence peaks occur and the maximum of the high-

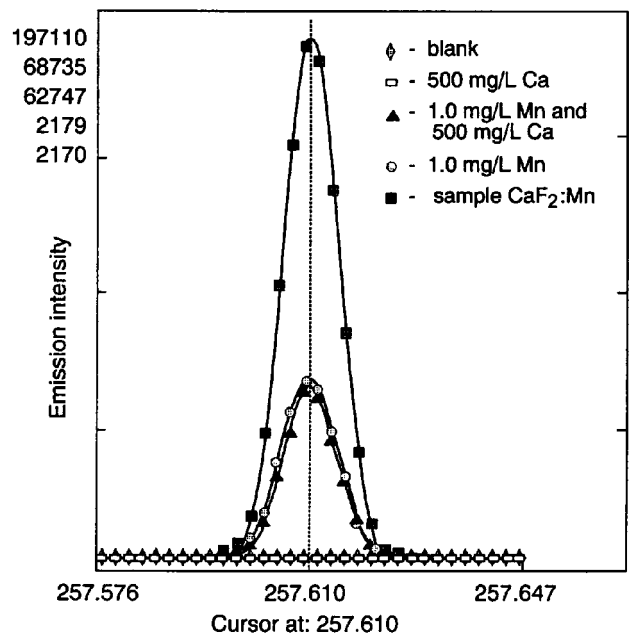


**Fig. 1.** Scan of manganese line Mn(II) at 257.610 nm.

**Table 3.** Results of ICP-AES and spectrophotometric analyses of powder of $CaF_2$: $MnF_2$ and $CaF_2$: Mn thermoluminophor (four replicates) with precision of determination (RSD)

| Sample | Mn, % (m/m) | | | | |
|---|---|---|---|---|---|
| | In initial solutions | ICP-AES | | Spectrophotometry | |
| | | $\bar{c} \pm s$ | RSD, % | $\bar{c} \pm s$ | RSD, % |
| $CaF_2$: $MnF_2$ | | | | | |
| 1 | 0.01 | 0.12±0.0012 | 1.00 | 0.10±0.0018 | 1.8 |
| 2 | 0.05 | 0.27±0.0026 | 0.98 | 0.28±0.0027 | 0.96 |
| 3 | 0.1 | 0.51±0.0049 | 0.96 | 0.49±0.0098 | 2.0 |
| 4 | 0.2 | 0.62±0.0055 | 0.88 | 0.59±0.012 | 2.0 |
| 5 | 0.4 | 1.49±0.0044 | 0.90 | 1.54±0.028 | 1.8 |
| 6 | 0.8 | 2.20±0.0094 | 0.63 | 2.12±0.044 | 2.1 |
| 7 | 1.0 | 2.53±0.017 | 0.69 | 2.50±0,048 | 1.92 |
| 8 | 1.2 | 2.39±0.019 | 0.80 | 2.46±0.042 | 1.71 |
| 9 | 1.6 | 1.63±0.011 | 0.65 | 1.55±0.029 | 1.87 |
| 10 | 2.0 | 1.78±0.016 | 0.65 | 1.73±0.04 | 2.3 |
| $CaF_2$: Mn | | | | | |
| 1 | 0.1 | 0.58±0.0042 | 0.72 | 0.62±0.014 | 2.2 |
| 2 | 0.2 | 0.68±0.0051 | 0.76 | 0.73±0.013 | 1.7 |
| 3 | 0.4 | 1.46±0.010 | 0.68 | 1.44±0.028 | 1.9 |
| 4 | 0.8 | 1.66±0.012 | 0.70 | 1.56±0.031 | 2.0 |

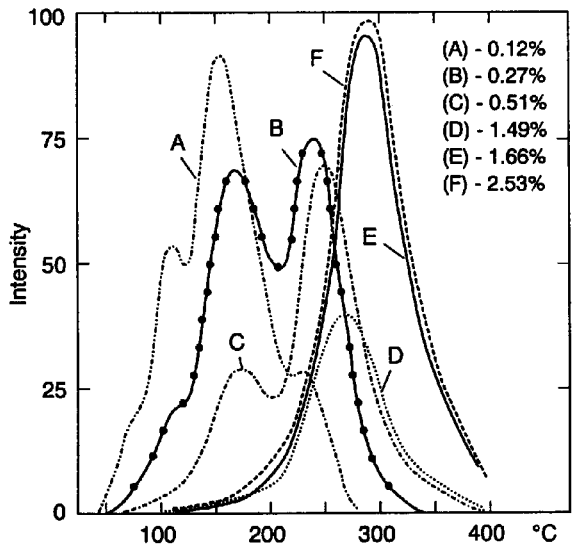


**Fig. 2.** Effects of the concentration of manganese on the intensity of glow curves. A–F, concentration of Mn (% m/m) in synthesized powders $CaF_2$: $MnF_2$.

temperature thermoluminescence peak is at quite a high temperature (290°C). The response of thermoluminescence intensity is linear up to $10^3$ Gy and the sensitivity of the detectors does not change after radiation with high doses.

Therefore they are suitable as extreme detectors. These detectors may be reused many times (up to 50) and all measurements may be carried out in air.

## CONCLUSIONS

The ICP-AES method is rapid and simple when compared to the spectrophotometric method, which is more complicated and time consuming. The manganese content has significant effects on the thermoluminescence properties of $CaF_2$: Mn thermoluminophors. Thermoluminophors containing 1.7–2.0% (m/m) of manganese are the most suitable materials for the preparation of thermoluminescence detectors.

## ACKNOWLEDGEMENTS

Financial support from the Estonian Science Foundation (grants Nos. 4587 and 3371) and Estonian Innovation Foundation (contract 29 it/97) is gratefully acknowledged. Thanks are due to Professor Risto Laitinen, University of Oulu, for the instrumental facilities that were used in this study.

## REFERENCES

1. Fairman, B., Hinds, M. W., Nelms, S. M., Penny, D. M. & Goodall, P. Atomic spectrometry update – industrial analysis: metals, chemicals and advanced materials. *J. Anal. At. Spectrom.*, 1998, **13**, 233–266.
2. Fairman, B., Hinds, M. W., Nelms, S. M., Penny, D. M. &. Goodall, P. Atomic spectrometry update – industrial analysis: metals, chemicals and advanced materials. *J. Anal. At. Spectrom.*, 1999, **14**, 1937–1969.
3. Gupta, R. K., Al-Ammar, A. & Barnes, R. M. Sample standard interaction during trace analysis of semiconductorgrade trimethylindium by inductively coupled plasma emission spectrometry. *J. Anal. At. Spectrom.*, 1999, **14**, 839–844.
4. Nickel, H. & Broekaert, J. A. C. Some topical applications of plasma atomic spectrochemical methods for the analysis of ceramic powders. *Fresenius' J. Anal. Chem.*, 1999, **363**, 145–155.
5. Paama, L., Pärnoja, E. & Perämäki, P. Trace element analysis of superconductor oxides by ICP-AES. *J. Anal. At. Spectrom.*, 2000, **15**, 571–572.
6. Paama, L., Perämäki, P. & Lajunen, L. H. J. Analysis of superconductor oxides $YBa_2Cu_3O_{8-x}$ by inductively coupled plasma atomic emission spectrometry and complexometric titration. *Anal. Chim. Acta*, 1996, **330**, 259–263.
7. Zarate-Morales, A. & Buentil, A. E. Environmental gamma dose measurements in Mexico City using TLD. *Health Phys.*, 1996, **71**, 358–361.
8. Vehl, D. L., Muron, D. I., Suijka, R. R., Vehar, D. W., Lorence, L. I., Westfall, R. L., Jones, S. C., Sweet, I. A. & Braunlich, P. Characterization of a two-dimensional thermoluminescent, dose-mapping system: uniformity, reproducibility and calibrations. *Rev. Sci. Instrum.*, 1994, **65**, 3243–3251.
9. Nicolae, M. & Lazar, M. Thermoluminescent dosimeter for monitoring of the environment around nuclear power plants. *Rev. Roum. Phys.*, 1985, **30**, 207.

10. Environmental Radiation Data. Report 75, July–September 1993, United States Environmental Protection Agency, Office of Radiation and Indoor Air. http://www.epa.gov/narel/erd75g.htm.
11. Miller, S. D. Environmental Radiation Detection via Thermoluminescence. PCT WO94/15227 (1994).
12. Schulman, J. R., Ginther, R. F., Kirk, K. D. & Goulart, H. S. Thermoluminescent dosimeter. Storage. Stability. Linearity. *Nucleonics*, 1960, **18**, 92–102.
13. Puite, K. J. & Arends, J. Trapping centers in $CaF_2$: Mn from thermoluminescence and thermally stimulated exoelectron emission measurements on undoped $CaF_2$ samples. In *Proceedings of the III International Conference on Luminescence Dosimetry, Resö Rept.*, 1971, **249**, 680.
14. Prokert, K. & Sommer, M. A new hypersensitive thermoluminophor based on the $CaF_2$. *Radiat. Prot. Dosim.*, 1998, **78**, 249–252.
15. Chakrabarti, K., Sharma, J. & Mathur, V. K. Laser bleaching of deep traps and reduction of zero dose problem in $CaF_2$: Mn dosimeters. *Radiat. Prot. Dosim.*, 1993, **47**, 155–158.
16. Miller, S. D., McDonald, J. C., Eichner, F. N. & Tomeraasen, P. L. System for Use with Solid State Dosimeter. US Patent No 4954707 (1990).
17. Lawniczak-Jablonska, K., Kachniarz, J., Spolnik, Z., Libera, J., Dynowska, E., Nadoln, A. & Sadowski, J. The use of Mn Lα line chemical effects in X-ray analysis to probe sample homogeneity. *J. Anal. At. Spectrom.*, 1999, **14**, 461–464.
18. Ferreyra, R. E., Camina, J. M., Marchevsky, E. & Luco, J. M. Simultaneous spectrophotometric determination of La, Ho, Mn 5-Br-PADAP complexes using multivariate calibration with partial least-squares (PLS) data evaluation. *Fresenius' J. Anal. Chem.*, 2000, **368**, 595–600.
19. Denks, V. P., Kerikmyae, M. P., Lust, A. L. & Savikhina, T. I. Photoluminescence of concentration series of $CaF_2$: Mn phosphors excited by VUV radiation. *Phys. Solid State*, 2000, **42**, 261–270.
20. Allsalu, M.-L., Kilk, I., Kuus, H., Lust, A. & Pedak, E. Method of Preparation of Thermoluminophor $CaF_2$, Activated with Manganese. Author's Certificate SU No 749095 (1980) (in Russian).
21. Lust, A. $CaF_2$: Mn termoluminofoori ja detektorite sünteesimetoodika. M.Sc. thesis, University of Tartu, Estonia, 1996.
22. Miller, J. C. & Miller, J. N. *Statistics for Analytical Chemistry*. Ellis Horwood, UK, 1984.

# Mangaani määramine termoluminestsentsmaterjalides induktiivse plasma aatomiemissioonspektromeetrilisel ja spektrofotomeetrilisel meetodil

Aime Lust, Lilli Paama, Mihkel Kerikmäe, Mare Must ja Paavo Perämäki

Mangaani sisaldus fluoriidide $CaF_2$: $MnF_2$ segus ja $CaF_2$: Mn termoluminofoorides määrati induktiivse plasma aatomiemissioonspektromeetria (ICP-AES) ja spektrofotomeetria meetodil. Võrreldi erinevaid mangaani emissioonijooni ja ICP-AES analüüs tehti kasutades emissioonijoont 257,610 nm juures. Spektrofotomeetrilise analüüsi puhul oksüdeeriti Mn(II)-ioonid permanganaatioonideks kaaliumperjodaadi abil. Olulisi erinevusi kahel meetodil saadud tulemuste vahel ei täheldatud. Termoluminofoorid sünteesiti mangaani kaasasadestamisel $CaF_2$-ga, varieerides Mn kontsentratsiooni vahemikus 0,01–2,0% (m/m). Kaasasadestatud fluoriidide segu kuumutati 1423 K juures inertse gaasi atmosfääris. Sünteesitud termoluminofooridel mõõdeti ka termovälja kiirguskõverad.

# II

OSL of Some TLD Detectors as the Indicator of Absorbed Dose.
Jaek, I.; Kerikmäe, M.; Lust, A.
*Rad. Prot. Dosim.*, **2002**, 100(1–4), 459–462.

Radiation Protection Dosimetry
Vol. 100, Nos 1–4, pp. 459–462 (2002)
Nuclear Technology Publishing

# OPTICALLY STIMULATED LUMINESCENCE OF SOME THERMOLUMINESCENT DETECTORS AS AN INDICATOR OF ABSORBED RADIATION DOSE

I. Jaek, M. Kerikmäe and A. Lust
Department of Physics and Chemistry
University of Tartu
Tähe 4, Tartu 51010, Estonia

**Abstract** — Stimulation spectra of several TLD materials in the short-wave spectral region are measured using the optically stimulated afterglow (OSA) method for determination of absorbed dose. Optical stimulation spectra are studied in the region of wavelengths lower than those of emission spectra. The effective optical stimulation bands have been found for examined materials in the regions of wavelengths which overlap with fluorescence excitation bands. Application of short-wave OSA bands for determination of absorbed dose is analysed.

## INTRODUCTION

Optically stimulated luminescence (OSL) has some advantages for indicating absorbed dose compared with thermoluminescence (TL). The repeated readout of the information is the most important one. Most conventional TL and OSL dosemeters have relatively low luminescence yield under stimulation. This means that the measuring technique based on simultaneous stimulation and registration of output light has limited possibilities because the spectral separation of luminescence and stimulating light cannot be very effective. Thus, only the quanta of lower energies than luminescence output are commonly used for stimulation. The complete stimulation spectrum can be measured using time-resolution instead of spectral separation. The intensity of optically stimulated afterglow (OSA) is measured relative to the time after the stimulating pulse of light. This method was used to measure complete stimulation spectra of quartz and alkali feldspars used in palaeodosimetry[1]. McKeever and others studied $Al_2O_3$:C afterglow between laser impulses[2]. Miller[3] has measured optical stimulation of the low-temperature TL peak of $CaF_2$:Mn, which gives the possibility of using organic binders. However, the stimulation in the region of shorter wavelengths was not used in these studies, despite the potential advantage of the time-resolution method.

## EXPERIMENTAL

The studied samples are listed in Table 1. $CaSO_4$:Dy and $CaF_2$:Mn were synthesised at the University of Tartu by co-precipitating activators ($Dy^{3+}$ and $Mn^{2+}$) with $CaSO_4$ and $CaF_2$, respectively, followed by high-temperature heating. LiF (TLD-100) and $Al_2O_3$:C were commercial products. The measuring apparatus is described elsewhere[1]. The delay time was 50 ms except for $CaF_2$:Mn, where $\Delta t$ was 150 ms. Measurements have been carried out at room temperature. The OSA stimulation spectra have been corrected with regard for the light intensity spectral distribution of the excitation radiation source (Xe lamp + SPM monochromator). The integrated emission value is acquired by PMT with a quartz window. Samples were dosed by X ray excitation. The heating rate was about $1°C.s^{-1}$ when glow curves and thermo-optical bleaching (TOB) were measured. TOB is measured using intermittent heating.

Contact author E-mail: galinap@physic.ut.ee

## RESULTS AND DISCUSSION

### OSA spectra

The OSA spectra of some TL materials were measured using the equipment with a short-wave limit of 250 nm. Both OSA spectra and luminescence output spectra are shown in Figure 1. As a rule, these materials have short-wave stimulation bands which effectively induce luminescence. In Table 1 the locations of the maxima of OSA bands $\lambda_{OSA}$, the maxima of emission spectra $\lambda_{em}$ and the ratio $I_1/I_2$ of the OSA signal values recorded at $\lambda_{OSA}(I_1)$ and at the wavelength of the stimulation corresponding to $\lambda_{em}(I_2)$ are presented.

These data demonstrate that the studied materials may be tried as OSL dosemeters using the OSA method in the short-wave region of the stimulating light.

### OSA method for determination of absorbed dose

The following conditions should be fulfilled to apply this method in practice:

(1) The stimulation bands should be connected with emptying of the proper 'dosemetric' traps revealed in TL. The thermo-optical bleaching curves (TOB) were measured to check this condition. TOB of

$Al_2O_3$:C at several stimulation wavelengths is shown in Figure 2. The decrease of intensity of dosemetric TL peaks at corresponding stimulating bands permits both to connect with the same traps (TL and OSL). The OSA method is useful to study deep traps which could be very important in practice (e.g. F-centres in LiF).

(2) The stimulating light should not excite recombination luminescence including thermoluminescence, i.e. should not increase the population of traps. The

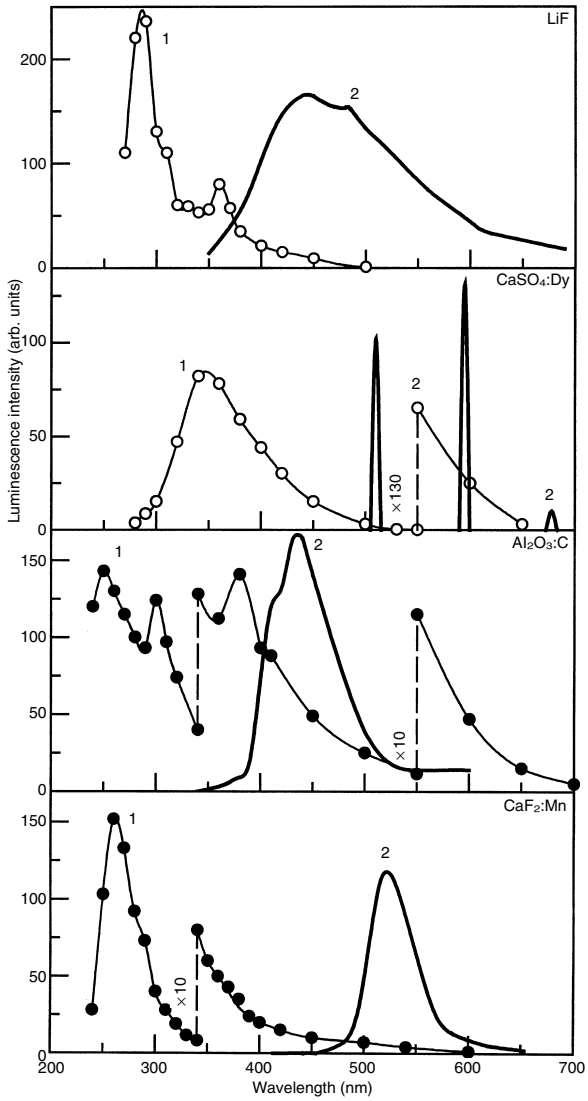


Figure 1. The OSA stimulation spectra (curves 1) and X ray luminescence (curves 2) of LiF, $CaSO_4$:Dy, $Al_2O_3$:C and $CaF_2$:Mn. Delay time $\Delta t$ = 50 ms except $CaF_2$:Mn where $\Delta t$ = 150 ms.

problem appears to be not easy because the requirement of quanta energy not to exceed the band gap is insufficient. The photoionisation of luminescence centres can also yield to the phosphorescence. So, one should check all the possible thermoluminescence excitation bands before using the OSA method, and restrict the stimulating light to prevent it from overlapping with TL excitation bands. The materials used here were checked against excitation by stimulating light and it was discovered that $Al_2O_3$:C only possesses a TL excitation band in the region of 300 nm (Figure 1, $\lambda \leq 300$ nm). This fact corresponds also to incomplete quenching of the OSA signal at the peak of the glow curve by short-wavelength stimulating light (Figure 2). The excitation of thermoluminescence by stimulating light in the region of 400 nm also occurs for some alkali feldspars used as palaeodosemeters.

(3) The general requirement for application of OSA methods in the region of short wavelength is the following:

$$\Delta t \gg \Delta\tau$$

where $\Delta\tau$ is the intrinsic decay time of fluorescence, and $\Delta t$ is the delay-time, or dead-time between stimulating light pulse and measuring of luminescence. This is a basic principle of separation of fluorescence and secondary phosphorescence (OSA signal). While the decay time of induced phosphorescence at room temperature is several tenths of a second, the dead-time before measurement should not be less than $10^{-3}$ s (milliseconds). This time seems to be long enough for most of conventional luminophors where $\Delta\tau \leq 10^{-5}$ s.

To achieve the maximum sensitivity, one uses short ($\approx$ 1.5 ms) delay times, but this is a problem in the case of luminescence impurities (centres) with forbidden

**Table 1. Samples studied.**

| No. | TL detector | $\lambda_{OSA}$ (nm) | $\lambda_{em}$ (nm) | $I_1/I_2$ | Notes |
|---|---|---|---|---|---|
| 1 | LiF(TLD-100) | 290 | 460/420 | >130 | $I_2$ value at 420 nm |
| 2 | $CaSO_4$:Dy | 350 | 510 | 80 | Line emission spectrum |
| 3 | $Al_2O_3$:C | 380 | 435 | 15 | |
| 4 | $CaF_2$:Mn | 270 | 520 | >200 | |

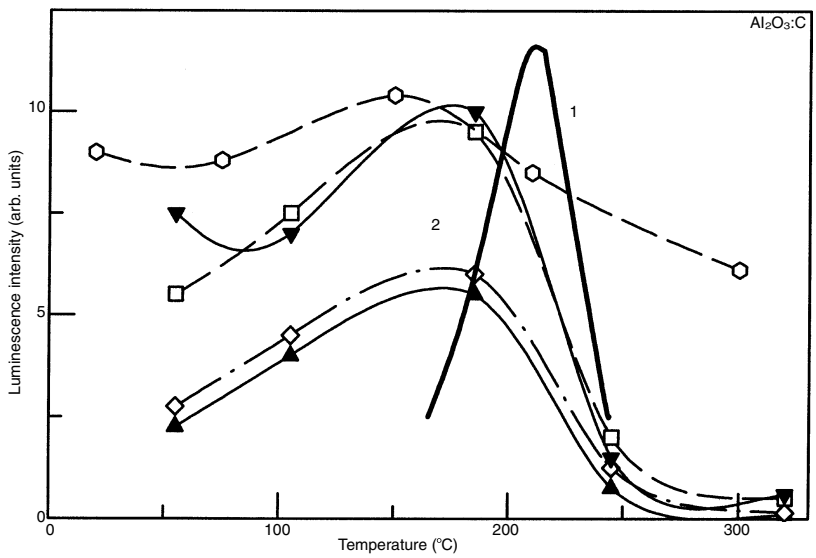


Figure 2. $Al_2O_3$:C after X ray excitation at room temperature: Curves: (1) TL glow curve; (2) thermo-optical bleaching (TOB) by stimulation at 300 (○), 400 (▼), 500 (□), 600 (◇), 700 (▲) nm. Heating rate about 1°C.s$^{-1}$. TOB is measured using intermittent heating.

transitions, which give long-time afterglow[4]. The materials with slow intrinsic decay times are difficult for distinguishing OSA signal from excited fluorescence. These difficulties could be illustrated by $Mn^{2+}$ in $CaF_2$:Mn. It gives typical afterglow of about 40 ms or longer when excited by light in the region 550–300 nm. So, one must exclude these bands of excitation from the stimulating light, e.g. filter out the excitation band of the 280 nm region from the stimulating light. This gives a possibility of decreasing a delay-time up to 150 ms. Without light filtering one has to prolong the delay-time up to 1 s or more. The lost phosphorescence integral can be compensated in this case by the sensitivity of the measuring equipment.

## SUMMARY

When the above mentioned conditions are fulfilled, the OSA response can be measured without any filters or spectral device, under stimulation of a halogen incandescent lamp. One of the suitable materials is $CaSO_4$:Dy, and probably also natural quartz. The OSA signal relative to the dose for $CaSO_4$:Dy is shown in Figure 3. The afterglow was stimulated by a complete unfiltered spectrum of a halogen incandescent lamp. As in case of TL, the dependence between OSA response and dose is linear in the studied range of doses.

## ACKNOWLEDGEMENTS

This study was supported by the Estonian Science grants No 4049, 3371 and by Estonian Innovation grant No 05197.

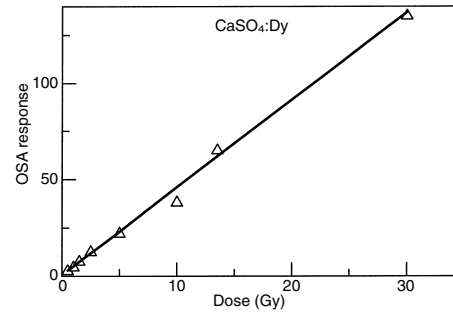


**Figure 3. The OSA signal versus dose for $CaSO_4$:Dy.**

## REFERENCES

1. Jaek, I., Hütt, G. and Streltsov, A. *Study of Deep Traps in Alkali Feldspars and Quartz by the Optically Stimulated Afterglow.* Radiat. Prot. Dosim. **84**(1–4), 467–470 (1999).
2. McKeever, S. W. S., Akselrod, M. S. and Markey, B. G. *Pulsed Optically Stimulated Luminescence Dosimetry using α-$Al_2O_3$:C.* Radiat. Prot. Dosim. **65**, 267–272 (1996).
3. Miller, S. D. *Composite Material Dosimeters.* US Patent, 5,569,927, October 29 (1999).
4. Blasse, G. *Materials Science of the Luminescence of Inorganic Solids*. In: Proc. Course on Luminescence of Inorganic Solids at International School on Atomic and Molecular Spectroscopy, Erice, Italy, June 1977. Luminescence of Inorganic Solids, Ed. by B. di Bartolo (New York and London: Plenum Press), pp. 457–494 (1978).

# III

$CaF_2$:Mn extreme dosimeter: Effects on Mn concentration
on thermoluminescence mechanisms and properties.
Danilkin, M.; Lust, A.; Kerikmäe, M.; Seeman, V.; Mändar, H.; Must, M.
*Rad. Meas.*, **2006,** 41, 677–681.

Available online at www.sciencedirect.com
ScienceDirect
Radiation Measurements 41 (2006) 677–681
Radiation Measurements
www.elsevier.com/locate/radmeas

# $CaF_2$:Mn extreme dosimeter: Effects of Mn concentration on thermoluminescence mechanisms and properties

Mikhail Danilkin*, Aime Lust, Mihkel Kerikmäe, Viktor Seeman, Hugo Mändar, Mare Must

*Faculty of Physics and Chemistry, University of Tartu, Tähe 4-101 51010, Tartu, Estonia*

Received 5 November 2005; received in revised form 19 March 2006; accepted 15 April 2006

**Abstract**

Concentration of manganese in $CaF_2$:Mn (TLD-400) is shown to exert the most essential influence on thermoluminescent (TL) properties. The TL curve demonstrates a single high-temperature peak only when $CaF_2$ is doped with a high manganese concentration, being close but still below the decomposition threshold of a solid solution. In case of lower manganese concentrations, the TL curve shows several peaks overlapping with each other. The optimum manganese concentration in thermoluminophor is found to be about 2.1–2.5 mol%. The influence of different factors on the actual Mn concentration in $CaF_2$:Mn is reported for the case where the material is prepared by the co-precipitation method. The $CaF_2$ crystal lattice stress due to the Mn incorporation is studied by means of the X-ray diffraction technique. The solid solution decomposition threshold is estimated. The EPR studies of both $\gamma$-irradiated and non-irradiated samples have demonstrated that the amount of $Mn^{2+}$ does not change as a result of the irradiation. The model of energy storage is suggested. It is based on a pair of $V_K$ and F centres, induced by radiation near $Mn^{2+}$, which immediately turns into an exciton-like state with a partial relaxation of the lattice stress caused by the Mn impurity. Partial relaxation of the lattice stress increases the thermal stability of the stored excitation.
© 2006 Elsevier Ltd. All rights reserved.

*PACS:* 29.40.Wk; 78.60.Kn; 78.55.Hx

*Keywords:* Solid-state detectors; Thermoluminescence; Calcium fluoride; Manganese; Solid solution; Soulubility threshold

author's personal copy

## 1. Introduction

Calcium fluoride doped with manganese is an important material for thermoluminescent (TL) dosimetry. It is suitable mostly for environmental dosimetry (Zarate-Morales and Buentil, 1996; Kalchgruber et al., 2002) rather than personal dosimetry, because it absorbs radiation like bones, not like tissue. This thermoluminophor linearly responds to the radiation dose in an extremely wide range of doses, from 0.5 mGy to about $10^3$ Gy (Schulman et al., 1960; Vehl et al., 1994). $CaF_2$:Mn has a single TL peak well above the room temperature (570–580 K). There are no losses from this peak at room temperature, and dose information can be stored for years. However, the TL curve depends substantially on the actual concentration and distribution of the doping agent ($Mn^{2+}$).

The lattice of $CaF_2$ could be represented as two cubic lattices inserted one into another: a cubic lattice composed of $F^-$ ions and a face-centred cubic lattice composed of $Ca^{2+}$ ions. Manganese substitutes for calcium at regular sites of $CaF_2$ lattice, and only divalent $Mn^{2+}$ is suitable to substitute $Ca^{2+}$ and to give luminescence. The smaller ionic radius of $Mn^{2+}$ compared to $Ca^{2+}$ (ionic radii of 8-coordinate $Mn^{2+}$ and $Ca^{2+}$ are 0.110 and 0.126 nm, respectively, see http://www.webelements.com) causes lattice strains in doped with Mn $CaF_2$. This makes the solid solution sensitive to the Mn concentration and complicates doping technologies. So, one needs to introduce Mn into $CaF_2$ lattice as uniformly as possible and to avoid oxidation of $Mn^{2+}$ to higher oxidation states at annealing. Once oxidised, manganese becomes unstable in the lattice and falls out of the solid solution. This causes TL dosimeters to degrade during cycled annealing while they are practically used, due to further

* Corresponding author. Tel.: +372 7 375253; fax: +372 7 376520.
*E-mail address:* danilkin@ut.ee (M. Danilkin).

1350-4487/$ - see front matter © 2006 Elsevier Ltd. All rights reserved.
doi:10.1016/j.radmeas.2006.04.020

oxidation and losses of $Mn^{2+}$. Mechanical mixing of the dopant with $CaF_2$ followed by annealing produces non-uniform and unstable solid solutions due to the low diffusion rate of $Mn^{2+}$ at the temperature of final annealing. The dopant is distributed more uniformly only when the starting material is obtained by co-precipitation of $MnF_2$ together with $CaF_2$ from the initial solution.

The aim of our study was to work out a technique of co-precipitation to obtain a thermoluminophor with required characteristics, and also to get around the problem of $Mn^{2+}$ oxidation both at the final annealing and during the practical operation. Our research has succeeded in developing the process of synthesis of a TL material $CaF_2$:$Mn^{2+}$, free of oxygen traces and very stable against oxidation: it can be used in air up to a hundred cycles without essential change in its properties (Lust, 1997; Kerikmäe, 2004; Allsalu et al., 1980). Here, we report the basic approaches that helped us to develop the technology of this TL material.

Many attempts have been made during the last 40 years to understand the TL mechanism of $CaF_2$:$Mn^{2+}$. Very different approaches have been used and different models were suggested (Alonso and Alcala, 1981; Mathur et al., 1986; McMasters et al., 1987; Allen and McKeever, 1990). Nevertheless, the issue is still open for investigations. We report here our experimental results and ideas concerning the mechanism of energy storage and release in thermoluminophor $CaF_2$:$Mn^{2+}$.

## 2. Experimental

The co-precipitation of the host material $CaF_2$ together with $MnF_2$ was carried out in a specially designed apparatus made of fluoroplast-4. Dilute solutions of $CaCl_2$, $MnCl_2$ and HF were added simultaneously at a regulated rate into the reaction vessel using peristaltic pumps. The reaction vessel was kept at an elevated temperature by means of a vapour bath, and the incoming solutions were agitated with a fluoroplast-made stirring rod. The precipitate was aged in the mother solution for 2–3 h. Then the precipitate was decanted and washed carefully, dried, and pre-annealed in air at 673 K for 2 h to remove the traces of water and fluoric acid. Traces of water cause oxidation of $Mn^{2+}$ as well as oxygen traces. To prevent $Mn^{2+}$ from oxidising, the starting materials should be also free of oxygen ($Ca(NO_3)_2$ cannot be used instead of $CaCl_2$). Pre-annealed precipitate was then placed in carbon-glass crucible and fired for 1/2 h at 1423 K in a quartz atmospheric tube under a protective flow of high-purity (99.999%) argon or nitrogen. When necessary, the finished thermoluminophor was pressed into tablets and fired in a protective atmosphere once again.

The resulting concentration of manganese in the finished thermoluminophor depends on the precipitation conditions and on the presence of additional dopants. The amount of manganese was varied in the starting materials from 0.01% to 2%. The actual concentration of Mn was assessed by spectrophotometrical analysis (the details are given in a previous work by Lust et al., 2002). The resulting accuracy and convergence of the technique used were high enough to give the standard deviation of about 1–2%. The eligibility of this analysis technique has been checked previously by comparing the results of the spectrophotometrical analysis with the data obtained by inductively coupled plasma atomic emission spectroscopy (Lust et al., 2002).

X-ray powder diffraction (XRPD) method was used for crystal phase analysis and cell parameter determination. XRPD data were collected using a computer-controlled Bragg–Brentano $\Theta$–$2\Theta$ powder diffractometer (equipped with a goniometer GUR-5 from diffractometer DRON-1). It has a 180 mm radius and works at 40 kV (20 mA) with CuK$\alpha$ ($\lambda = 1.5405981$ Å) radiation collimated with Soller slits (aperture 2.5°) and a 1 mm divergence slit. Soller slits (aperture 1,5°) were also used in the diffracted beam. A 0.03 mm Ni filter, a 0.25 mm receiving slit and a scintillation detector were used in the step-scanning mode (5 s for each step of 0.02°2$\Theta$) in the angular range of 8–160°2$\Theta$. A software system AXES (Mändar et al., 1999) was used to treat raw data (peak detection, fitting with pseudo-Voigt function and cell refinement). For cell refinement, an independent zero angle correction was made and applied to the diffraction angle. Rietveld analysis (computer program FULLPROF, by Rodriguez-Carvajal, 1997) was used to determine the lattice stoichiometry.

The EPR spectra of $Mn^{2+}$ were studied with X-band EPR spectrometers (8.87 GHz with a 100 kHz magnetic field modulation and 9.1 GHz with a 975 kHz magnetic field modulation). The spectra were measured at the room temperature.

The TL curves were measured with a semiautomatic TLD reader based on a thermocontroller OMRON E5CK and a photomultiplier tube with a current–frequency converter. Both the thermocontroller and the data acquisition system were connected to a computer. The measurements were carried out at a constant heating rate (0.5 K/s).

The TL materials were irradiated with a $^{60}$Co $\gamma$-radiation source (doses 100, 200 and 400 Gy) to study the radiation effects, the TL curves and other manifestations of stored dose information. The reference dose irradiator 6527B (Sweden) equipped with a $^{90}$Sr/$^{90}$Y $\beta$-radiation source was used to give lower doses (0.1–1.0 Gy).

## 3. Results and discussion

The TL curve appearance in $CaF_2$:Mn (the number and positions of the TL peaks) depends solely on the manganese concentration and distribution. The TL curves for different Mn concentrations (actually determined in finished luminophors concentrations) are shown in Fig. 1. The results demonstrate a good reproducibility since our previous study (Lust et al., 2002). The TL curve is composed of several peaks overlapping each other if the Mn concentration is low. At higher Mn concentrations, the TL peaks are shifted towards higher temperatures, and a single strong TL peak appears near 570 K. Fractional annealing shows, however, that the TL peak is not elementary and still consists of several close overlapping peaks. Nevertheless, the distribution of the activation energies of the traps becomes obviously narrower at higher Mn concentrations. This fact assumes probably that the disorder caused by an Mn impurity in $CaF_2$ lattice (Barkyoumb and Mansour, 1992) turns into

Author's personal copy

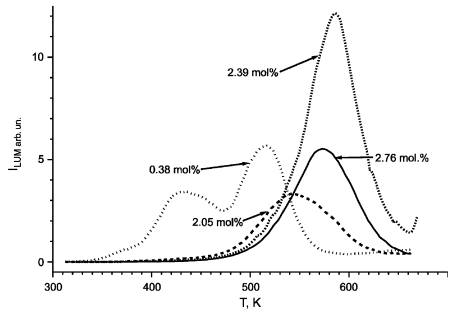


Fig. 1. TL curves after 0.25 Gy irradiation for different concentrations of Mn in $CaF_2$.

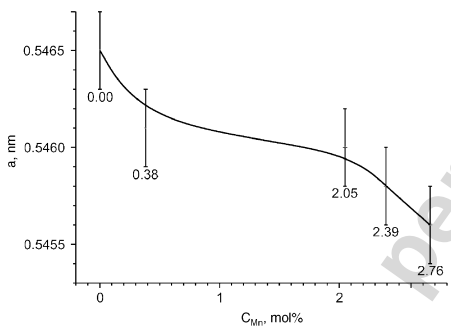


Fig. 2. Crystal lattice constant of $CaF_2$:Mn versus Mn concentration.

some ordered clusters when the concentration of Mn increases. This could be a preliminary stage of manganese falling out of a solid solution. X-ray diffraction analysis has not revealed separate phases of Mn-containing substances. However, the lattice constant decreases slightly but systematically when the concentration of $Mn^{2+}$ ions increases (see Fig. 2). This can be explained by substituting $Ca^{2+}$ ions by smaller $Mn^{2+}$ ions (the ionic radii of 8-coordinate $Mn^{2+}$ and $Ca^{2+}$ are 0.110 and 0.126 nm, respectively, see http://www.webelements.com). The stoichiometry analysis has not revealed any changes in the occupancies of Ca and F atoms in the lattice, the only exception being the sample with the highest concentration of $Mn^{2+}$ (2.76 mol%). The best fit between the observed and calculated diffraction pattern has been obtained for this sample with the occupancy of Ca equal to 0.88(±0.05) and the occupancy of F equal to 0.85(±0.05). This sample demonstrates also a TL peak of a lower intensity with the maximum situated at a lower temperature when compared with the sample with 2.39 mol% of Mn. This indicates that the Mn concentration of 2.76 mol%

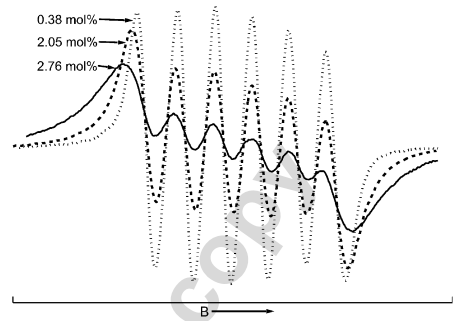


Fig. 3. EPR spectra of $Mn^{2+}$ for different concentrations of Mn in $CaF_2$.

lies close to the threshold of the solid solution decomposition. $Mn^{2+}$–$F^-$ distances in different fluoride compounds with hexahedral coordination of Mn were studied by Barriuso and Moreno, 1984. The distances $Mn^{2+}$–$F^-$ are usually smaller than $Ca^{2+}$–$F^-$ distance in $CaF_2$, hence, the $Mn^{2+}$ substitution for $Ca^{2+}$ causes stress and distortions in the $CaF_2$ lattice: $Ca^{2+}$–$F^-$ distances are decreased and $Mn^{2+}$–$F^-$ distances are increased against their usual values. These lattice deformations terminate the amount of manganese in the $CaF_2$:Mn solid solution. Also, the lattice stress affects the activation energies of the traps involved in TL.

The increasing displacement of $F^-$ ions caused by $Mn^{2+}$ also affects the EPR spectrum of $Mn^{2+}$. The EPR studies of $CaF_2$:Mn have a long history (Lay and Nolle, 1967; Garifullina and Stepanov, 1973; Gehlhoff and Ulrici, 1980; Kuroda et al., 2001). The superhyperfine structure (SHFS) caused by eight closest to $Mn^{2+}$ $^{19}F$ nuclei can be only resolved in single crystals. In our powder samples, the hyperfine structure from $^{55}Mn$ is observed, while a SHFS of $^{19}F$ nuclei is averaged through different orientations of the microscopic crystals, and thereby causes a uniform broadening of the EPR lines. Due to the displacement of $Mn^{2+}$ and $F^-$ ions at increasing Mn concentrations, the average distance between $Mn^{2+}$ and $F^-$ decreases, and the interaction with $^{19}F$ nuclei becomes stronger. This makes SHFS stronger and causes extra broadening of the averaged EPR lines compared with the broadening raised by the dipole–dipole interaction. The broadening of the EPR lines of $Mn^{2+}$ is illustrated in Fig. 3 for three different concentrations of manganese.

We have studied the EPR spectra of the samples irradiated with different radiation doses, up to 400 Gy. Radiation has been proved to produce no effect on the amount of $Mn^{2+}$ in $CaF_2$:Mn. This means that the energy storage cannot be explained by charge transformations of $Mn^{2+}$. Moreover, we have studied the effect of well-known quenching impurities (Co, Ni, Fe) on the storage characteristics of $CaF_2$:Mn. These impurities have not demonstrated any quenching effect on either energy storage or release. The only influence they exert on the thermoluminophor is the reduction of the manganese concentration

Author's personal copy

due to concurrent co-precipitation. This causes the TL curve to become wider towards low temperatures and to show peaks typical for lower concentrations of Mn. The absence of non-linear quenching effects as well as the absence of charge transformations of $Mn^{2+}$ makes recombination models for the energy storage and transfer untenable. Hence, the process of energy storage should be explained with some intracentre mechanism.

The study of the optical absorption and excitation spectra of $\gamma$-irradiated $CaF_2$:Mn single crystals (Mathur et al., 1986) has revealed radiation-induced absorption bands. F-centre formation near $Mn^{2+}$ was suggested to explain the observed data (Mathur et al., 1986; Allen and McKeever, 1990). We suppose that an F-centre and a $V_K$-centre appear together near manganese due to the displacement of an F-anion into the interstitial position. These complex defects would disappear rapidly at room temperature when they occur in regions of $CaF_2$ lattice free of impurities. However, when these defects are formed in a pair near $Mn^{2+}$, the lattice strains induced by the impurity exert a partial relaxation. Then, the electron–hole interaction causes an exciton-like state to be formed near $Mn^{2+}$. Both electron–hole coupling energy and lattice stress relaxation increase the thermal stability of the radiation-induced complex defect. So, after a partial relaxation, the energy stored near manganese freezes. This energy can be transferred to manganese only after a thermal activation or under UV stimulation. Optically stimulated luminescence for $CaF_2$:Mn has been studied and reported earlier (Allen and McKeever, 1990; Jaek et al., 2002).

The suggested model explains most of the observed experimental data. The highest thermal stability of defects and highest temperature of TL peak maximum occur at a highest possible concentration of manganese, which lies still below the threshold of decomposition of the solid solution. This concentration corresponds to a maximal possible extent of the lattice stress induced by $Mn^{2+}$.

## 4. Conclusive remarks

Our aim was to find the optimal concentration of the doping agent (Mn) in $CaF_2$. This concentration should be low enough to keep a solid solution far from the decomposition threshold, and also, should be high enough to obtain a single high-temperature TL peak of sufficiently high intensity. The actual amount of manganese in $CaF_2$:Mn is influenced by the concentration of manganese in the initial solution as well as by the conditions of co-precipitation. So, the amount of manganese in the co-precipitate is affected by the factors like the rate of adding the solutions into the reaction vessel, the ratio of calcium and fluoride ions, and also the ageing time. The amount of manganese in the precipitate versus the ratio of $Ca^{2+}$:$F^-$ is shown in Table 1.

The excess of $F^-$ ions and a longer ageing time increase the amount of co-precipitated manganese. In order to obtain a co-precipitate of $CaF_2$–$MnF_2$ in the form of fine microscopic crystals, one should add the solutions into the reaction vessel very slowly. The most suitable rates of adding solutions were the following: $CaCl_2$—2.5 ml/min, HF—2.8 ml/min. Ageing time of 2 h appears to be sufficient, as the amount of manganese in the co-precipitate does not increase when the ageing time is increased above 2 h. The optimum concentration of the manganese in the co-precipitated precursor is found to be about 2.1–2.5 mol%. It decreases only slightly after the final firing of the precursor.

Table 1
Dependence of co-precipitated Mn on the $Ca^{2+}$ to $F^-$ ratio[a]

| Conc. of $Mn^{2+}$ in the initial solution (mol%) | Ratio of concentrations, $[Ca^{2+}]$:$[F^-]$ | Concentration of $Mn^{2+}$ in the co-precipitate (mol%) |
|---|---|---|
| 0.262 | 1:2.5 | 2.32 |
| 0.262 | 1:2.2 | 1.59 |
| 0.262 | 1:1.9 | 1.07 |
| 0.262 | 1:1.7 | 0.49 |

[a]Solutions were added at a rate of 2.4 $cm^3$/min, ageing time was 3 h.

The manganese content in commercial $CaF_2$:Mn (TLD 400) is about 4.3 mol%. TLD materials with still higher concentration of manganese were also used, however, in routine applications they are closed in glass ampoules or covered with protective enamels. In our opinion, extra-high concentration of manganese complicates routine work with this material making it unstable due to the oxidation of manganese in the air and due to the decomposition of a solid solution during cycled readouts.

## Acknowledgements

Financial support from Estonian Scientific Foundation is acknowledged gratefully (Grants GFKKM 5198 and GFKKM 5779). We are also thankful to the Cancer Clinic of the University of Tartu for the help with a high-dose $\gamma$-irradiation of the samples.

## References

Allen, P., McKeever, S.W.S., 1990. Studies of PTTL and OSL in TLD-400. Radiat. Prot. Dosim. 33, 19–22.

Allsalu, M.-L.J., Kilk, I.R., Kuus, H.J., Lust, A.L., Pedak, E.J., 1980. Method of preparation of thermoluminophor based on doped with manganese calcium fluoride. Inventors certificate of SU No. 749085.

Alonso, P.J., Alcala, R., 1981. Excitation spectra and fluorescent lifetime measurements of $Mn^{2+}$ in $CaF_2$ and $CdF_2$. J. Lumin. 22, 321–333.

Barkyoumb, J.H., Mansour, A.N., 1992. Electronic and atomic structure of Mn-doped $CaF_2$: an X-ray-absorption near-edge structure and extended X-ray-absorption fine-structure study. Phys. Rev. B. 46 (14), 8768–8776.

Barriuso, M.T., Moreno, M., 1984. Investigation of the $Mn^{2+}$–$F^-$ distance for $Mn^{2+}$ in fluoride lattices with hexahedral coordination. Chem. Phys. Lett. 112 (2), 165–168.

Garifullina, R.L., Stepanov, V.G., 1973. Exchange interaction-coupled $Mn^{2+}$ pairs in $CaF_2$ and $SrF_2$. Sol. State Phys. 15 (7), 2169–2172 (in Russian).

Gehlhoff, W., Ulrici, W., 1980. Transition metal ions in crystals with the fluorite structure. Phys. Stat. Sol. (b) 102, 11–59.

Jaek, I., Kerikmäe, M., Lust, A., 2002. Optically stimulated luminescence of some thermoluminescent detectors as an indicator of absorbed dose. Radiat. Prot. Dosim. 100 (14), 459–462.

Kalchgruber, R., Göksu, H.Y., Hochhäuser, E., Wagner, G.A., 2002. Monitoring environmental dose rate using Riso TL/OSL readers with built-in sources: recommendations for users. Radiat. Meas. 35, 585–590.

Author's personal copy

Kerikmäe, M., 2004, Some luminescent materials for dosimetric applications and physical research. Ph.D. Thesis, University of Tartu.

Kuroda, S., Marumoto, K., Kihara, H., Ofuchi, H., Tabuchi, M., Takeda, Y., Banshchikov, A.G., Sokolov, N.S., Yakovlev, N.L., 2001. Electron spin resonance study of low-dimensional magnetic properties of $MnF_2$–$CaF_2$ superlattices. Jpn. J. Appl. Phys. 40, L1151–L1153.

Lay, F.M., Nolle, A.W., 1967. Paramagnetic resonance and relaxation and dielectric loss in $CaF_2$ crystals containing $Mn^{2+}$, $OH^-$ and oxygen. Phys. Rev. 163 (2), 266–275.

Lust, A., 1997. Method of synthesis of $CaF_2$:Mn thermoluminescent material and detectors. M.Sc. Thesis, University of Tartu.

Lust, A., Paama, L., Kerikmäe, M., Must, M., Perämäki, P., 2002. Determination of manganese in thermoluminescent materials by inductively coupled plasma atomic emission spectrometry and spectrofotometry. Proc. Estonian Acad. Sci. Chem. 51 (2), 126–133.

Mathur, V.K., Abbundi, R.J., Brown, M.D., McKeever, S.W.S., 1986. Radiation induced defects in Mn doped $CaF_2$. Radiat. Effects 99, 9–14.

Mändar, H., Felsche, J., Mikli, V., Vajakas, T., 1999. AXES 1.9: new tools for estimation of crystallite size and shape by Williamson–Hall analysis. J. Appl. Crystallogr. 32, 345–350.

McMasters, D.W., Jassemnejad, B., McKeever, S.W.S., 1987. Some observations regarding the effects of background rare-earth impurities on the thermoluminescence and optical absorption of $CaF_2$–Mn. J. Phys. D 20, 1182–1187.

Rodriguez-Carvajal, 1997. J. FULLPROF version 3.5. Laboratoire Leon Brillouin (CEA-CNRS), F-91191 Gif sur Yvette, France.

Schulman, J.R., Ginther, R.J., Kirk, R.D., Goulart, H.S., 1960. Thermoluminescent dosimeter. His storage, stability, linearity. Nucleonics 18, 92–102.

Vehl, D., Muron, D.I., Suijka, R.R., Vehar, D.W., Lorence, L.I., Westfall, R.L., Jones, S.C., Sweet, I.A., Braunlich, P., 1994. Characterization of a two-dimentional, thermoluminescent, dosemapping system: uniformity, reproducibility and calibrations. Rev. Sci. Instrum. 65, 3243–3251.

Zarate-Morales, A., Buentil, A.E., 1996. Environmental gamma-dose measurements in Mexico-City using TLD. Health Phys. 71, 358–361.

Author's personal copy

# IV

Magnetic manifestations of thermoluminescence excitation in $CaF_2$:Mn (TLD-400).
Danilkin, M.; Kirillov, A.; Klimonsky, S.; Kuznetsov, V.; Lust, A.; Mändar, H.;
Seeman, V. *Rad. Meas.*, **2007** (available online at
http://dx.doi.org/10.1016/j.radmeas.2007.01.079).

ARTICLE IN PRESS

Available online at www.sciencedirect.com

ScienceDirect

Radiation Measurements

Radiation Measurements ▮▮▮ (▮▮▮▮) ▮▮▮–▮▮▮

www.elsevier.com/locate/radmeas

# Magnetic manifestations of thermoluminescence excitation in $CaF_2$:Mn (TLD-400)

Mikhail Danilkin[a,*], Aleksei Kirillov[a], Sergei Klimonsky[b], Vyacheslav Kuznetsov[b], Aime Lust[a], Hugo Mändar[a], Vladimir Nikiforov[c], Arno Ratas[a], Aleksandr Ruchkin[c], Viktor Seeman[a]

[a]*University of Tartu, Faculty of Physics and Chemistry, Tähe 4-101, Tartu 51010, Estonia*
[b]*Mendeleyev University of Chemical Technology of Russia, Miusskaya Sqr. 9, Moscow, Russia*
[c]*Moscow State University, Department of Low-Temperature Physics and Superconductivity, 119899, Moscow, Russia*

Received 17 December 2006; accepted 31 January 2007

**Abstract**

Magnetic susceptibility as a function of temperature (4–250 K) and EPR spectra at room temperature were studied for thermoluminescence detectors (TLD) $CaF_2$:Mn with either stored dose information or cleaned dose by annealing. No essential variations of $Mn^{2+}$ number in detectors were found due to dose storage; however, the exchange interactions between manganese ions are observed as deviations from Curie–Weiss law. These deviations are removed when samples are irradiated with high doses (250–500 Gy) and appear again after dose annealing. The effect is regarded as indirect evidence of trapped exciton formation in the close vicinity of $Mn^{2+}$ impurity, with the exchange interaction being destroyed by fluorine displacement from regular lattice position. The unusually high stability of trapped at impurity excitons is explained by partial relaxation of lattice distortion caused by substitution of $Ca^{2+}$ with a smaller $Mn^{2+}$.
© 2007 Elsevier Ltd. All rights reserved.

*Keywords:* Solid-state detectors; Thermoluminescence; Calcium fluoride; Manganese; Exchange interactions in clusters

## 1. Introduction

TLD material $CaF_2$:Mn is important for measuring extreme doses, due to its linear responsibility in very wide range of doses. However, the mechanism of energy storage and release in this material is not still clear in detail. The dependence of the thermoluminescence (TL) curve for $CaF_2$:Mn on the manganese concentration has been discussed in our previous paper (Danilkin et al., 2006). The substitution of calcium in $CaF_2$ with smaller divalent manganese, which has more covalent chemical bonds, causes both local distortions of crystal lattice around manganese and also small but detectable decrease in lattice constant. The higher the concentration of Mn, the larger are the displacements of fluoride ions around Mn. We have supposed that the displacement of fluorine towards $Mn^{2+}$ causes extra broadening of $Mn^{2+}$ EPR lines due to increased unresolved super hyperfine structure from $^{19}F$ nuclei. The TL curve becomes more uniform with increasing manganese concentration up to solid solution decomposition, and also the main TL curve maximum occurs at higher temperature. Summarising these facts, and also the fact of $Mn^{2+}$ concentration being unchanged after irradiation of samples with high doses, we have suggested that the energy is stored in the vicinity of $Mn^{2+}$ in a form of exciton. Radiation-induced displacement of one of fluorine in the vicinity of Mn causes a pair of $V_K$ centre and F centre to appear. The pair of defects keeping both electron and hole is immediately transformed into exciton. This model was developed for self-trapped excitons (STE) (e.g., Lindner et al., 2001). However, STE have very short lifetimes in pure $CaF_2$ and cannot explain the energy storage effects. The unusually increased stability of trapped excitons in our case can be explained by partial relaxation of the distorted lattice in the vicinity of $Mn^{2+}$. The higher the concentration of Mn, the larger are local distortions of crystal lattice, and hence, the deeper relaxation occurs when a metastable state with stored energy is formed through a trapped exciton.

* Corresponding author. Tel.: +372 7 375253; fax: +372 7 375264.
*E-mail address:* danilkin@ut.ee (M. Danilkin).

1350-4487/$ - see front matter © 2007 Elsevier Ltd. All rights reserved.
doi:10.1016/j.radmeas.2007.01.079

Please cite this article as: Danilkin, M., et al., Magnetic manifestations of thermoluminescence excitation in $CaF_2$:Mn (TLD-400). Radiat. Meas. (2007), doi: 10.1016/j.radmeas.2007.01.079

To verify the model by EPR, one should observe the disturbed $Mn^{2+}$ centres which appear after storing dose information. It is difficult to characterise these low-symmetry centres without single crystals so essential for effective EPR studies. However, the crystal growth of $CaF_2$ with large Mn concentration would be a heavy task, regarding noticeable lattice distortions caused by Mn impurity. We have obtained another indirect evidence of this model by studying the deviations of magnetic susceptibility from Curie–Weiss law.

## 2. Experimental

The samples were prepared by co-precipitating $MnF_2$ together with $CaF_2$ and subsequent firings of luminophor in air at 673 K, and then in protecting inert gas atmosphere at 1423 K, as described in our previous work (Danilkin et al., 2006). The tablets were cold-pressed from powder, with precautions against pressing-out manganese impurity (the effect is known at high Mn concentrations and high pressure applied). The actual concentrations of Mn both in tablets and powder samples were checked by spectrophotometric analysis (the details are presented by Lust et al., 2002).

EPR studies were performed at room temperature with X-band EPR spectrometer (8.87 GHz, 100 kHz magnetic field modulation).

The samples were irradiated with a $^{60}Co$ gamma-radiation source (doses from 10 to 500 Gy), and also with X-ray tube (45 kV, 16 mA, W-anode, doses above 2000 Gy). Smaller doses (0.1–1.0 Gy) were given using reference irradiator 6527B (Sweden), equipped with $^{90}Sr/^{90}Y$ source.

Magnetic susceptibility of TLD tablets was measured using quantum magnetometer equipped with superconductive magnet and superconductive screen (device is assembled and operating at Physics Chair of D. Mendeleev University of Chemical Technology of Russia). The thermal insulation of sample from liquid He environment makes the measurements possible in a wide range of temperatures (2–350 K).

## 3. Results and discussion

There were no variations of EPR signal of $Mn^{2+}$ detected when the samples were irradiated with doses 10–500 Gy. The small degradation of $Mn^{2+}$ spectrum intensity occurs after irradiation with doses above 2500 Gy. This degradation is accompanied with increase in the intensity of somewhat weak additional spectrum of low-symmetry centres observed around the main six lines of $Mn^{2+}$. Probably, these are low-symmetry $Mn^{2+}$ centres one would expect to see after dose storage, however, it is very difficult to say something about these centres, because the observed spectrum is too weak and composed of broad orientation-averaged lines in powder samples. One needs single crystals for effective studies of the nature of the observed object.

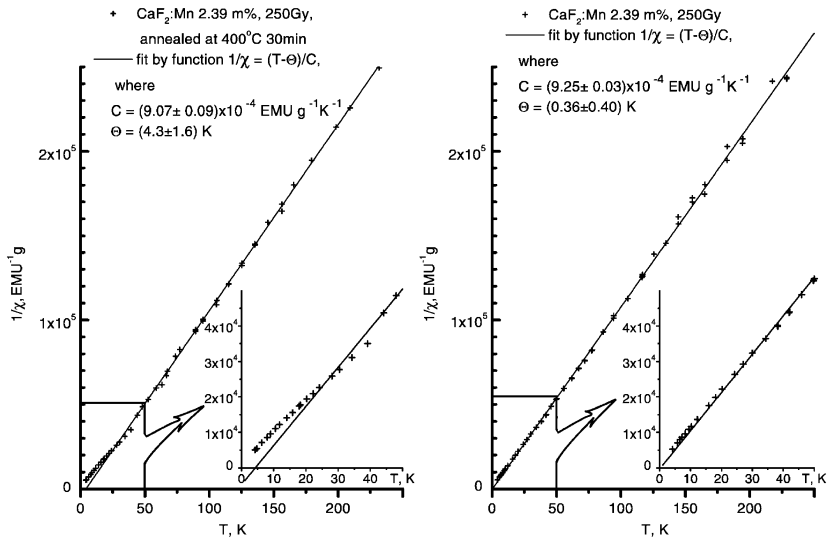


Fig. 1. Inverse magnetic susceptibility versus temperature. Deviations from Curie–Weiss law are observable at low temperatures when sample is annealed after irradiation, while there are practically no deviations in the sample irradiated with a dose of 250 Gy.

Please cite this article as: Danilkin, M., et al., Magnetic manifestations of thermoluminescence excitation in $CaF_2$:Mn (TLD-400). Radiat. Meas. (2007), doi: 10.1016/j.radmeas.2007.01.079

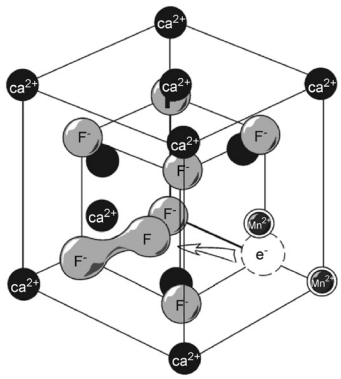


Fig. 2. A schematic model of relative positions of two $Mn^{2+}$ and exciton trapped near $Mn^{2+}$ impurity ions.

On the other hand, magnetic susceptibility studies demonstrated an interesting radiation effect: the exchange interactions between $Mn^{2+}$ ions observed as deviations from Curie–Weiss law could be removed by irradiation with dose of 250–500 Gy and restored back by dose annealing (see Fig. 1). To explain the observed effect, one could suppose that fluoride ions are transferring magnetic exchange interaction between $Mn^{2+}$ ions. The exchange between $Mn^{2+}$ is destroyed when irradiation of samples causes the displacement of fluorine from its regular sites. The displacement of fluorine into interstitial position is the first step of exciton formation (Lindner et al., 2001). While STE has very short lifetime in a perfect lattice, the exciton trapped near Mn impurity would be stabilised due to partial relaxation of lattice distortions caused by Mn impurity. The higher the Mn concentration, the more stable are trapped in the vicinity of Mn excitons due to increased relaxation of distorted lattice. This model could explain the increase of shift of TL peak position towards the higher temperatures with the increase of Mn concentration up to a threshold of solid solution decomposition (Danilkin et al., 2006). Actually, there are two superimposed effects. $Mn^{2+}$ is distributed in $CaF_2$ lattice non-uniformly. It is clustered into certain configurations, depending on the solid solution proportions. Transition from one cluster configuration to another is accompanied with very abrupt changes in TL curve structure, while accretion of the same type clusters causes only smooth changes in existing trapping energies. The observed deviations from Curie–Weiss law are also different in the case of different cluster configurations. However, the details of magnetic interactions will be reported later.

The model of trapped near $Mn^{2+}$ exciton is represented schematically in Fig 2. Chosen positions of two $Mn^{2+}$ ions substituting for $Ca^{2+}$ have to show as the contiguous to both $Mn^{2+}$ fluoride-ion (and thus capable to transfer magnetic exchange) has been removed at excitation. The relative positions of two $Mn^{2+}$ ions and exciton shown in Fig. 2 represent not the only but one of possible configurations. Both two $Mn^{2+}$ and trapped exciton will occupy rather different positions depending on Mn concentration, with trapping energy being determined by those relative positions of defects. The closer $Mn^{2+}$ impurities are one to another, the stronger are lattice distortions, and hence, the excited lattice exerts more relaxation when exciton is created. So, one would expect an increase of exciton bound energy at the expense of lattice relaxation when the concentration of Mn increases. This model explains both abrupt changes in the TL curve (transition from one configuration to another) and relatively small shifts of existing TL maxima (accumulation of the lattice strains).

## Acknowledgements

Financial support from Estonian Scientific Foundation is acknowledged gratefully (Grants GFKKM 5198 and GFKKM 5779). We are also thankful to Nina Melnikova for her help with data treatment.

## References

Danilkin, M., Lust, A., Kerikmäe, M., Seeman, V., Mändar, H., Must, M., 2006. $CaF_2$:Mn extreme dosimeter: effects of Mn concentration on thermoluminescence mechanisms and properties. Radiat. Meas. 41, 677–681.

Lindner, R., Williams, R.T., Reichling, M., 2001. Time-dependent luminescence of self-trapped excitons in alkaline earth fluorides excited by femtosecond laser pulses. Phys. Rev. B 63, 075110.

Lust, A., Paama, L., Kerikmäe, M., Must, M., Perämäki, P., 2002. Determination of manganese in thermoluminescent materials by inductively coupled plasma atomic emission spectrometry and spectrophotometry. Proc. Estonian Acad. Sci., Chem. 51 (2), 126–133.

Please cite this article as: Danilkin, M., et al., Magnetic manifestations of thermoluminescence excitation in $CaF_2$:Mn (TLD-400). Radiat. Meas. (2007), doi: 10.1016/j.radmeas.2007.01.079

$Eu^{2+}$ and $Eu^{3+}$ centers formation at synthesis of $CaF_2$:Eu luminophors. Danilkin, M.I.; Beloussov, A.P.; Klimonsky, S.O.; Kuznetsov, V.D.; Lust, A.L.; Nikiforov, V.N.; Paama, L.N.; Rammo, I.H.; Seeman, V.O. (submitted for publication to *Journal of Applied Spectroscopy, Minsk*).

# Формирование центров $Eu^{2+}$ и $Eu^{3+}$ при синтезе $CaF_2$:Eu люминофоров.

М.И. Данилкин*[1], А.П. Белоусов[1], С.О. Климонский[2], В.Д. Кузнецов[2], А.Л. Луст[1], В.Н. Никифоров[3], Л.Н. Паама[1], И.Х. Раммо[1]. В.О. Сееман[1]

[1]Физико-химический факультет Тартуского университета, 51010, ул. Тяхе 4-101, Тарту, Эстонская республика

[2]Факультет естественных наук РХТУ им. Д.И. Менделеева, 125047 Миусская пл.9, Москва А-47, Российская Федерация

[3]Кафедра физики низких температур и сверхпроводимости Физического факультета МГУ им. М.В. Ломоносова, Ленинские Горы, Москва 119899, Российская Федерация

Исследовалось влияние методов синтеза $CaF_2$:Eu люминофоров на зарядовое состояние европия. Показано, что $Eu^{3+}$ преобладает над $Eu^{2+}$ в образцах, полученных путем соосаждения европия со фторидом кальция, причем отношение $Eu^{3+}/Eu^{2+}$ растет с увеличением общего количества европия. Частичная перезарядка европия происходит во время прокаливания образцов из-за изменения баланса избыточного фтора. Проведены иссследования люминесценции, магнитной восприимчивости и ЭПР синтезированных образцов. Показано, что европий образует в твердом растворе крупные упорядоченные кластеры, определяющие как люминесцентные, так и магнитные свойства материала.
Ключевые слова: Фторид кальция, европий, люминесценция, магнитная восприимчивость, ЭПР, обменные взаимодействия.

# $Eu^{2+}$ and $Eu^{3+}$ centres formation at synthesis of $CaF_2$:Eu luminophors.

M.I. Danilkin*[1], A.P. Beloussov[1], S.O. Klimonsky[2], V.D. Kuznetsov[2], A.L. Lust[1], V.N. Nikiforov[3], L.N. Paama[1], I.H. Rammo[1], V.O. Seeman[1]

[1]Faculty of Physics and Chemistry of the University of Tartu, 51010 Tähe 4-101, Tartu, Estonian Republic

[2]Faculty of Natural Sciences of Mendeleev' University of Chemical Technology of Russia, 125047 Miusskaya pl. 9, Moscow A-47, Russia

[3]Department of Low Temperature Physics and Superconductivity, Physics Faculty M.V. Lomonosov Moscow State University, Leninskie Gory, Moscow 119899 Russia

The influence of synthesis methods on the charge state of europium in $CaF_2$:Eu luminophors has been studied. $Eu^{3+}$ is shown to prevail over $Eu^{2+}$ in the samples obtained by co-precipitaion of europium together with calcium fluoride, the $Eu^{3+}/Eu^{2+}$ ratio increasing at the increase of total europium amount. Partial charge transformation of europium takes place at annealing of samples due to the changes of extra fluorine balance. Luminescence, magnetic susceptibility and EPR studies of the synthesized samples were carried out. Europium is shown to constitute large orderd clusters in the solid solution affecting both luminescent and magnetic properties of the material.

Key words: Calcium fluoride, europium, luminescence, magnetic susceptibility, EPR, excange interactions.

## ВВЕДЕНИЕ

История исследования $CaF_2$:Eu люминофоров насчитывает уже много лет. Поглощение и люминесценция $Eu^{2+}$ в кристаллах $CaF_2$ исследовались еще Феофиловым [1], а в наши дни промышленные монокристаллические сцинтилляторы $CaF_2:Eu^{2+}$ применяются даже в таких экзотических областях, как поиск темной материи [2]. Тем не менее, наиболее детальные или же самые недавние исследования посвящены свойствам либо двухзарядного [3,4], либо трехзарядного [5,6] европия по отдельности, а также двухфотонным процессам на двухзарядном европии в $CaF_2$ [7]. Зарядовые превращения европия в $CaF_2$ исследовались только в связи с попытками объяснения механизма термолюминесценции [8], а также в связи с изучением роли кислорода как компенсатора заряда трехзарядных примесей. В то же время, совсем недавно появились сообщения о выращенном монокристалле смешанного фторида кальция и европия [9], где содержится 35% европия, причем только в состоянии $Eu^{3+}$. Эти монокристаллы не содержат кислорода в качестве компенсатора заряда, и предлагаются в качестве нового сцинтилляционного материала для детекторов рентгеновского излучения в системах безопасности и, возможно, для медицинских применений. Высокое содержание европия и довольно сложная процедура выращивания бескислородных монокристаллов существенно удорожают этот материал. Керамический материал с похожими свойствами и гораздо меньшим содержанием европия может оказаться недорогой альтернативой с большими шансами на практическое применение. Поэтому управление зарядовым состоянием европия при синтезе $CaF_2$:Eu люминофоров представляет практический интерес. Настоящая работа посвящена не только вопросу синтеза люминофоров с заданным состоянием европия и структурой центров люминесценции, но также проблемам и методам исследования европия в разных зарядовых состояниях,

поскольку мы столкнулись с интересными фундаментальными аспектами поведения европия во фториде кальция. В работе сопоставляются результаты, полученные методами измерения люминесценции, ЭПР и магнитной восприимчивости образцов $CaF_2$:Eu.

## ТЕХНИКА ЭКСПЕРИМЕНТА

Исследованные образцы подразделяются на две группы по способу приготовления. Одна группа изготовлена путем механического смешивания $CaF_2$ (о.с.ч. 6-2) и $Eu_2(CO_3)_3$ с последующим прокаливанием шихты при температуре 1173 K либо 1373 K в атмосфере особо чистого азота (99.999%) в течение 45 минут. В этих образцах концентрация европия варьировалась от 0.0257 до 0.1028 ат.% (0.05-0.20 вес.%). Содержание европия в готовых люминофорах этой группы не анализировалось, поскольку европий при прокаливании не улетучивается. Вторая группа образцов была приготовлена путем соосаждения основания люминофора вместе с активатором при реакции в растворе. Реакция проводилась в специально сконструированном сосуде из фторопласта-4. Маточный раствор в сосуде был подкислен HCl, вода использовалась трижды дистиллированная. В реакционный сосуд непрерывно и с заданной скоростью подавались с помощью перистальтических насосов разбавленные растворы $NH_4F$ и $CaCl_2$, причем в последний добавляли $Eu_2(CO_3)_3$ и тоже подкисляли HCl до растворения карбоната европия. В ряде случаев (образцы с нечетными номерами) карбонат европия вводили также и в маточный раствор, где он растворялся благодаря кислой среде. Во время реакции раствор в сосуде перемешивался фторопластовой мешалкой, а сосуд подогревался водяным паром. По завершении подачи реагентов осадок подвергали старению в маточном растворе в течение 2 часов. После старения осадок отделяли декантированием, промывали, снова декантировали и сушили, после чего проводили предварительный отжиг на воздухе при температуре 673 K в течение 2 часов. Температура предварительного отжига выбиралась так, чтобы она оказывалась недостаточной для внедрения во фторид кальция следов кислорода, но достаточной для надежного удаления всех следов кислот. Затем, аналогично первой группе образцов, шихта помещалась в тигель из стеклоуглерода и прокаливалась при 1373 K в течение 45 минут в атмосфере особо чистого азота. Концентрация европия во второй группе образцов варьировалась в растворах от 0.1028 ат.% до 0.3084 ат.% (0.2-0.6 вес.%), причем в нечетных образцах указанное количество европия вводилось и в маточный, и в подаваемый раствор, что удваивало введенную концентрацию. Фактическая же концентрация европия в шихте и в готовом люминофоре отличалась от вложенной, происходило значительное ее увеличение в процессе соосаждения. Поэтому реальную концентрацию европия в готовых образцах

определяли методом атомно-эмиссионного анализа с индукционно-связанной плазмой (ICP-AES). Методика анализа подробно изложена в работе [10]. Ниже дана сводная таблица исследованных образцов (Таблица 1).

Люминесценция образцов исследовалась с помощью люминесцентного спектрофотометра Hitachi 650-60, состоящего из двух одинаковых монохроматоров: один – для канала возбуждения, другой – для канала люминесценции (200-850 нм, 1.5 нм разрешение). Источник света – дуговая ксеноновая лампа мощностью 150 Вт. Прибор сопряжен с компьютером для непосредственного приема данных, с дискретизацией не хуже 12-13 двоичных разрядов. Спектры измерялись при комнатной температуре. Использовалось внутрицентровое возбуждение, 350 нм для $Eu^{2+}$ и 392 нм для $Eu^{3+}$. Для получения спектров люминесценции с более высоким спектральным разрешением применялся монохроматор МДР-6 (ЛОМО) с ФЭУ-100, с возбуждением образцов ртутной лампой постоянного тока СВД-305-3. Коротковолновая часть спектра лампы в окрестности линии ртути 365 нм выделялась фильтром УФС-6. Для уменьшения рассеянного возбуждающего света перед монохроматором ставился фильтр ЖС-18. При используемых в эксперименте щелях разрешение было не хуже 0.7 нм.

Магнитные измерения проводились с помощью квантового магнитометра, собранного на кафедре физики РХТУ [11]. Образцы для измерений запаивались в кварцевые ампулы, имевшие тонкую перегородку ниже средней части. Нижняя часть ампулы вакуумировалась и отпаивалась, затем образец осторожно насыпался на перегородку и тоже отпаивался под вакуумом. Вклад перегородки в отсчет был диамагнитным, но из-за малой толщины перегородки и высокой чистоты кварца пренебрежимо малым, и поэтому не учитывался. Для улучшения теплообмена ампулы насыщались гелием путем диффузии через кварцевые стенки при комнатной температуре. Возвратно-поступательное движение измеряемого образца между приемными петлями сверхпроводящего трансформатора магнитного потока осуществлялось с помощью пневмо-гидравлического привода. Образец при этом находился в антидьюаре, что позволяло измерять магнитную восприимчивость в широком диапазоне температур, от 4.2 K до 300 K. Измерения выполнялись при фиксированных значениях магнитного поля: для образца №3 – при 35.64 мТл; для №4 – при 71.21 мТл; для образцов №7,8,10 – при 65.67 мТл. Массы образцов были порядка 70 мг, что обеспечивало точность измерений восприимчивости не хуже $\pm 5*10^{-9}$ ед.CGS/г.

Спектры ЭПР измерялись на спектрометре X-диапазона с частотой 9.2 гГц и модуляцией магнитного поля 975 кГц. Измерения ЭПР проводились как при комнатной температуре, так и при температуре жидкого азота (77 K). Для определения g-фактора Eu2+ в качестве репера

использовался сигнал Cr3+ в кристалле MgO, который помещался в резонатор вместе с исследуемым образцом.

## РЕЗУЛЬТАТЫ И ОБСУЖДЕНИЕ

В спектрах люминесценции большинства образцов, полученных механическим смешиванием, присутствует только одна широкая полоса излучения $Eu^{2+}$, возбуждаемая при 350 нм. Максимум излучения немного, но систематически сдвигается в сторону более длинных волн с ростом концентрации европия, с 423 до 427.5 нм, что соответствует энергетическому сдвигу порядка 0.03 эВ. Интенсивность полосы люминесценции $Eu^{2+}$ растет с увеличением концентрации европия. В образцах, полученных путем соосаждения, ситуация с люминесценцией $Eu^{2+}$ иная. Интенсивность широкой полосы $Eu^{2+}$ начинает убывать с ростом общей концентрации европия, причем сильнее всего она уменьшается у образцов, где европий вводился одновременно и  в маточный раствор, и в подаваемый раствор хлорида кальция. Интенсивность люминесценции $Eu^{2+}$ в таких образцах всегда ниже, чем при введении европия только в подаваемый раствор, несмотря на вдвое большее количество вводимого европия. Положение максимума излучения для всех образцов, полученных путем соосаждения, приходится на 425-426 нм. При переходе к возбуждению 392 нм во всех этих образцах наблюдается линейчатый спектр $Eu^{3+}$. При этом возбуждении видна также широкая полоса люминесценции $Eu^{2+}$, что позволяет наглядно видеть, как с ростом концентрации европия уменьшается доля $Eu^{2+}$ и возрастает доля $Eu^{3+}$. Особенно эффективно образуется трехзарядный европий при одновременном введении активатора и в маточный раствор, и в добавляемый раствор $CaCl_2$. Семейство спектров люминесценции, записанных при возбуждении 392 нм для образцов №№1-5, представлено на Рис.1. На рисунке не показана люминесценция образца №10, у которого также наблюдался очень слабый линейчатый спектр $Eu^{3+}$. Обнаружение люминесценции $Eu^{3+}$ в одном из приготовленных путем механического смешивания образцов, причем в образце с наибольшим общим количеством европия, указывает на тенденцию увеличения доли трехзарядного европия в люминофорах с ростом общей его концентрации вне зависимости от метода и условий синтеза. Впрочем, условия синтеза оказывают сильное дополнительное влияние на соотношение концентраций $Eu^{2+}/Eu^{3+}$.

Запрещенные переходы трехзарядных редкоземельных ионов обладают высокой чувствительностью к симметрии окружения.  Поэтому структура излучательных переходов в спектре люминесценции $Eu^{3+}$ позволяет судить о симметрии и строении центров излучения. Наиболее чувствителен $Eu^{3+}$ к наличию или отсутствию инверсной симметрии. Самый общий

подход применительно к $Eu^{3+}$ был сформулирован Блассе [12]: при наличии инверсной симметрии будет преобладать магнитно-квадрупольный переход $^5D_0 – {}^7F_1$ вблизи 590 нм, а при отклонении от этой симметрии – электрические дипольные переходы $^5D_0 – {}^7F_J$, где J=2,4,6, расположенные в красной и инфракрасной области. При этом первый из дипольных переходов $^5D_0 – {}^7F_2$ оказывается интенсивнее всех прочих только если отклонение от инверсной симметрии незначительно. С первого взгляда на спектры люминесценции (Рис. 1) можно заключить, что центры с инверсной симметрией преобладают, а у центров с отклонением от инверсной симметрии эти отклонения значительные, поскольку переходы $^5D_0 – {}^7F_2$ и $^5D_0 – {}^7F_4$ имеют практически одинаковую интенсивность. Несколько удивляет схожесть относительных интенсивностей линий для всех образцов, что может косвенно указывать на формирование некоторой одинаковой структуры независимо от концентрации европия. В таблице 2 приводится отношение интенсивностей всех переходов к интенсивности магнитно-квадрупольного перехода $^5D_0 – {}^7F_1$ для каждого из пяти первых образцов. Небольшое отличие заметно лишь у образца №4, где спектр $Eu^{3+}$ самый слабый, и поэтому отличие может быть вызвано погрешностями при вычитании темнового сигнала. Детальный анализ структуры центров излучения $Eu^{3+}$ в $CaF_2$ и процессов их формирования проводился в работах [5,6,13] методами лазерной спектроскопии и последовательных отжигов образцов при разных температурах. Сопоставление наших спектров люминесценции с приведенными в работах [5,6] моделями позволяет отнести центры люминесценции к типам R и Q, то есть, к димерам, тройкам, или даже к более крупным кластерам, содержащим еще большее количество ионов $Eu^{3+}$. В приведенных на Рис. 1 спектрах отдельные линии не разрешаются, поэтому целесообразно обратиться как к спектрам возбуждения люминесценции (люминесценция регистрировалась для перехода $^5D_0$-$^7F_1$ около 590 нм), так и к спектрам люминесценции, снятым с более высоким разрешением (вкладка на Рис.1). Спектр возбуждения для образца №5 с максимальным содержанием трехзарядного европия приведен на Рис. 2. Показанный участок спектра содержит три группы линий, одновременное присутствие которых возможно лишь для парных, тройных или более сложных центров [5,6,13]. Спектр люминесценции этого же образца, снятый с более высоким разрешением, приведен на вкладке рисунка 1. Линии излучения $Eu^{3+}$ снова не удается полностью разрешить, но видна причина – их значительное уширение. Кроме того, можно видеть, что структура спектра несколько сложнее, чем можно было бы ожидать при простом суммировании спектров парных и тройных центров. Неоднородное уширение линий и сложная структура спектра позволяет предположить, что трехзарядный европий внедряется во фторид кальция неравномерно и образует крупные кластеры из большого числа ионов.

Возможно, структура этих кластеров близка к структуре недавно полученного кристалла $Ca_{0.65}Eu_{0.35}F_{2.35}$ [9], на что может указывать и общее сходство спектров люминесценции наших образцов и этого кристалла.

Значительная неоднородность распределения европия в $CaF_2$ проявляется особенно сильно в магнитных свойствах этих люминофоров. Закон Кюри-Вейсса хорошо выполняется только в низкотемпературном интервале, от 4.2 до 60 K (см. вкладку на Рис. 3). Согласно выражению $\chi(T) = \chi_0 + C/(T-\Theta)$ можно выделить независящую от температуры часть восприимчивости $\chi_0$ и парамагнетизм, связанный с ионами $Eu^{2+}$ (ионы $Eu^{3+}$ находятся при низких температурах в немагнитном состоянии $^7F_0$). При более высоких температурах количественный анализ кривых магнитной восприимчивости затруднен, так как отделить восприимчивость ионов $Eu^{2+}$ от быстро растущей при приближении к комнатной температуре восприимчивости $Eu^{3+}$ достаточно сложно. Ясно, однако, что растущая восприимчивость $Eu^{3+}$ должна была бы приводить к отклонению зависимостей $(\chi-\chi_0)^{-1}(T)$ вниз, между тем в действительности наблюдаются значительные отклонения вверх (Рис. 3). Высокотемпературные участки кривых характеризуются существенно меньшими значениями константы Кюри-Вейсса, чем низкотемпературные, и большими, порядка 150 K и даже больше, значениями парамагнитной температуры Кюри $\Theta$. Это может быть объяснено тем, что ионы $Eu^{2+}$ группируются в крупные упорядоченные образования, в составе которых они связаны сильным ферромагнитным обменным взаимодействием. Обменное взаимодействие, наряду с изменением постоянной кристаллической решетки в кластерах, может быть причиной замеченного нами сдвига максимума полосы излучения двухзарядного европия. Прояснить этот вопрос могли бы детальные исследования температурных зависимостей люминесценции. Интересно отметить, что отклонения от закона Кюри-Вейсса увеличиваются и обменное взаимодействие усиливается в образцах, содержащих значительное количество трехзарядного европия. Этот факт позволяет предложить механизм образования крупных кластеров, содержащих $Eu^{2+}$. Изначально шихта после соосаждения и предварительного прокаливания обладает лишь красной люминесценцией $Eu^{3+}$. После прокаливания шихты при высокой температуре часть европия восстанавливается. Дело в том, что компенсатором заряда для $Eu^{3+}$ служит междоузельный фторид-анион. Большинство парных и более сложных центров содержит один избыточный междоузельный фторид-анион на каждый такой сложный центр, поэтому существует механизм улучшения зарядового баланса с удалением лишнего фтора за счет усложнения структуры кластера и увеличения в нем числа ионов $Eu^{3+}$ [6,13]. При нарушении баланса фторид-анионов европий может легко

восстанавливаться до $Eu^{2+}$. При этом ионный радиус европия увеличивается, и его перемещение вдаль от кластера оказывается затруднено. Таков может быть путь образования сложных упорядоченных магнитных кластеров $Eu^{2+}$ в $CaF_2$. Интересно отметить, что избыток фтора действует совсем не однозначно. Лишь небольшой избыток фторид-анионов имеет окислительное действие на европий, тогда как значительный избыток фтора, наоборот, оказывает восстанавливающее действие. Аналогичное действие галогенов на европий наблюдалось ранее в сульфиде кальция [14]. Эта особенность позволяет управлять зарядовым состоянием европия в $CaF_2$.

При низких температурах величина постоянной составляющей магнитной восприимчивости $\chi_0$ может быть определена с небольшой погрешностью порядка 1-5%. Вклад в $\chi_0$ дают диамагнитная восприимчивость матрицы и парамагнетизм Ван-Флека ионов $Eu^{3+}$; с ростом количества $Eu^3$ величина $\chi_0$ возрастает. Для получения «чистого» вклада $Eu^{3+}$ в $\chi_0$ из значения $\chi_0$ мы вычли диамагнитную восприимчивость основного вещества, $CaF_2$. Однако расчет концентрации $Eu^{3+}$, выполненный по формуле для магнитной восприимчивости $Eu^{3+}$ в кристаллическом поле кубической симметрии [15], дает значительно завышенные значения его концентрации, превышающие общее количество европия в образцах. Это косвенно подтверждает, что $Eu^{3+}$ входит в состав сложных кластеров, поскольку известно, что низкосимметричное окружение приводит к повышению парамагнетизма Ван-Флека [16,17].

Можно сопоставить вклад $Eu^{3+}$ в $\chi_0$ и площадь S под его группой линий излучения около 590 нм для трех образцов:

№10: $\chi_0(Eu^{3+}) = 0.43 \times 10^{-6}$ ед.CGS/г и S=31 усл. ед.;

№4: $\chi_0(Eu^{3+}) = 1.14 \times 10^{-6}$ ед.CGS/г и S=54 усл. ед.;

№3: $\chi_0(Eu^{3+}) = 2.17 \times 10^{-6}$ ед.CGS/г и S=176 усл. ед.

Видно, что растут и интенсивность люминесценции $Eu^{3+}$, и $\chi_0$, но количественные пропорции не выполняются. Расхождение может быть связано именно с тем, что в упорядоченных кластерах ионы $Eu^{3+}$ вносят иной вклад в $\chi_0$, чем в случае высокосимметричных изолированных центров [16,17].

Спектры ЭПР $Eu^{2+}$ в $CaF_2$ исследовались ранее и в монокристаллах, и в порошках, но нередко разные исследователи приводят совершенно разные значения g-фактора и публикуют разные спектры [18,19]. Полученное нами значение 1.973±0.001 ближе всех к значению 1.971±0.001, полученному в работе [20]. Значение g-фактора получено нами из предположения, что центральная наиболее интенсивная изотропная линия спектра $Eu^{2+}$ (Рис. 4) обусловлена электронным переходом $m_S$=+1/2 — $m_S$=-1/2, причем сверхтонкая структура от ядер $^{151}Eu$ и

$^{153}$Eu не разрешается в порошке из-за усреднения. Расхождение значений, полученных разными авторами, связано, видимо, с сильным обменном взаимодействием, которое значительно искажает спектр ЭПР. При концентрации около 0.1 мол% даже в механически смешанных образцах изолированных ионов $Eu^{2+}$ уже больше не существует, а в случае превращения части трехзарядного европия из упорядоченных кластеров в двухзарядный ситуация еще более усложняется. Достаточно сравнить спектры ЭПР для образцов №10 и №3, приведенные на Рис.4. Обращает на себя внимание тот факт, что спектр простирается в широком диапазоне магнитных полей, где помимо усредненного спектра изолированных ионов $Eu^{2+}$ наблюдаются также спектры и ассоциированных с дефектами, и охваченных обменными взаимодействиями ионов $Eu^{2+}$. Заметим, что в спектре образца №10 еще присутствуют остатки сглаженной структуры, а у образца №3, полученного соосаждением, они уже почти не видны. У этого образца и отклонения магнитной восприимчивости от закона Кюри-Вейсса тоже более значительные, и преобладает в нем $Eu^{3+}$. Таким образом, именно трехзарядный европий провоцирует упорядоченную кластеризацию, оказываясь затем в случае восстановления до $Eu^{2+}$ вовлеченным в сильное обменное взаимодействие.

## ВЫВОДЫ

С ростом концентрации европия в $CaF_2$ начинает преобладать $Eu^{3+}$. Особенно мало двухзарядного европия образуется в образцах, полученных при соосаждении активатора, добавленного одновременно в раствор $CaCl_2$ и в маточный раствор. Баланс избыточного фтора играет важную роль, поскольку основным компенсатором заряда в отсутствие кислорода оказывается междоузельный фторид-анион. Механизм баланса избыточного фтора, основанный на удалении избытка фтора с увеличением количества $Eu^{3+}$ в составе сложного центра, способствует увеличению размера упорядоченных европиевых кластеров в $CaF_2$. Частичное восстановление европия до состояния $Eu^{2+}$ не сопровождается его удалением из упорядоченных кластерных образований, и поэтому двухзарядный европий во фториде кальция оказывается охвачен сильным обменным взаимодействием.

## БЛАГОДАРНОСТИ

Авторы выражают благодарность Н.А. Мельниковой за помощь в обработке данных. Финансовая помощь Эстонского Научного Фонда (грант 5779) также заслуживает благодарности.

## ЛИТЕРАТУРА


1. П.П. Феофилов. Опт. и спектр., 1(7) (1956) 992-1001
2. Y. Shimizu, M. Minowa, W. Suganuma, Y. Inoue. Phys.Lett. B633 (2006) 195-200
3. P. Kisliuk, H.H. Tippins, C.A. Moore, and S.A. Pollack. Phys. Rev. 171(2) (1968) 336-342
4. А.Е. Никифоров, А.Ю. Захаров, В.А. Чернышев, М.Ю. Угрюмов, С.В. Котоманов. ФТТ 45(5) (2003) 822-825
5. R.J. Hamers, J.R. Wietfeldt, J.C. Wright. J. Chem. Phys. 77(2) (1982) 683-692
6. Kathleen M. Cirillo-Penn, J.C. Wright. Phys. Rev. B41(15) (1990) 10799-10807
7. W. Kaiser, C.G.B. Garrett. Phys. Rev. Lett. 7 (1961) 229-231
8. S.M. Dhopte, P.L. Muthal, V.K. Kondawar, S.V. Moharil. J. Lumin. 54 (1992) 95-101
9. K. Shimamura, N. Shiran, A. Gektin, V. Voronova, V. Nesterkina, N. Ichinose, E. Villora, T. Shshido. Functional materials, 11(4) (2004) 676-679
10. L. Paama, E. Pärnoja, M. Must, P. Perämäki. J. Anal. At. Spectrom., 16 (2001) 1333-1336
11. В.Д. Кузнецов. Приборы и техника эксперимента, 4 (1985) 196-201
12. G. Blasse: in Luminescence of Inorganic Solids, edited by B. Di Bartolo, Plenum Press, New York and London (1978) 457-494
13. Kathleen M. Cirillo-Penn, J.C. Wright. J. Lumin. 48&49 (1991), 505-508
14. М. Данилкин, М, Муст, Э. Педак, Э. Пярноя, Г. Рясный, В. Семан, И. Шпиньков, Л. Шпинькова. ЖПС 62(3) (1995), 186-191
15. W.P. Wolf, J.H. Van Vleck. Phys. Rev. 118(6) (1960) 1490-1492
16. S. Bhattacharyya. J. Appl. Phys. 80(9), (1996) 5213-5217
17. В.Т. Калинников, Ю.В. Ракитин. "Введение в магнетохимию. Метод статической магнитной восприимчивости в химии". М.: Наука, 1980. 302 с. с илл.
18. J.M. Baker, B. Bleaney, W. Hayes. Proc. Roy. Soc. (London) A247 (1958) 141-151
19. S.V. Upadeo, T.K. Gundurao, S.V. Moharil. J. Phys.: Condens. Matter 6 (1994), 9459-9468
20. А.А. Маненков, А.М. Прохоров. ДАН СССР, 107 (1956) 402-404

**Подписи к рисункам.**

Рис. 1. Спектры люминесценции $Eu^{2+}$ и $Eu^{3+}$ в образцах №№1-5 (T=300 K), снятые при возбуждении 392 нм. Спектры умножены на коэффициент 1.5 при $\lambda$>550 нм. На вставке – спектр люминесценции $Eu^{3+}$ образца №5 (T=300 K), снятый с разрешением порядка 0.7 нм при возбуждении ртутной лампой (линия 365 нм).

Рис. 2. Спектр возбуждения (T=300 K) для излучательного перехода $^5D_0$ – $^7F_1$ в образце №5 (группа линий около 590 нм в спектре люминесценции).

Рис. 3. Обратная магнитная восприимчивость образца №3 как функция температуры. На вкладке показана низкотемпературная часть зависимости магнитной восприимчивости от температуры. Параметры $C$, $\Theta$ и $\chi_0$, определены подгонкой закона Кюри-Вейсса при низкой температуре.

Рис. 4. Спектры ЭПР $Eu^{2+}$ в образцах $CaF_2$:Eu №10 и №3 (T=300 K).

Таблица 1. Список исследованных образцов

| № | Концентрация европия в растворах, ат.% | Концентрация европия, найденная анализом, ат.% | Концентрация европия, введенная при смешивании, ат.% | Температура прокаливания T, K |
|---|---|---|---|---|
| 1 | 0.1028 в воде и 0.1028 в $CaCl_2$ | 1,467 | —— | 1373 |
| 2 | 0.1028 только в воде | 1,493 | —— | 1373 |
| 3 | 0.2056 в воде и 0.2056 в $CaCl_2$ | 2,727 | —— | 1373 |
| 4 | 0.2056 только в воде | 1,639 | —— | 1373 |
| 5 | 0.3084 в воде и 0.3084 в $CaCl_2$ | 4,351 | —— | 1373 |
| 6 | 0.3084 только в воде | 2,137 | —— | 1373 |
| 7 | $Eu_2(CO_3)_3$ смешали механически с $CaF_2$ | —— | 0,0257 | 1373 |
| 8 | $Eu_2(CO_3)_3$ смешали механически с $CaF_2$ | —— | 0,0514 | 1373 |
| 9 | $Eu_2(CO_3)_3$ смешали механически с $CaF_2$ | —— | 0,1028 | 1173 |
| 10 | $Eu_2(CO_3)_3$ смешали механически с $CaF_2$ | —— | 0,1028 | 1373 |

Таблица 2. Отношение интенсивностей спектральных линий $Eu^{3+}$ для образцов, полученных путем соосаждения.

| | Образцы | | | | |
|---|---|---|---|---|---|
| переходы: | Nr5 | Nr4 | Nr3 | Nr2 | Nr1 |
| $^5D_0$-$^7F_1$ | 1,00 | 1,00 | 1,00 | 1,00 | 1,00 |
| $^5D_0$-$^7F_2$ | 0,34 | 0,42 | 0,35 | 0,37 | 0,36 |
| $^5D_0$-$^7F_4$ | 0,38 | 0,42 | 0,38 | 0,35 | 0,36 |

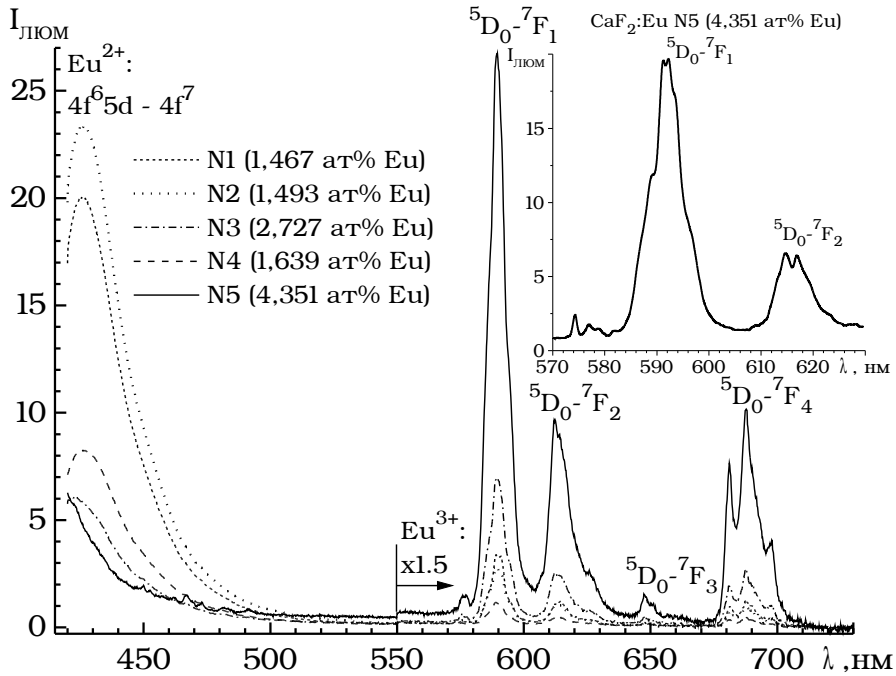
I_ЛЮМ
Eu2+:
4f65d - 4f7
N1 (1,467 ат% Eu)
N2 (1,493 ат% Eu)
N3 (2,727 ат% Eu)
N4 (1,639 ат% Eu)
N5 (4,351 ат% Eu)
5D0-7F1
Eu3+:
x1.5
5D0-7F2
5D0-7F3
5D0-7F4
λ ,нм
CaF2:Eu N5 (4,351 ат% Eu)
I_ЛЮМ
5D0-7F1
5D0-7F2
λ , нм

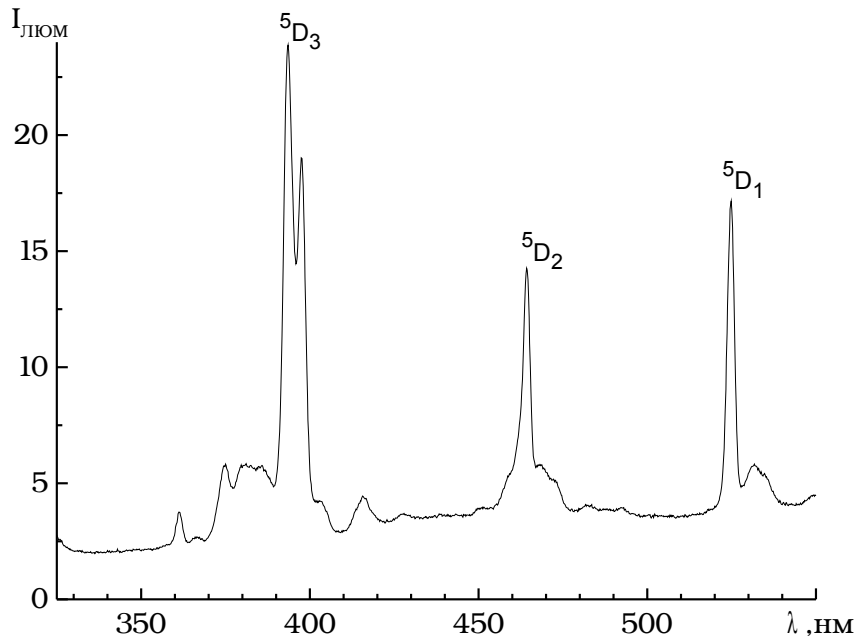
I люм
5D3
5D2
5D1
0
5
10
15
20
350
400
450
500
λ ,нм

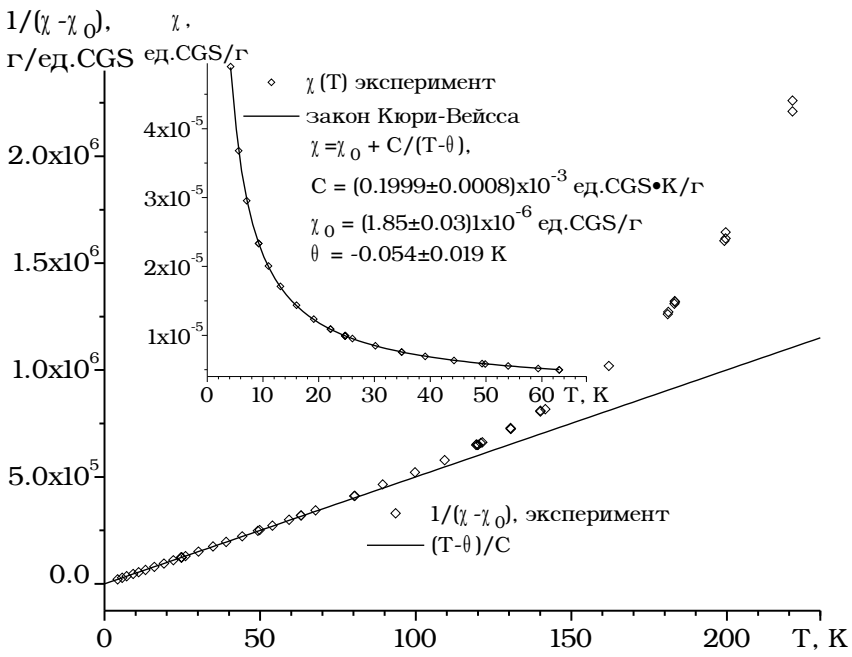
1/(χ -χ 0), г/ед.CGS
χ, ед.CGS/г
χ (T) эксперимент
закон Кюри-Вейсса
χ =χ 0 + C/(T-θ),
C = (0.1999±0.0008)x10-3 ед.CGS•K/г
χ 0 = (1.85±0.03)1x10-6 ед.CGS/г
θ = -0.054±0.019 K
T, K
1/(χ -χ 0), эксперимент
(T-θ)/C
T, K

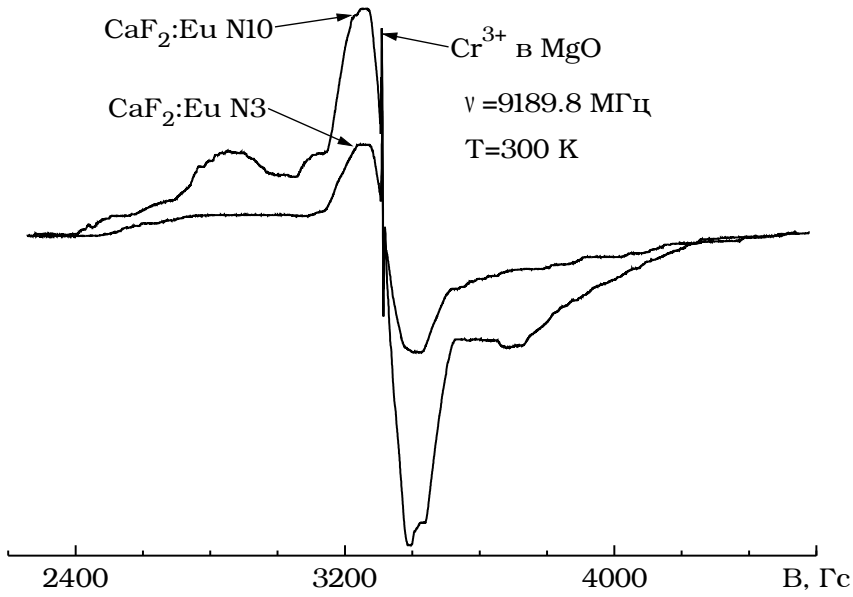
CaF2:Eu N10
Cr3+ в MgO
CaF2:Eu N3
ν =9189.8 МГц
T=300 K
2400
3200
4000
B, Гс

# CURRICULUM VITAE

## Aime Lust


| | |
|---|---|
| Born | March 15, 1942, Kohtla-Järve, Estonia |
| Citizenship | Estonian |
| Marital Status | single |
| Address | Institute of Chemical Physics, University of Tartu,<br>2 Jakobi Str. 51014, Tartu, Estonia |
| Phone: | +372 737 5253 |
| Fax: | +372 737 5264 |
| E-mail: | aime@beryll.physic.ut.ee |


### Education

| | |
|---|---|
| 1961–1965 | University of Tartu, Department of Chemistry |
| 1997 | M.Sc. (physical and analytical chemistry) |
| 2004– ..... | University of Tartu, Department of Chemistry, Ph.D.student<br>doctoral advisor sen.reasercher Mikhail Danilkin |

### Professional emploiment

| | |
|---|---|
| 1998– ..... | University of Tartu, Institute of Chemical Physics, researcher |
| 1993–1998 | same, chemist |
| 1968–1993 | University of Tartu, Chair of analytical chemistry,younger researcher |
| 1966–1968 | same, senior laboratory assistant |

### Scientific activity

Methods of synthesis of thermoluminophors and investigation of their characteristics. TLD dosimetry. Investigation and work-out of new luminescent materials, energy storage and release in luminophors.

## Main Scientific publications


1. V. P. Denks, M. P. Kerikmäe, A. L. Lust and T. I. Savikhina. Photoluminescence of Concentration Series of $CaF_2$:Mn Phosphors Excited by VUV. Radiation.Physics of the Solid State, 2000, vol. 42(2), pp. 261–267.
2. I. Jaek, M. Kerikmäe and A. Lust. OSL of Some TLD Detectors as the Indicator of Absorbed Dose. Radiation Protection Dosimetry, 2002, vol.100 (1–4), pp. 459–462.
3. Aime Lust, Lilli Paama, Mihkel Kerikmäe, Mare Must and Paavo Perämäki. Determination of Manganese in Thermoluminescence Materials by Inductively Coupled Plasma Atomic Emission Spectroscopy and Spectrophotometry. Proc. Estonian Acad. Sci.Chem., 2002, vol. 51(2),pp. 126–133.
4. Mikhail Danilkin, Aime Lust, Mihkel Kerikmäe, Viktor Seeman, Hugo Mändar, Mare Must. $CaF_2$:Mn extreme dosimeter: Effects on Mn concentration on thermoluminescence mechanisms and properties. Radiation Measurements, 2006, vol. 41, pp. 677–681.
5. Mikhail Danilkin, Mihkel Kerikmäe, Aleksei Kirillov, Aime Lust, Arno Ratas, Lilli Paama and Viktor Seeman. Thermoluminescent detector $Li_2B_4O_7$: Mn,Si-false dose problem. Proc. of Estonian Acad. Sci.Chem., 2006, vol. 55 (3), pp.123–131.
6. Mikhail Danilkin, Aleksei Kirillov, Sergei Klimonsky, Vyacheslav Kuznetsov, Aime Lust, Hugo Mändar, Vladimir Nikiforov, Arno Ratas, Aleksandr Ruchkin, Viktor Seeman. Magnetic manifestations of thermoluminescence excitation in $CaF_2$:Mn (TLD–400). Radiation measurements, 2007 (available online at doi:10.1016/j.radmeas.2007.01.079 ).
7. M. Danilkin, A. Beloussov, A. Lust, L. Paama, I. Rammo, S. Klimonsky, V. Kuznetsov, V. Nikiforov, V. Seeman. $Eu^{2+}$ and $Eu^{3+}$ centers formation at synthesis of $CaF_2$:Eu luminophors. (submitted for publication to Journal of Applied Spectroscopy, Minsk).

# CURRICULUM VITAE

## Aime Lust


| | |
|---|---|
| Sündinud: | 15. märts 1942, Kohtla-Järve |
| Kodakondsus: | Eesti |
| Perekonnaseis: | vallaline |
| Aadress: | Keemilise füüsika instituut, Tartu Ülikool, Jakobi 2, 51014 |
| Tel. | +372 737 5253 |
| Fax | +372 737 5264 |
| e-mail: | aime@beryll.physic.ut.ee |


### Haridus

| | |
|---|---|
| 1961–1965 | Tartu Ülikool, keemiaosakond |
| 1997 | M.Sc. (füüsikaline ja analüütiline keemia) |
| 2004– | Tartu Ülikooli keemiaosakonna doktorant, juhendaja vanemteadur Mihhail Danilkin |

### Teenistuskäik

| | |
|---|---|
| 1998– | Tartu Ülikool, keemilise füüsika instituut, teadur |
| 1993–1998 | samas, keemik |
| 1968–1993 | Tartu Ülikool, analüütilise keemia kateeder, nooremteadur |
| 1966–1968 | samas, vanemlaborant |

### Teadustegevus

Peamised uurimisvaldkonnad: Termoluminofooride süntees ja nende omaduste uurimine. Uute luminestsentsmaterjalide süntees ja kasutamine. Lisandite jaotus tahketes lahustes. Ioniseeriva kiirguse energia salvestamine ja vabastamine luminofoorides.

**Tähtsamad teaduspublikatsioonid**


1. V. P. Denks, M. P. Kerikmäe, A. L. Lust and T. I. Savikhina. Photoluminescence of Concentration Series of $CaF_2$:Mn Phosphors Excited by VUV Radiation. Physics of the Solid State, 2000, vol. 42(2), pp. 261–267.
2. I. Jaek, M. Kerikmäe and A. Lust. OSL of Some TLD Detectors as the Indicator of Absorbed Dose. Radiation Protection Dosimetry, 2002, vol. 100(1–4), pp. 459–462.
3. Aime Lust, Lilli Paama, Mihkel Kerikmäe, Mare Must and Paavo Perämäki. Determination of Manganese in Thermoluminescence Materials by Inductively Coupled Plasma Atomic Emission Spectroscopy and Spectrophotometry. Proc. Estonian Acad. Sci.Chem., 2002, vol. 51 (2), pp.126–133.
4. Mikhail Danilkin, Aime Lust, Mihkel Kerikmäe, Viktor Seeman, Hugo Mändar, Mare Must. $CaF_2$:Mn extreme dosimeter: Effects of Mn concentration on thermoluminescence mechanisms and properties. Radiation Measurements, 2006, vol.41, pp. 677–681.
5. Mikhail Danilkin, Mihkel Kerikmäe, Aleksei Kirillov, Aime Lust, Arno Ratas, Lilli Paama, and Viktor Seeman. Thermoluminescent detector $Li_2B_4O_7$:Mn,Si – a false dose problem. Proc. Estonian Acad. Sci. Chem. 2006, vol. 55(3), pp. 123–131.
6. Mikhail Danilkin, Aleksei Kirillov, Sergei Klimonsky, Vyacheslav Kuznetsov, Aime Lust, Hugo Mändar, Vladimir Nikiforov, Arno Ratas, Aleksandr Ruchkin, Viktor Seeman. Magnetic manifestations of thermoluminescence excitation in $CaF_2$:Mn (TLD-400). Radiation Measurements (available online at doi:10.1016/j.radmeas.2007.01.079 )
7. M. Danilkin, A. Beloussov, A. Lust, L. Paama, I. Rammo, S. Klimonsky, V. Kuznetsov, V.Seeman. $Eu^{2+}$ and $Eu^{3+}$ centers formation at synthesis of $CaF_2$ luminophors(submitted for publication to Journal of Applied Spectroscopy, Minsk).

# DISSERTATIONES CHIMICAE UNIVERSITATIS TARTUENSIS

1. **Toomas Tamm.** Quantum-chemical simulation of solvent effects. Tartu, 1993, 110 p.
2. **Peeter Burk.** Theoretical study of gas-phase acid-base equilibria. Tartu, 1994, 96 p.
3. **Victor Lobanov.** Quantitative structure-property relationships in large descriptor spaces. Tartu, 1995, 135 p.
4. **Vahur Mäemets.** The $^{17}O$ and $^{1}H$ nuclear magnetic resonance study of $H_2O$ in individual solvents and its charged clusters in aqueous solutions of electrolytes. Tartu, 1997, 140 p.
5. **Andrus Metsala.** Microcanonical rate constant in nonequilibrium distribution of vibrational energy and in restricted intramolecular vibrational energy redistribution on the basis of slater's theory of unimolecular reactions. Tartu, 1997, 150 p.
6. **Uko Maran.** Quantum-mechanical study of potential energy surfaces in different environments. Tartu, 1997, 137 p.
7. **Alar Jänes.** Adsorption of organic compounds on antimony, bismuth and cadmium electrodes. Tartu, 1998, 219 p.
8. **Kaido Tammeveski.** Oxygen electroreduction on thin platinum films and the electrochemical detection of superoxide anion. Tartu, 1998, 139 p.
9. **Ivo Leito.** Studies of Brønsted acid-base equilibria in water and non-aqueous media. Tartu, 1998, 101 p.
10. **Jaan Leis.** Conformational dynamics and equilibria in amides. Tartu, 1998, 131 p.
11. **Toonika Rinken.** The modelling of amperometric biosensors based on oxidoreductases. Tartu, 2000, 108 p.
12. **Dmitri Panov.** Partially solvated Grignard reagents. Tartu, 2000, 64 p.
13. **Kaja Orupõld.** Treatment and analysis of phenolic wastewater with microorganisms. Tartu, 2000, 123 p.
14. **Jüri Ivask.** Ion Chromatographic determination of major anions and cations in polar ice core. Tartu, 2000, 85 p.
15. **Lauri Vares.** Stereoselective Synthesis of Tetrahydrofuran and Tetrahydropyran Derivatives by Use of Asymmetric Horner-Wadsworth-Emmons and Ring Closure Reactions. Tartu, 2000, 184 p.
16. **Martin Lepiku.** Kinetic aspects of dopamine $D_2$ receptor interactions with specific ligands. Tartu, 2000, 81 p.
17. **Katrin Sak.** Some aspects of ligand specificity of P2Y receptors. Tartu, 2000, 106 p.
18. **Vello Pällin.** The role of solvation in the formation of iotsitch complexes. Tartu, 2001, 95 p.

19. **Katrin Kollist.** Interactions between polycyclic aromatic compounds and humic substances. Tartu, 2001, 93 p.
20. **Ivar Koppel.** Quantum chemical study of acidity of strong and superstrong Brønsted acids. Tartu, 2001, 104 p.
21. **Viljar Pihl.** The study of the substituent and solvent effects on the acidity of OH and CH acids. Tartu, 2001, 132 p.
22. **Natalia Palm.** Specification of the minimum, sufficient and significant set of descriptors for general description of solvent effects. Tartu, 2001, 134 p.
23. **Sulev Sild.** QSPR/QSAR approaches for complex molecular systems. Tartu, 2001, 134 p.
24. **Ruslan Petrukhin.** Industrial applications of the quantitative structure-property relationships. Tartu, 2001, 162 p.
25. **Boris V. Rogovoy.** Synthesis of (benzotriazolyl)carboximidamides and their application in relations with *N*- and *S*-nucleophyles. Tartu, 2002, 84 p.
26. **Koit Herodes.** Solvent effects on UV-vis absorption spectra of some solvatochromic substances in binary solvent mixtures: the preferential solvation model. Tartu, 2002, 102 p.
27. **Anti Perkson.** Synthesis and characterisation of nanostructured carbon. Tartu, 2002, 152 p.
28. **Ivari Kaljurand.** Self-consistent acidity scales of neutral and cationic Brønsted acids in acetonitrile and tetrahydrofuran. Tartu, 2003, 108 p.
29. **Karmen Lust.** Adsorption of anions on bismuth single crystal electrodes. Tartu, 2003, 128 p.
30. **Mare Piirsalu.** Substituent, temperature and solvent effects on the alkaline hydrolysis of substituted phenyl and alkyl esters of benzoic acid. Tartu, 2003, 156 p.
31. **Meeri Sassian.** Reactions of partially solvated Grignard reagents. Tartu, 2003, 78 p.
32. **Tarmo Tamm.** Quantum chemical modelling of polypyrrole. Tartu, 2003. 100 p.
33. **Erik Teinemaa.** The environmental fate of the particulate matter and organic pollutants from an oil shale power plant. Tartu, 2003. 102 p.
34. **Jaana Tammiku-Taul.** Quantum chemical study of the properties of Grignard reagents. Tartu, 2003. 120 p.
35. **Andre Lomaka.** Biomedical applications of predictive computational chemistry. Tartu, 2003. 132 p.
36. **Kostyantyn Kirichenko.** Benzotriazole — Mediated Carbon–Carbon Bond Formation. Tartu, 2003. 132 p.
37. **Gunnar Nurk.** Adsorption kinetics of some organic compounds on bismuth single crystal electrodes. Tartu, 2003, 170 p.
38. **Mati Arulepp.** Electrochemical characteristics of porous carbon materials and electrical double layer capacitors. Tartu, 2003, 196 p.

39. **Dan Cornel Fara.** QSPR modeling of complexation and distribution of organic compounds. Tartu, 2004, 126 p.
40. **Riina Mahlapuu.** Signalling of galanin and amyloid precursor protein through adenylate cyclase. Tartu, 2004, 124 p.
41. **Mihkel Kerikmäe.** Some luminescent materials for dosimetric applications and physical research. Tartu, 2004, 143 p.
42. **Jaanus Kruusma.** Determination of some important trace metal ions in human blood. Tartu, 2004, 115 p.
43. **Urmas Johanson.** Investigations of the electrochemical properties of polypyrrole modified electrodes. Tartu, 2004, 91 p.
44. **Kaido Sillar.** Computational study of the acid sites in zeolite ZSM-5. Tartu, 2004, 80 p.
45. **Aldo Oras.** Kinetic aspects of dATPαS interaction with $P2Y_1$ receptor. Tartu, 2004, 75 p.
46. **Erik Mölder.** Measurement of the oxygen mass transfer through the air-water interface. Tartu, 2005, 73 p.
47. **Thomas Thomberg.** The kinetics of electroreduction of peroxodisulfate anion on cadmium (0001) single crystal electrode. Tartu, 2005, 95 p.
48. **Olavi Loog.** Aspects of condensations of carbonyl compounds and their imine analogues. Tartu, 2005, 83 p.
49. **Siim Salmar.** Effect of ultrasound on ester hydrolysis in aqueous ethanol. Tartu, 2006, 73 p.
50. **Ain Uustare.** Modulation of signal transduction of heptahelical receptors by other receptors and G proteins. Tartu, 2006, 121 p.
51. **Sergei Yurchenko.** Determination of some carcinogenic contaminants in food. Tartu, 2006, 143 p.
52. **Kaido Tämm.** QSPR modeling of some properties of organic compounds. Tartu, 2006, 67 p.
53. **Olga Tšubrik.** New methods in the synthesis of multisubstituted hydrazines. Tartu. 2006, 183 p.
54. **Lilli Sooväli.** Spectrophotometric measurements and their uncertainty in chemical analysis and dissociation constant measurements. Tartu, 2006, 125 p.
55. **Eve Koort.** Uncertainty estimation of potentiometrically measured ph and $pK_a$ values. Tartu, 2006, 139 p.
56. **Sergei Kopanchuk.** Regulation of ligand binding to melanocortin receptor subtypes. Tartu, 2006, 119 p.
57. **Silvar Kallip.** Surface structure of some bismuth and antimony single crystal electrodes. Tartu, 2006, 107 p.
58. **Kristjan Saal.** Surface silanization and its application in biomolecule coupling. Tartu, 2006, 77 p.
59. **Tanel Tätte.** High viscosity $Sn(OBu)_4$ oligomeric concentrates and their applications in technology. Tartu, 2006, 91 p.

60. **Dimitar Atanasov Dobchev**. Robust QSAR methods for the prediction of properties from molecular structure. Tartu, 2006, 118 p.
61. **Hannes Hagu**. Impact of ultrasound on hydrophobic interactions in solutions. Tartu, 2007, 81 p.
62. **Rutha Jäger.** Electroreduction of peroxodisulfate anion on bismuth electrodes. Tartu, 2007, 142 p.
63. **Kaido Viht.** Immobilizable bisubstrate-analogue inhibitors of basophilic protein kinases: development and application in biosensors. Tartu, 2007, 88 p.
64. **Eva-Ingrid Rõõm.** Acid-base equilibria in nonpolar media. Tartu, 2007, 156 p.
65. **Sven Tamp.** DFT study of the cesium cation containing complexes relevant to the cesium cation binding by the humic acids. Tartu, 2007, 102 p.
66. **Jaak Nerut.** Electroreduction of hexacyanoferrate(III) anion on Cadmium (0001) single crystal electrode. Tartu, 2007, 180 p.
67. **Lauri Jalukse.** Measurement uncertainty estimation in amperometric dissolved oxygen concentration measurement. Tartu, 2007, 112 p.